# A STUDY ON USING GLASS MICRO-SPHERES IN EROSION RESISTANT COATINGS AND POLYMER COMPOSITES

A THESIS SUBMITTED IN PARTIAL FULFILLMENT OF THE REQUIREMENTS FOR THE DEGREE OF

Doctor of Philosophy

In

Mechanical Engineering

By

**GAURAV GUPTA**

(511 ME 104)

Under the supervision of

**Prof. Alok Satapathy**

Associate Professor

Department of Mechanical Engineering

National Institute of Technology,

Rourkela


**DEPARTMENT OF MECHANICAL ENGINEERING**

**National Institute of Technology**

**Rourkela (India)**

2015

*Dedicated To*

*My Beloved*

*Grand Parents*

# National Institute of Technology
# Rourkela

# C E R T I F I C A T E

This is to certify that the thesis entitled ***A Study on using Glass Microspheres in Erosion Resistant Coatings and Polymer Composites*** submitted by **GAURAV GUPTA** to National Institute of Technology, Rourkela for the award of the degree of **Doctor of Philosophy** in *Mechanical Engineering* is an authentic record of research work carried out by him under my guidance and supervision.

The work incorporated in this thesis has not been, to the best of my knowledge, submitted to any other University or Institute for the award of a degree or diploma.

Date:

Place:

**Prof. Alok Satapathy**
Associate Professor
Department of Mechanical Engineering,
National Institute of Technology
Rourkela

# ACKNOWLEDGEMENT

Endeavors are never achieved alone; there are always several supportive hands. This thesis too is a meticulous result of the guidance of many such people around me who have brought me all through the way. So, I would like to thank them all for their presence in my life in a small way**.** I feel myself extremely fortunate to be involved in a challenging research work of this kind. It has enriched my life, giving me an opportunity to work in a new area of science and technology. It has enhanced my understanding and thinking ability and after the completion of my work, I experienced a feeling of self-gratification.

I would first like to express my deep sense of gratitude to my guide **Prof. Alok Satapathy** who is an embodiment of knowledge, perseverance and tolerance for his excellent guidance, extraordinary effort and support during my research work. Without him this thesis would not have been materialized. One can never possibly wish for a better adviser and path maker in life. I would also like to express my sincere gratitude to the Head of the Department of Mechanical Engineering **Prof. S. S. Mahapatra** for his timely help during the entire course of my research work.

I wish to record my heartfelt thanks and gratitude to my parents who have been a constant source of endless inspiration and support for me through one way or the other from the very childhood and who stood by me whatsoever, at all difficult phases of my life.

I would specially like to thank **Mrs. Susmita Satapathy** for her constant motivation and fruitful comments without which I would not have been evolved as a good researcher.

I owe a lot to my friend **Alok Agrawal** who encouraged and supported me a lot for this research. I am extremely thankful to my co-researchers **Pravat Ranjan Pati, Debasmita Mishra, Madhusmita Sahu, Abhishek Sharma, Johan Banjare, Yagya Ku. Sahu, Saurabh Chandraker, Srimant Ku. Mishra, Alok Ku. Jha, Vivek Mishra and Saurabh Sharma** for helping me in every way they could and for making the past few years more delightful.

At last but not the least, I thank **Almighty God** for giving me an opportunity to work in such an environment with such good and knowledgeable people around.

Date:

Place:

**Gaurav Gupta**
(Research Scholar)
Roll No. 511 ME 104
Dept. of Mechanical Engineering
National Institute of Technology
Rourkela

# List of Figures


**Figure 2.1** Sequence of events during thermal spraying

**Figure 2.2** Conventional plasma spraying process

**Figure 2.3** Factors affecting erosive wear of polymers and composites

**Figure 3.1** Unmodified epoxy resin chain

**Figure 3.2** Tri-ethylene-tetramine (hardener used for epoxy matrix)

**Figure 3.3** Polypropylene chain (n is the number of polymerized unit)

**Figure 3.4** Plasma spray set-up

**Figure 3.5** General arrangement of the plasma spraying equipment

**Figure 3.6** Schematic diagram of the plasma spraying process

**Figure 3.7** Pictorial view of plasma sprayed coating samples

**Figure 3.8** Schematic view of the plasma sprayed coatings

**Figure 3.9** Composite fabrication by hand lay-up process

**Figure 3.10** Injection molding machine

**Figure 3.11** Compression molding machine

**Figure 3.12** Elcometer 456 thickness gauge

**Figure 3.13** PC-2000 Electronic Tenso-meter (Horizontal table model)

**Figure 3.14** Loading pattern during coating pull out test

**Figure 3.15** Scanning electron microscope

**Figure 3.16** X-ray diffractometer

**Figure 3.17** Leitz micro-hardness tester

**Figure 3.18** Instron 1195 universal testing machine

**Figure 3.19** Composite samples for tensile test

**Figure 3.20** **(a)** Loading arrangement for tensile test

**(b)** Loading arrangement for flexural strength test

**Figure 3.21** Unitherm$^{TM}$ Model 2022 tester

**Figure 3.22** **(a)** Schematic diagram of erosion test rig

**(b)** Solid particle erosion test set-up

**Figure 4.1** **(a)** Particle size analysis of borosilicate glass micro-spheres

**(b)** SEM micrographs of BGM powder prior to coating

**Figure 4.2** Variation of coating thickness for BGM and BGM-$Al_2O_3$ with torch input power

**Figure 4.3** Variation of coating thickness for BGM and BGM-$TiO_2$ with torch input power

**Figure 4.4** Variation of coating deposition efficiency for BGM and BGM-$Al_2O_3$ with torch input power

**Figure 4.5** Variation of coating deposition efficiency for BGM and BGM-$TiO_2$ with torch input power

**Figure 4.6** Variation of coating adhesion strength for BGM and BGM-$Al_2O_3$ with torch input power

**Figure 4.7** Variation of coating adhesion strength for BGM and BGM-$TiO_2$ with torch input power

**Figure 4.8** X-ray diffractogram of the BGM coating

**Figure 4.9** X-ray diffractogram of the BGM-$Al_2O_3$ coating

**Figure 4.10** X-ray diffractogram of the BGM-$TiO_2$ coating

**Figure 5.1** SEM micrographs of uneroded (5.1 a, b)/eroded (5.1 c, d) surfaces of the BGM coatings

**Figure 5.2** SEM micrographs of uneroded (5.2 a, b) and eroded (5.2 c, d) surfaces of the BGM+$Al_2O_3$ coatings

**Figure 5.3** SEM micrographs of uneroded (5.3 a) and eroded (5.3 a, b, c) surfaces of the BGM+$TiO_2$ coatings

**Figure 5.4** Effect of control factors on erosion rate for BGM coatings

**Figure 5.5** Effect of control factors on erosion rate for 'BGM + $Al_2O_3$'coatings

**Figure 5.6** Effect of control factors on erosion rate for 'BGM + $TiO_2$'coatings

**Figure 5.7** Three layer neural network (BGM coatings)

**Figure 5.8** Three layer neural network ('BGM + $Al_2O_3$' coatings)

**Figure 5.9** Three layer neural network ('BGM + $TiO_2$' coatings)

**Figure 5.10** Effect of impact velocity on erosion rate for different (a) impingement angle (b) erodent size for BGM coatings

**Figure 5.11** Effect of impact velocity on erosion rate for different (a) impingement angle (b) erodent size for BGM + $Al_2O_3$ coatings

**Figure 5.12** Effect of impact velocity on erosion rate for different (a) impingement angle (b) erodent size for BGM + $TiO_2$ coatings

**Figure 5.13** Comparison of erosion rates of BGM coatings obtained from different methods

**Figure 5.14** Comparison of erosion rates of 'BGM + $Al_2O_3$' coatings obtained from different methods

**Figure 5.15** Comparison of erosion rates of 'BGM + $TiO_2$' coatings obtained from different methods

**Figure 6.1** Micro-hardness of glass micro-sphere filled composites

**Figure 6.2** Tensile strength of glass micro-sphere filled composites

**Figure 6.3** Tensile modulus of glass micro-sphere filled composites

**Figure 6.4** Flexural strength of glass micro-sphere filled composites

**Figure 6.5** Impact strength of glass micro-sphere filled composites

**Figure 6.6** Thermal conductivity of glass micro-sphere filled composites

**Figure 7.1** SEM micrographs of uneroded and eroded surfaces of the epoxy composites

**Figure 7.2** SEM micrographs of uneroded and eroded surfaces of the polypropylene composites

**Figure 7.3** Effect of control factors on erosion rate for EP-BGM composites

**Figure 7.4** Effect of control factors on erosion rate for PP-BGM composites

**Figure 7.5** Three layer neural network (EP-BGM)

**Figure 7.6** Three layer neural network (PP-BGM)

**Figure 7.7** Effect of impact velocity on erosion rate for different (a) BGM content (b) impingement angle for EP-BGM composite

**Figure 7.8** Effect of BGM content on erosion rate for different (a) impact velocity (b) impingement angle for PP-BGM composite

**Figure 7.9** Comparison of erosion rates of EP-BGM composites obtained from different methods

**Figure 7.10** Comparison of erosion rates of PP-BGM composites obtained from different methods

**Figure 7.11** Effect of impingement angle on erosion rate of epoxy-BGM composites

**Figure 7.12** Effect of impingement angle on erosion rate of PP-BGM composites

**Figure 7.13** Comparison of wear rates of composites under different test conditions

*****

# List of Tables


**Table 2.1** Principal characteristics and features of important thermal spray variants employing powders as feedstock

**Table 3.1** Some important properties of glass microspheres

**Table 3.2** Properties of $Al_2O_3$ and $TiO_2$

**Table 3.3** Some important properties of epoxy

**Table 3.4** Properties of homo-polymer M110 polypropylene

**Table 3.5** Elemental composition of AISI 1018 mild steel

**Table 3.6** Elemental composition of Al 6061 aluminium

**Table 3.7** Mixtures used for coating deposition

**Table 3.8** Operating parameters during coating deposition

**Table 3.9** Epoxy composites filled with glass microspheres

**Table 3.10** Main parameters during the injection molding

**Table 4.1** Coating porosity at different torch input power for different feed materials

**Table 4.2** Coating micro-hardness at different torch input power for different feed materials

**Table 5.1** Experimental design using $L_{16}$ orthogonal array and the wear test results for BGM coatings

**Table 5.2** S/N ratio response table for erosion rate of BGM coatings

**Table 5.3** Experimental design using $L_{16}$ orthogonal array and the wear test results for 'BGM + $Al_2O_3$' and 'BGM + $TiO_2$' coatings

**Table 5.4** S/N ratio response table for erosion rate of 'BGM + $Al_2O_3$' coatings

**Table 5.5** S/N ratio response table for erosion rate of 'BGM + $TiO_2$' coatings

**Table 5.6** Results of the confirmation experiments for erosion rate

**Table 5.7** Comparison of experimental and predicted values for erosion rate

**Table 5.8** Input parameters for training (BGM coatings)

**Table 5.9** Input parameters for training ('BGM + $Al_2O_3$' coatings)

**Table 5.10** Input parameters for training ('BGM + $TiO_2$' coatings)

**Table 5.11** Percentage error between experimental result and ANN prediction

**Table 6.1** Measured and theoretical densities along with the void fractions of the composites

**Table 6.2** Mechanical properties of the composites

**Table 7.1** Experimental design using $L_{16}$ orthogonal array and the wear test results for epoxy and polypropylene composites

**Table 7.2** S/N ratio response table for erosion rate of EP-BGM composites

**Table 7.3** S/N ratio response table for erosion rate of PP-BGM composites

**Table 7.4** Results of the confirmation experiments for erosion rate

**Table 7.5** Comparison between experimental and predicted values for erosion rate

**Table 7.6** Input parameters for training (EP-BGM)

**Table 7.7** Input parameters for training (PP-BGM)

**Table 7.8** Percentage error between experimental result and ANN prediction

*****

# *ABSTRACT*

*The present work reports the performance of a new class of glass micro-sphere based coatings and glass micro-sphere filled polymer composites with emphasis on the general trends observed in their properties and erosion wear behavior. A wealth of property data has been generated by conducting various tests under controlled laboratory conditions and the analysis of the test results is presented in the thesis.*

*The quality of coating in terms of mechanical, micro-structural and functional characteristics depends on a large number of variables that include both materials as well as operational parameters. While the composition of coating material and the substrate play an important role in determining the coating quality, the influence of plasma torch input power is also equally important; this is reflected in the research findings of the present investigation. This work suggests that glass micro-spheres are coatable and deposition of such coatings on metallic substrates using plasma spraying route is possible. The variations of different coating characteristics such as coating adhesion strength, deposition efficiency, coating thickness and micro-hardness with the plasma torch input power are evident in the illustrations presented in this thesis. These coatings possess desirable characteristics such as good adhesion strength, hardness etc. Pre-mixing of micro-sized $Al_2O_3$ or $TiO_2$ particles improves the coatability of glass micro-spheres. Such coatings also exhibit improved interfacial adhesion strength. The strength is greatly affected by the plasma torch input power.*

*Glass micro-sphere possesses ample reinforcing potential to be used as a functional filler in both thermoset and thermoplastic polymers. Successful fabrication of epoxy composites reinforced with glass micro-spheres is possible by simple hand-lay-up technique. Similarly, glass micro-sphere filled polypropylene composites can be fabricated by injection/compression molding routes. These glass micro-sphere filled composites possess very low amount of*

*porosity (maximum ≈ 2%) and improved micro-hardness. They also exhibit improved impact strength as compared to that of the neat polymers. The tensile and flexural strength of the composites are affected, though marginally, by the weight fraction of glass micro-spheres in the composites. With improved hardness, these composites have the potential to be used in wear related applications.*

*Solid particle erosion wear characteristics of glass micro-sphere coatings and glass micro-sphere filled polymer composites have been successfully analyzed using Taguchi technique. Significant factors affecting the erosion rate of these coatings and composites are identified through successful implementation of signal-to-noise response approach. Two predictive models; one based on artificial neural networks (ANN) approach and the other on Taguchi approach are proposed in this work. It is demonstrated that these models well reflect the effects of various factors on the wear loss and their predictive results are consistent with the experimental observations. Neural computation is successfully applied in this investigation to predict and simulate the wear response of these coatings and composites under various test conditions within and beyond the experimental domain.*

*****

# CONTENTS


| Chapter | | Chapter Title | Page |
|---|---|---|---|
| **Chapter 1** | **INTRODUCTION** | | 1 |
| | 1.1 | Background and Motivation | 1 |
| | 1.2 | Thesis Outline | 4 |
| **Chapter 2** | **LITERATURE REVIEW** | | 6 |
| | 2.1 | On Thermal Spraying | 6 |
| | 2.2 | On Plasma Spray Coatings | 10 |
| | 2.3 | On Particulate filled Polymer Composites | 13 |
| | 2.4 | On Glass Micro-sphere filled Polymer Composites | 17 |
| | 2.5 | On Wear and it's Classification | 19 |
| | 2.6 | On Erosion Wear Characteristics of Ceramic Coatings | 22 |
| | 2.7 | On Erosion Wear Characteristics of Polymer Composites | 26 |
| | 2.8 | On Implementation of Design-of-Experiments and Artificial Neural Networks in Wear Analysis | 30 |
| | 2.9 | Knowledge Gap in Earlier Investigations | 33 |
| | 2.10 | Objectives of the Present Research | 34 |
| | | **Chapter Summary** | |
| **Chapter 3** | **MATERIALS AND METHODS** | | 36 |
| | 3.1 | Materials | 36 |
| | 3.2 | Deposition of the Coatings | 40 |
| | 3.3 | Composite Fabrication | 45 |
| | 3.4 | Coating Characterization | 49 |
| | 3.5 | Composite Characterization | 52 |
| | 3.6 | Erosion Wear Behaviour | 57 |

3.7 Process Optimization and Taguchi Method 57

3.8 Artificial Neural Network 59

**Chapter Summary**

**Chapter 4** Results and Discussion - I 61

**COATING CHARACTERIZATION**

4.1 Characterization of Coating Material 61

4.2 Characterization of Coatings 62

**Chapter Summary**

**Chapter 5** Results and Discussion - II 77

**EROSION WEAR RESPONSE OF PLASMA SPRAYED GLASS MICRO-SPHERE COATINGS**

5.1 Morphology of Coating Surfaces 77

5.2 Erosion Test Results and Taguchi Analysis 80

5.3 Confirmation Experiment 85

5.4 Wear Rate Estimation using Predictive Equation 86

5.5 ANN Based Prediction 88

**Chapter Summary**

**Chapter 6** Results and Discussion - III 99

**COMPOSITE CHARACTERIZATION**

6.1 Physical Characterization of the Composites 99

6.2 Mechanical Characterization of the Composites 100

**Chapter Summary**

**Chapter 7** Results and Discussion - IV 108

**EROSION WEAR RESPONSE OF GLASS MICRO-SPHERE FILLED POLYMER COMPOSITES**

7.1 Morphology of Composite Surfaces 108

7.2 Erosion Test Results and Taguchi Analysis 111
7.3 Confirmation Experiment 114
7.4 Wear Rate Estimation using Predictive Equation 115
7.5 ANN Based Prediction 116
7.6 Effect of Impingement Angle on Erosion Rate 123
7.7 Discussion 124
**Chapter Summary**

**Chapter 8 SUMMARY AND CONCLUSIONS** 127
8.1 Summary of Research Findings 128
8.2 Conclusions 131
8.3 Recommendations for Potential Applications 133
8.4 Scope for Future Work 134

**REFERENCES** 135

**APPENDICES**
**A1 List of Publications**
**A2 Brief Bio-data of the Author**
**Prints of Published/Accepted Papers**

*****

Chapter 1

# INTRODUCTION

## 1.1 Background and Motivation

Micro-sized spheres of glass are being manufactured for a wide variety of uses in research, medicine, consumer goods and various industries. But its potential as a coating material and as a reinforcing element in polymers has not been adequately explored. Glass micro-spheres have several advantages and can be preferred over irregular ones in many engineering applications due to their low surface area to volume ratio, high density, free flowing ability and close sizing etc. [1]. In view of this, the present work attempts to explore the possibility of developing plasma sprayed glass microsphere coatings and glass microsphere filled polymer composites.

Plasma spray coating is a thermal spraying process that combines particle melting, quenching and consolidation in a single operation. It utilizes the exotic properties of the plasma medium to impart new functional properties to both conventional as well as non-conventional materials. The process involves injection of powder particles (metallic, ceramic or cermet powders) into the plasma jet created by heating an inert gas in an electric arc confined within a water-cooled nozzle. Plasma spraying has certain additional advantages over other competing surface modification techniques. By virtue of the high temperature and high enthalpy of the thermal plasma jet, any powder, which melts without decomposition or sublimation, can be coated keeping the substrate temperature as low as $50^{o}$C. The coating process is fast and the thickness can go from a few tens of microns to a few mm. It is a continuous process and can be used to deposit ceramics, metals, alloys and composites.

Plasma spraying is extensively used in hi-tech industries like aerospace, nuclear energy as well as conventional industries like textiles, chemicals, plastics and

paper mainly as wear resistant coatings in crucial components. It is a very large industry with applications in corrosion, abrasion and temperature resistant coatings and in the production of monolithic shapes [2]. This process can be applied to coat on variety of substrates of complicated shape and size using metallic, ceramic and/or polymeric consumables. The production rate of the process is very high and the coating adhesion is also adequate. It has therefore a very wide range of applicability, e.g., as thermal barrier coatings, wear resistant coatings etc. Wear resistant coatings are used to combat wear especially in cylinder liners, pistons, valves, spindles, textile mill rollers etc. Alumina ($Al_2O_3$), titania ($TiO_2$) and zirconia ($ZrO_2$) are considered as some of the conventional wear resistant coating materials [3]. These materials form good adherent coatings on metallic substrates and are used in various thermal as well as tribological applications. Though a lot of studies have been devoted to the development of various wear resistant coatings, no attempt has so far been made for deposition of glass micro-sphere coatings for wear resistance purpose.

Similarly, use of solid glass micro-spheres (glass bead) as reinforcing filler in polymer composites has been rare. Polymers and their composites form a very important class of tribo-engineering materials and are invariably used in machine and structural components, where wear performance in non-lubricated condition is a key parameter for the material selection. Over the past few decades, it is found that polymers have replaced many of the conventional metals/materials in various applications due to their many advantages such as ease of processing, productivity, cost reduction etc. [4]. In most of these applications, the properties of polymers are modified by using fillers to suit the desired requirements. Hard particulate fillers consisting of ceramic or metal particles and fiber-fillers made of glass are being used these days to dramatically improve the mechanical and wear properties of many composites [5, 6]. But the potential of glass micro-spheres for such use in polymeric matrices has rarely been explored.

Studies on tribo-performance of such materials are becoming increasingly relevant and significant as these are often used in hostile workplaces where they

are subjected to different wear situations. *Wear* is defined as the damage to a solid surface usually involving progressive loss of materials, owing to relative motion between the surface and a contacting substance or substances [7]. It is a material response to the external stimulus and can be mechanical or chemical in nature. There are quite a few terms to describe various wear modes which can be clubbed into four principal categories viz. abrasion, adhesion, erosion and surface fatigue [8]. Generally, abrasive wear occurs when two surfaces in contact move against each other and the harder particle in one cut through the other. This form of wear is prevalent when a tangential motion causes the material removal by the simultaneous micro-ploughing and micro-cutting [7]. However, wear due to localized bonding between contacting solid surfaces leading to material transfer between the two surfaces or the loss from either surface is termed as adhesive wear. Similarly, surface fatigue is another wear process that takes place when tiny wear particles are dislodged from a surface by fracture on repeated rolling or sliding on the surface. Owing to a repeated loading action, sub-surface cracks grow from pre-existing defects, join hands with other vicinal cracks and finally come to the surface removing a small chunk of material [8]. In the erosion wear mode, a progressive loss of material occurs from a solid surface due to mechanical interaction between that surface and a fluid, a multi-component fluid, or impinging liquid or solid particles [9].

Solid particle erosion (SPE) wear, which results from solid particles moving at various velocities and striking the surface of a material at various angles, is one of the most encountered wear modes [10, 11]. In some cases, SPE is an useful phenomenon, as in sandblasting and high-speed abrasive water jet cutting but it is a serious problem in many industrial systems including steam and jet turbines, pipelines and valves carrying particulate matter and fluidized bed combustion systems [12]. Solid particle erosion is to be expected whenever hard particles are entrained in a gas or liquid medium impinging on a solid at any significant velocity. In both cases, particles can be accelerated or decelerated and their directions of motion can be changed by the fluid.

Statistical methods have commonly been used for analysis, prediction and/or optimization of a number of engineering processes. Such methods enable the user to define and study the effect of every single condition possible in an experiment where numerous factors are involved. Solid particle erosion is a complex wear phenomena in which a number of control factors collectively determine the performance output (i.e. the wear rate) and there is enormous scope here for implementation of appropriate statistical techniques for process optimization. But unfortunately, such studies have not been adequately reported so far. The present research work addresses to this aspect by adopting a statistical approach called Taguchi experimental design. This technique provides a simple, systematic and efficient methodology for the analysis of the control factors.

Against this background, an attempt has been made in this research work to develop borosilicate glass microsphere (BGM) based coatings and composites and to study their erosion wear performance using design-of-experiment and artificial neural networks.

### 1.2 Thesis Outline

The remainder of this thesis is organized as follows:

**Chapter 2** Includes a literature review designed to provide a summary of the base of knowledge already available involving the issues of interest. It presents the research works on plasma spray coatings as well as particulate reinforced polymer composites reported by various investigators.

**Chapter 3** Includes a description of the raw materials and the test procedures. It presents the details of development of coatings and fabrication of composites as well as the characterization of coatings and composites under investigation and also an explanation of the Taguchi experimental design and ANN.

**Chapter 4** Presents the physical and mechanical properties of the coatings under this study.

**Chapter 5** Includes the erosion wear characteristics of BGM, BGM-$Al_2O_3$ and BGM-$TiO_2$ coatings.

**Chapter 6** Presents the physical and mechanical properties of the composites under this study.

**Chapter 7** Includes the erosion wear characteristics of epoxy-BGM and polypropylene-BGM composites.

**Chapter 8** Provides summary of the research findings, outlines specific conclusions drawn from both the experimental and analytical efforts and suggests ideas and directions for future research.

*****

Chapter 2

# LITERATURE REVIEW

The purpose of this literature review is to provide background information on the issues to be considered in this thesis and to emphasize the relevance of the present study. This treatise embraces various aspects of plasma spray coatings and particulate filled polymer composites with a special reference to their erosion wear characteristics. This chapter includes reviews of available research reports:

- On Thermal Spraying
- On Plasma Spray Coatings
- On Particulate filled Polymer Composites
- On Glass Micro-Sphere filled Polymer Composites
- On Wear and its Classification
- On Erosion Wear Characteristics of Ceramic Coatings
- On Erosion Wear Characteristics of Polymer Composites
- On Implementation of Design-of-Experiments and Artificial Neural Networks in Wear Analysis

At the end of the chapter a summary of the literature survey and the knowledge gap in the earlier investigations are presented. The specific objectives of the present research work are also outlined.

## 2.1 On Thermal Spraying

Thermal spraying represents a group of widely used surface modification processes for the production of various overlay protective coatings to improve the surface characteristics of engineering and structural components. The origin of the concept of thermal spraying actually dates back to the early part of $20^{th}$ century when a Swiss engineer, Max Schoop and his associates developed a

metal coating by blasting a surface with metal dust. Today it is globally considered as a potential alternative to traditional coating manufacturing techniques such as hard chrome electro-plating and has emerged as an important tool of increasingly sophisticated surface engineering technology to produce a range of protective coatings as well as for restoration of worn parts in engineering components [13-16]. In fact, a large variety of hard materials (including ceramics and cermets) can be deposited on a cold or moderately pre-heated substrate [17, 18], thus obtaining very hard coatings while preventing thermal alteration of the substrate itself (which invariably occurs in other hard facing processes, such as in welding). This is a key requirement when design tolerances must be satisfied, thin-walled components are being considered or heat-sensitive materials (like Al or Mg alloys) are being processed.

Process Fundamentals:

Thermal spraying is a generic term used for processes wherein the deposited layer is developed by melting the material to be coated in a high temperature zone and propelling the molten droplets onto the substrate. In other words, all the variant processes of the thermal spray technique generally involve the following features:

- The coating material to be sprayed is heated in a flame or in an arc so that it is substantially molten.
- The molten material is accelerated in a gas stream and propelled onto the substrate surface to be coated.
- The partially/fully molten particles flatten upon impacting the substrate and subsequently cool and coalesce to yield the desired coating.

A graphical illustration depicting the above sequence of the events leading to the formation of the coating by a thermal spray process is provided in Figure 2.1. The consumable coating material can be in the forms of wire, rod or powder although use of feedstock in the form of spray-grade powders is most popular.

Virtually any material that melts without sublimation can be sprayed. The sprayed coatings are built up layer by layer and, although the desired thickness of the deposit may vary depending upon the application, the protective coatings are typically 100-500 microns thick.

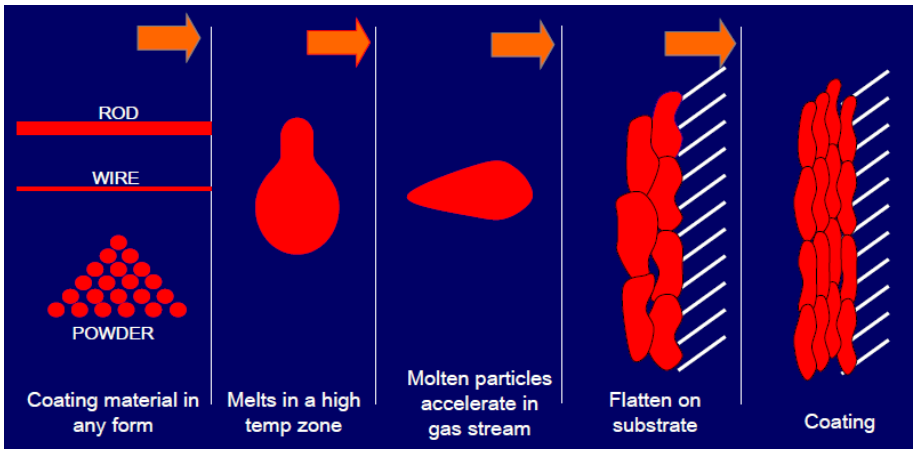


**Figure 2.1** Sequence of events during thermal spraying

Thermal Spray Variants:

On the basis of the heat source employed for melting the feedstock, thermal spraying processes are classified into different categories. Table 2.1 presents the variety of thermal processes, now available for coating purpose, as a consequence of the above advancements in this technology along with their principal characteristics. While the process fundamentals and the surface preparation methods are similar for every variant, each of the processes included in Table 2.1 differs significantly in the manner in which the high temperature zone is generated and consequently, in equipment design.

Applications of Thermal Sprayed Products:

In thermal spraying, due to high flame temperature, typically higher than $5000^0$C, a satisfactory melting state can be achieved, which is beneficial for formation of a dense coating structure. Ceramic coatings produced by thermal spray techniques are increasingly and widely used in these days for a range of industrial applications to provide friction wear and erosion resistance, corrosion

protection and even thermal insulation [19-28]. Oxide ceramics such as alumina, zirconia, titania, chromia, silica and yttria are being widely used as surface coating materials to improve resistance to wear, cavitation, fretting and corrosion [19, 29-33] and in some cases to provide lubrication and thermal insulation [34]. They are especially useful in applications where resistance to wear and corrosion are required simultaneously. It is seen that as far as surface modification of engineering and structural components is concerned, ceramic materials with high hardness, high resistance to thermal and corrosive conditions and relatively low densities offer many advantages over metallic and polymeric materials [19, 35].

**Table 2.1** Principal characteristics and features of important thermal spray variants employing powders as feedstock

| | **Flame** | **Air Plasma** | **Detonation Spray** | **HVOF** | **Cold Spray** |
|---|---|---|---|---|---|
| Feedstock Form | Powder/Wire | Powder | Powder | Powder | Powder |
| Heat Source | Oxy-fuel combustion | Plasma Flame | Controlled Detonation | Oxy-fuel combustion | Resistance heater to preheat gas |
| Flame Temp. ($^0$C) | 3,000-3,500 | 10,000-15,000 | 3,000-3,500 | 3,000-3,500 | No flame; max. gas preheat 600 $^0$C |
| Gas Velocity (m/s) | <300 | 400-500 | 3,000 | 1,500-2,000 | 2,500-3,000 |
| Particle Temp. ($^0$C) | 1,500-2,200 | 2,700-3,500 | 1,500-2,000 | 1,500-2,000 | 400-600 |
| Particle Velocity (m/s) | 50-100 | 100-200 | 600-800 | 600-800 | 800-1000 |

The present day status of thermal spraying as the major means of depositing protective coatings has been the result of the astounding progress made in several allied fields during the past three or four decades. Introduction of plasma torches has been considered to be the most significant development in the field of thermal spraying as it has provided an impetus to the accelerated growth of this technology. The plasma arcs and their variations have been the foundation

of the thermal spray industry for more than two decades and are widely used to obtain a range of protective coatings for numerous industrial applications.

## 2.2 On Plasma Spray Coatings

Plasma: the fourth state of matter

Plasma is considered to be the fourth state of matter, consisting of a mixture of electrons, ions and neutral particles, although overall it is electrically neutral. Most simply, plasma may be defined as nothing but a partially ionized state of gas. The degree of ionization of a plasma is the proportion of atoms that have lost (or gained) electrons and in the case of thermal plasmas, this is controlled mostly by temperature. Plasma technology involves the creation of a sustained electric arc by the passage of electric current through a gas in a process referred to as electrical breakdown. Because of the electrical resistivity across the system, significant heat is generated, which strips away electrons from the gas molecules resulting in an ionized gas stream known as *plasma*. At about $2000^0$C, gas molecules dissociate into the atomic state and when the temperature is raised to about $3000^0$C, gas molecules lose electrons and become ionized. In this state, gas has a liquid-like viscosity at atmospheric pressure and the free electric charges confer relatively high electrical conductivities that can approach those of metals [36]. A non-transferred DC arc plasma has been conventionally used for coating purposes and is most widely employed in the thermal spray industries.

Plasma spray coating:

Plasma spray coating technique utilizes the exotic properties of the plasma medium to effect physical, chemical or metallurgical reactions to produce metallic and ceramic coatings for a variety of applications. Plasma spray coating is an economical and effective surface modification method applied to various machine parts to reduce degradation. It is gaining importance in many critical areas of application due to the fact that it provides increased design flexibility and its high deposition rate, so that the parts made up from a combination of

materials with widely differing physical and chemical properties could be employed [37, 38]. Plasma sprayed ceramic coatings have been widely used for machine parts as well as in structural applications in order to improve resistance to wear, corrosion, oxidation and heat flow [39-44]. In plasma spraying, a coated layer is formed on a substrate surface by spraying melted powders on to the substrate at a high speed using a high-temperature plasma heat source. The microstructure and properties of plasma sprayed coatings depend on the design of the plasma torch, the operating parameters including torch input power, plasma forming gases and flow rates, spray distance, feedstock composition, feed rate and injection parameters etc.

Plasma sprayed coatings are produced by introducing powder particles of the feedstock material into a plasma jet, which melts them and propels towards the substrate. The formation of a coating depends on the interaction between a droplet and the substrate or the previously deposited layers, i.e. spreading of a droplet, the formation of a splat (lamella) and its solidification. The difference in the degree of a splat flattening results in the difference in porosity and its shape as well as distribution and these factors could affect also the bonding between lamellae. A schematic diagram of plasma spray process is shown in Figure 2.2.

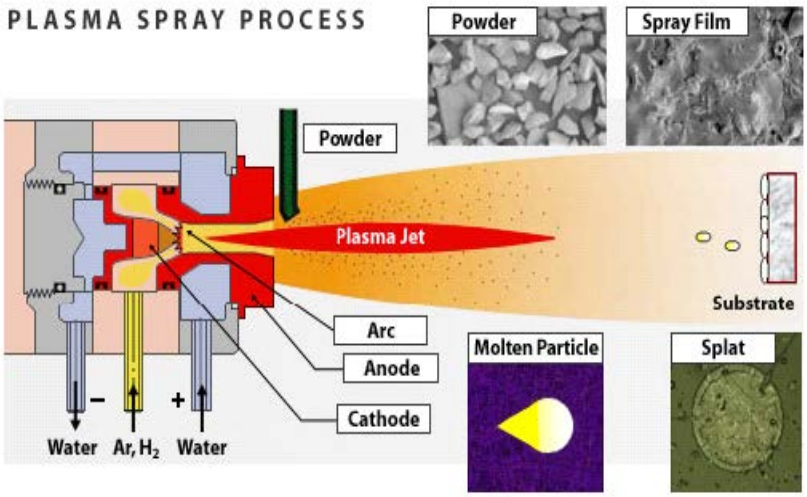


**Figure 2.2** Conventional plasma spraying process

Plasma spray set-up:

An arc is created between tungsten tipped copper cathode and an annular copper anode (both water cooled). The plasma generating gas is forced to pass through the annular space between the electrodes. While passing through the arc, the gas undergoes ionization in the high temperature environment resulting plasma. The ionization is achieved by collisions of electrons of the arc with the neutral molecules of the gas. The plasma protrudes out of the electrode encasement in the form of a flame. The consumable material, in the powdered form, is poured into the flame in metered quantity. The powder melts immediately and absorbs the momentum of the expanding gas and rushes towards the target to form a thin deposited layer. The next layer deposits onto the first one immediately after the deposition of first layer and thus the coating builds up layer by layer [8, 2, 45, 46]. The temperature in the plasma arc can be as high as $10{,}000^{0}$C. Elaborate cooling arrangement is required to protect the plasmatron (i.e., the plasma generator) from excessive heating.

A typical plasma spraying equipment consists of the following modules [47]:

1. The Plasmatron
2. The Power Supply Unit
3. The Powder Feeder
4. The Coolant Water Supply Unit
5. The Control Unit

Process parameters in plasma spraying

In plasma spraying one has to deal with a lot of process parameters, which determine the degree of particle melting, adhesion strength and deposition efficiency of the powder [48]. An elaborate listing of these parameters and their effects are reported in the literature [49-51]. Some important parameters are arc power, plasma gas, carrier gas, mass flow rate of powder, torch to base distance, spraying angle, substrate cooling, powder related variables, preheating of the substrate, angle of powder injection etc.

The requirements for plasma spraying

1. *Roughness of the Substrate Surface***:** A rough surface provides a good coating adhesion and enough room for anchorage of the splats facilitating bonding through mechanical inter-locking.

2. *Cleanliness of the Substrates***:** The substrate to be sprayed on must be free from any dirt or grease or any other material that might prevent intimate contact of the splat and the substrate. For this purpose the substrate must be thoroughly cleaned (ultrasonically, if possible) with a solvent before spraying.

3. *Bond Coat:* Materials like ceramic are normally not sprayed directly onto metals, owing to a large difference between their thermal expansion coefficients (α). So bond coat is required for these types of coatings. For example, in wear related applications, an alumina and Ni-Al top and bond coats combination can be used [52]. In thermal barrier applications, CoCrAlY or Ni-Al bond coat and zirconia top coat are popular [53].

4. *Cooling Water:* For cooling purpose distilled water should be used, whenever possible. Normally a small volume of distilled water is re-circulated into the gun and it is cooled by an external water supply from a large tank. Sometime water from a large external tank is pumped directly into the gun [47].

## 2.3 On Particulate filled Polymer Composites

Composites are combinations of two materials in which one of the materials, called the reinforcing phase, is in the form of fiber sheets or particles and are embedded in the other material called the matrix phase. The primary functions of the matrix are to transfer stresses between the reinforcing fibers/particles and to protect them from mechanical and/or environmental damage whereas the

presence of fibers/particles in a composite improves its mechanical properties such as strength, stiffness etc.

Most commonly used matrix materials are polymeric in nature. The reasons for this are two-fold. In general the mechanical properties of polymers are inadequate for many structural purposes. In particular their strength and stiffness are low compared to metals and ceramics. These difficulties are overcome by reinforcing other suitable materials with polymers. Secondly, the processing of polymer matrix composites need not involve high pressure and does not require high temperature. Also equipment required for manufacturing polymer matrix composites are simpler. Broadly, polymer composites can be classified into two groups on the basis of reinforcing material: Fiber Reinforced Polymer (FRP) and Particle Reinforced Polymer (PRP).

Particles used for reinforcing include ceramics, small mineral particles, metal powders such as aluminium and amorphous materials, including polymers and carbon black. Particulate filled polymer composites have been used extensively in various fields due to their low production cost and the ease with which they can be formed into complex shapes. Besides, they behave almost isotropically and are not as sensitive as long fiber composites to the mismatch of thermal expansion between the matrix and the reinforcement [54, 55]. Generally, particulate fillers are used in polymers for a variety of reasons such as cost reduction, improved processing, density control, optical effects, thermal conductivity, modified electrical and magnetic properties, flame retardancy, improved hardness and wear resistance.

Hard particulate fillers consisting of ceramic or metal particles and fiber-fillers made of glass are being used these days to improve the performance of polymer composites to a reasonable extent [56]. Various kinds of polymers and their composites filled with metal particles have a wide range of industrial applications such as heaters, electrodes [57], composites with thermal durability at high temperature etc. [58]. Similarly, ceramic filled polymer composites have

also been the subject of extensive research in last two decades. When silica particles are added into a polymer matrix, they play an important role in improving electrical, mechanical and thermal properties of the composites [5, 6]. The mechanical properties of particulate filled polymer composites are known to be dependent strongly on the particle size, particle-matrix interface adhesion and particle loading. In this regard, Sumita et al. [59] underlined the interest of replacing micro-scale silica by its nano-scale counterpart, since silica nanoparticles possess superior mechanical properties. Smaller particle size yields higher fracture toughness also for calcium carbonate filled high density polyethylene [60]. Similarly, epoxy filled with smaller alumina trihydrate particles shows higher fracture toughness [61]. Thus, particle size is being reduced rapidly and many recent studies have focused on how single-particle size affects mechanical properties [62-68]. Yamamoto et al. [69] reported that the structure and shape of silica particle have significant effects on the mechanical properties such as fatigue resistance, tensile and fracture properties. Nakamura et al. [70-72] discussed the effects of size and shape of silica particle on the strength and fracture toughness based on particle-matrix adhesion and also found an increase in the flexural and tensile strength as specific surface area of particles increased. Pukanszky et al. [73] highlighted the mechanisms of interfacial interactions in particulate filled composites. Nicolais and Nicodemo [74] studied the effect of particle shape on tensile properties of glassy thermoplastic composites. While most of these investigations have focused either on the particle shape or on particle size, the study made by Patnaik et al. [75] reported that the mechanical properties of polyester based hybrid composites are highly influenced also by the type and content of the filler materials.

Lauke and Fu [76] developed a theoretical model for the fracture toughness of particulate/polymer composites by considering a simple geometrical model of particle-particle interaction in a regular particle arrangement. They also discussed the influence of structural properties such as particle volume fraction

and matrix mechanical properties on fracture toughness. Jerabek et al. [77] studied filler/matrix-debonding and micro-mechanisms of deformation in particulate filled polypropylene composites under tension.

Padhi and Satapathy [78, 79] reported on processing, characterization and wear analysis of short glass fiber-reinforced polypropylene composites filled with blast furnace slag particles. They also predicted and simulated the erosion wear behavior of these composites. Tagliavia et al. [80] made an analysis of flexural properties of composites filled with hollow particles. They studied the flexural properties of hollow-glass particle filled vinyl ester composites, which are used in marine applications. Weidenfeller et al. [81] made a detailed study on cooling behavior of particle filled polypropylene composites during injection molding process. Hassan et al. [82] studied morphological and mechanical properties of carbonized waste maize stalk as reinforcement for eco-composites. Omar et al. [83] investigated on the particle size dependence on the static and dynamic compression properties of polypropylene/silica composites.

Thermal behaviour of various particulate filled composites has also been reported by researchers in the past. Nayak et al. [84] conducted a computational and experimental investigation on thermal conductivity of particle reinforced epoxy composites. Bishay et al. [85] studied the electrical, mechanical and thermal properties of polyvinyl-chloride (PVC) composites filled with aluminium powder. Agrawal and Satapathy [86] developed a heat conduction model and investigated on thermal conductivity enhancement of AlN/epoxy composites. They further investigated thermal and dielectric properties of polymers (epoxy and polypropylene) reinforced with micro-sized AlN particles [87]. Their results show that incorporation of AlN in both the resin increases the effective thermal conductivity and glass transition temperature whereas coefficient of thermal expansion of composite decreases favorably. The dielectric constant of the composite also found to get modified with filler content.

## 2.4 On Glass Micro-sphere filled Polymer Composites

Spherical glass beads are being used in many industries, due to certain advantages such as strong filling ability, smooth spherical surface, small and well distributed internal stress in the products and good processibility of the filled materials. Studies on the structure-property correlation of glass micro-sphere filled polymers have been made by several researchers over the past 20 years [88-94]. Even then, thermal, mechanical and tribological behaviour of such composites has remained a relatively less studied area. Glass micro-spheres are being used commercially with various resin matrices, both thermoplastics and thermosets, to improve the physical and mechanical properties of the resins [95]. Among the mechanical properties, hardness, modulus of elasticity and fracture toughness are known to be improved with the incorporation of glass micro-spheres in brittle resin matrices [96-98]. The tensile strength and ductility (elongation to break), on the other hand, decreases with the increase in filler volume fraction [99, 100]. Glass micro-spheres are preferred as fillers especially when composite properties such as isotropy or low melt viscosity are important. They are considered to be a reinforcement which does not create a source of stress concentration in the matrix unlike other long fibers which have sharp edges leading to stress generation in the matrix and in turn early failure of the composites.

Sahu and Broutman [89] have studied in considerable detail the mechanical and fracture properties of glass sphere filled epoxy and polyester resins with various particle-matrix interface conditions. Mallick and Broutman [93] presented a possible explanation for the strength behaviour of glass micro-sphere filled brittle resin composites and described the flexural, compressive and fracture properties of brittle epoxy matrix composite containing glass beads of 15 micron average particle size.

Few research works have also been reported recently on glass micro-sphere filled thermoplastics and concept of linear elastic fracture mechanics (LEFM)

has been widely employed to study the fracture toughness of such thermoplastic composites [94-98]. Sanchez-Soto et al. [99] analyzed the fracture behaviour of a material model composed of polysterene and solid glass beads and found out that small quantities of glass beads are enough to modify polystyrene fracture behaviour changing the propagation mode, which tends to stabilize as more quantity of beads are added to the matrix. Faulkner and Schmidt [101] studied the rheological and mechanical properties of glass bead filled polypropylene (PP) composites and noted that the relative tensile modulus and relative flexural modulus were both linear functions of bead fraction. Lepez et al. [102] carried out thermo-rheological analysis of glass micro-sphere filled high density polyethylene (HDPE) and polystyrene (PS) melts and proposed a new empirical model that allowed the prediction of complex viscosity of the composite melts. Ou and Yu [103] investigated the effects of the interfacial adhesion on the micro-damage and the rheological behaviour of glass bead filled nylon. Li et al. [104] analyzed the dynamic and mechanical properties of glass micro-sphere filled low density polyethylene composites using a dynamic mechanical analyser. Lee and Yee [105] investigated the major energy dissipation mechanisms of glass micro-sphere filled epoxies based on the previously established knowledge about the micro-mechanical deformations occurring during the fracture.

Liang [106, 107] gave an insight about the tensile and flexural properties of hollow glass micro-sphere (HGM) filled acrylonitrile-butadiene-styrene (ABS) and polyvinyl-chloride (PVC) composites. Gupta et al. [80, 108] compared the tensile and compressive characteristics of vinyl-ester/glass-microballoon syntactic foams and also did a microscopic examination of their compressive fracture features. They also analyzed the flexural and compressive properties of hollow-particle filled composites and found a similar kind of observation [109]. Hollow glass micro-spheres have low density and so they reduce the weight of the composites to a great extent, but according to Kim and Khamis [110], their addition tends to reduce the Young's modulus and ultimate strength of the

composites. Even specific values of flexural stiffness are only marginally increased for high volume fractions of spheres but this difficulty can be overcome by using rigid inorganic particles; so solid glass micro-sphere might serve as a good alternative. Ferreira et al. [111] investigated the effects of hollow glass micro-sphere filled hybrid composites and studied on the addition of short fiber reinforcements on the mechanical behaviour of epoxy composites. In a recent study, Kushvaha and Tippur [112] investigated the effects of filler shape (characterized by the aspect ratio), filler volume fraction and loading rate on fracture toughness of glass-epoxy composites.

Few works have also been reported in the past on the thermal and electrical behaviour of glass micro-sphere filled polymers. Yung et al. [113] and Zhu et al. [114] investigated the thermal, mechanical as well as the dielectric properties of such HGM filled composites and concluded that the properties of composites are mainly dependent on the characteristics of HGMs. Liang [115] estimated the thermal conductivity for polypropylene/hollow glass bead composites and found that the estimated and measured thermal conductivity decreased roughly linearly with increasing the HGM volume fraction. Recently Mishra and Satapathy [116] have developed a theoretical model and proposed a correlation to estimate the effective thermal conductivity of micro-sphere filled polymers. They have also reported extensively on thermal properties of glass micro-spheres filled epoxy composites [117].

## 2.5 On Wear and its Classification

Wear is the process occurring at the interfaces between interacting bodies and is usually hidden from investigators by the wearing components. However, this obstacle has been gradually overcome by scientists, revealing an intricate world of various wear modes and mechanisms. The widest definition of wear, which has been recognized for at least 50 years, includes the loss of material from a surface, transfer of material from one surface to another or movement of material within a single surface [4]. Although a narrower definition of wear has

been proposed as 'progressive loss of substances from the operating surface of a body occurring as a result of relative motion at the surface [118], the wide range of engineering applications of concern to the tribologists is served better by a broader definition. A simple and useful statement is that wear is 'damage to a solid surface, generally involving progressive loss of material, due to relative motion between that surface and a contacting substance or substances' [7]. This includes:

1. Degradation by the displacement of material within the surface (leading to changes in surface topography without loss of material), as well as the more usual case of material removal,

2. The wear processes common in machines in which one surface slides or rolls against another, either with or without the presence of a deliberately applied lubricant, and

3. The more specialized types of wear which occur when the surface is abraded by hard particles moving across it, or is eroded by solid particles or liquid drops striking it or by the collapse of cavitation bubbles in a liquid.

This definition, quite deliberately tells nothing about the mechanisms by which the degradation takes place. These may be purely mechanical, for example involving plastic deformation or brittle fracture or they may involve significant chemical aspects, like oxidation of a metal or hydration of a ceramic; in many practical cases, both chemical and mechanical processes play a role [10].

A fundamental scheme to classify wear was first outlined by Burwell and Strang [119]. Later, Burwell [120] modified the classification to include five distinct types of wear, namely:

1. Abrasive wear: Abrasive wear or abrasion is generally defined as the wear that is caused by the displacement of material from a solid surface due to hard particles sliding along the surface and cutting grooves on the softer surfaces. It accounts for most of the failures in practice. This hard material

may originate from one of the two surfaces, rubbing against each other. In sliding mechanisms, abrasion can arise from the existing asperities on one surface (if it is harder than the other), from the generation of wear fragments which are repeatedly deformed and hence get work hardened or oxidized until they become harder than either or both of the sliding surfaces or from the adventitious entry of hard particles, such as dirt from outside the system.

2. Adhesive wear: Adhesive wear can be defined as wear due to localized bonding between contacting solid surfaces leading to material transfer between the two surfaces or the loss from either surface. For adhesive wear to occur, it is necessary for the surfaces to be in intimate contact with each other. Surfaces, which are held apart by lubricating films, oxide films etc. reduce the tendency for adhesion to occur.

3. Surface fatigue: Wear of a solid surface can also be caused by fracture arising from material fatigue. The term 'fatigue' is broadly applied to the failure phenomenon where a solid is subjected to cyclic loading involving tension and compression above a certain critical stress. Repeated loading causes the generation of micro-cracks, usually below the surface, at the site of a pre-existing point of weakness. On subsequent loading and unloading, the micro-crack propagates. Once the crack reaches the critical size, it changes its direction to emerge at the surface and thus flat sheet like particles is detached during wearing. The number of stress cycles required to cause such failure decreases as the corresponding magnitude of stress increases. Vibration is a common cause of fatigue wear.

4. Corrosive wear: Most metals are thermodynamically unstable in air and react with oxygen to form an oxide, which usually develop layer or scales on the surface of metal or alloys when their interfacial bonds are poor. Corrosion wear is the gradual eating away or deterioration of unprotected metal surfaces by the effects of the atmosphere, acids, gases, alkalis etc. This

type of wear creates pits and perforations and may eventually dissolve metal parts.

5. Erosive wear: In tribology, erosive wear can be defined as the progressive loss of original material from a solid surface due to mechanical interaction between that surface and a fluid, a multi-component fluid or impinging liquid or solid particles. Like all kinds of wear, erosion also causes significant damage in many machine parts. When the angle of impingement is small, the wear produced is closely analogous to abrasion.

## 2.6 On Erosion Wear Characteristics of Ceramic Coatings

Many industrial processes make use of plasma sprayed ceramic coatings, whose reproducibility is good, once the optimal set of spray parameters has been found. Hard ceramic coatings produced by plasma spraying or by other techniques are being increasingly employed in wear related applications and therefore the wear behaviour of such ceramic coatings has emerged as an area for extensive research in last few decades [121-123]. Much research related to the basic wear mechanisms of plasma sprayed oxides exists, since such coatings have been studied for a long time [30, 124-126]. There exists a few works on comparing them to the characteristics of other thermally sprayed wear resistant coatings, electroplating and nickel electroless plating as well [127, 128]. Furthermore, to fully assess the industrial applicability of thermally sprayed coatings in general and of plasma sprayed coatings in particular, wear maps should be experimentally obtained and it is currently being done for massive sintered ceramics [129-131]. Today a variety of materials, e.g., carbides, oxides, metallic etc. belonging to the above category are available commercially. The wear resistant coatings can be broadly classified into the following categories [2]:

- Carbides: WC, TiC, SiC, ZrC, $Cr_2C_3$ etc.
- Oxides: $Al_2O_3$, $Cr_2O_3$, $TiO_2$, $ZrO_2$ etc.
- Metallic: NiCrAlY, Triballoy etc.
- Diamond

As already mentioned, plasma sprayed coatings are being used now a days as erosion resistant coatings in a wide variety of applications [40, 132-134]. Extensive research shows that the deposition parameters like energy input to the plasma and the powder properties affect the porosity, splat size, phase composition, coating hardness etc. [29, 135-141]. These in turn, have an influence on the erosion wear resistance of the coatings. Quantitative studies of the combined erosive effect of repeated impacts are very useful in predicting component lifetimes, in comparing the performance of materials and also in understanding the underlying damage mechanisms involved.

It is well known that resistance of engineering components encountering the attack of erosive environments during operation can be improved by applying hard ceramic coatings on their surfaces. Alonso et al. [142] experimented with the production of plasma sprayed erosion-resistant coatings on carbon-fiber-epoxy composites and studied their erosion behaviour. The microstructure and properties of these coatings were studied and their erosion characteristics were determined experimentally in an erosion-testing device. Tabakoff and Shanov [143] designed a high temperature erosion test facility to obtain erosion data in the range of operating temperatures experienced in compressors and turbines. In addition to the high temperatures, this facility properly simulates all the erosion parameters important from the aerodynamic point of view. These include particle velocity, angle of impact, particle size, particle concentration and sample size.

Kulu et al. [144-147] have carried out significant research in the field of erosion resistant coatings and have reported that under extreme conditions (high hardness and strength of erodents, high velocity and pressure, cyclic impact load, elevated temperatures etc.) solid particle erosion (SPE) is a serious problem for many industrial equipment. Response of a material to SPE is a complex function of the physical properties of the target, the impacting particles and the erosive environment [148]. Many erosion mechanisms have been proposed in the past

and have been supported by the experimental data from erosion tests. Various models for the erosion of bulk metals, glass and ceramics have also been proposed [149] usually considering different combinations of micro-cutting, plastic deformation, melting, fatigue and fracture mechanisms [150]. According to Finnie and McFadden [151], there are four principal factors that influence the erosion behaviour of a material: the erodent velocity and particle size, the impact angle and the properties of the eroded material.

Few reports are available in the existing literature on erosion behaviour of alumina coatings. The resistance to erosion of such coatings depends upon inter-splat cohesion, shape, size and hardness of erodent particles, particle velocity, angle of impact and the presence of cracks and pores [29, 152-155]. The slurry and particle erosion response of flame sprayed alumina coatings have also been reported in the literature [156]. It is seen that high particle velocity enhances the erosion rate and the erosion rate reaches a maximum for an impact angle of $90^0$. The loss of material is by the progressive removal of splats and can be attributed to the presence of defects and pores in the inter-splat regions within the coating. Similar observations have also been reported for the plasma sprayed alumina coatings subjected to an erosive wear caused by the $SiO_2$ particles [157].

Branco et al. [158] examined the room temperature solid particle erosion of zirconia and alumina based ceramic coatings with different levels of porosity and varying microstructure and mechanical properties. The erosion tests were carried out by a stream of alumina particles with an average size of 50 μm at a velocity of 70 m/s, carried by an air jet with impingement angle of $90^0$. The results of this study indicated that there is a strong relationship between the erosion rate and the coating porosity. Similarly, Mishra et al. [159] investigated the erosion characteristics of plasma sprayed alumina-titania coating deposited on mild steel substrates. They reported that the erosion wear rate varied with the erodent dose, the angle of impact, erodent velocity, stand-off distance and also

with the erodent size. This study revealed that premixing of titania in alumina significantly improves the resistance of the coating to solid particle erosion.

Ercenk et al. [160] studied the effects of impingement angle and SiC reinforcement on the erosion wear behavior of basalt based glass and glass-ceramic coatings. Erosion tests were realized by using corundum media at the different impingement angles and velocities. The test results showed that the addition of SiC in the basalt based coatings resulted in enhancement of erosive wear resistance of glass and glass-ceramic coatings. Krishnamurthy et al. [161] examined the solid particle erosion behavior of plasma sprayed alumina and calcia-stabilized zirconia coatings on Al-6061 substrate. Satapathy [3] carried out an extensive research on erosion wear behaviour of plasma sprayed red mud coatings under different test conditions. This study revealed that impact velocity and the impingement angle are the significant factors that influence the erosion rate of the coatings to a great extent. Subsequently, Sahu et al. [162] performed tribo-performance analysis of plasma sprayed fly ash-aluminum coatings using experimental design and artificial neural network. These coatings exhibit improved resistance to solid particle erosion when the fly ash is premixed with aluminum powder prior to the coating deposition.

Different models have been proposed that allow estimation of the stresses that a moving particle will impose on a target during erosion [163]. It has been experimentally observed by many investigators that during the impact, the target can be locally scratched, extruded, melted and/or cracked in different ways [164-166]. The imposed surface damage will vary with the target material, erodent particle, impact angle, erosion time, particle velocity, temperature and atmosphere [164, 167]. Over the years, the state of the information on solid particle erosion of metals and coatings has been reviewed time to time by Kosel [12], Tilly [164], Engel [168], Preece and Macmillan [169], Hutchings [170], Finnie et al. [171], Ruff and Wiederhom [172], Shewmon and Sundararajan [173], Sundararajan [174], Levy [175] and many others [27, 32, 40, 176-184].

## 2.7 On Erosion Wear Characteristics of Polymer Composites

Polymer composites acquire an important place when it comes to operating in a dusty environment where resistance to erosion becomes a prime requirement. The subject of erosion wear of polymer composites has been receiving substantial research attention since past few decades. Interest in this area is commensurate with the increasing utilization of composites in aerospace, transportation and process industries, in which they can be subjected to multiple solid or liquid particle impacts. Some examples of these applications are pipe lines carrying sand slurries in petroleum refining, helicopter rotor blades [185, 186], pump impeller blades, high speed vehicles and aircrafts operating in desert environments, water turbines, aircraft engines [187], missile components, canopies, radomes, wind screens [188] and outer space applications [189]. Differences in erosion behavior of various types of polymer composites are caused by the amount, type, orientation and properties of the reinforcement on the one hand and by the type and properties of the matrix and its adhesion to the fibers/fillers on the other [190].

Erosion studies have been conducted in the past for a variety of reasons and an exhaustive database regarding the effect of impact related (impact velocity and impingement angle), particle related (hardness, size and shape) and material related (hardness, ductility and microstructure) variables on the erosion behavior of metals and alloys is already available in the literature. Many have attempted to correlate the erosion rate with such variables. Finnie [149], after 40 years of involvement with erosion research, presented an article in 1995 on the past and the future of erosion. In this article, the influencing parameters and dominating mechanisms during solid particle erosion are reviewed for metals and ceramics. In the same year, another article was published by Meng and Ludema [191] providing information about the existing wear models and prediction equations. This article is more general as it discussed all the frictional phenomena termed to ‘wear’ including also the solid particle erosion. Friedrich et al. [192], in the year 2002, reported in detail, on wear of polymer composites including SPE. The

material removal during erosion is dependent on many inter-related factors that include the properties and structures of the target material, the macro/micro-exposure conditions and the physical/chemical characteristics of the erodent particles. The combination of all these factors results in erosion rates those are peculiar to specific sets of conditions. In general, various factors, which influence the erosive wear performance of polymers and their composites, are shown in Figure 2.3.

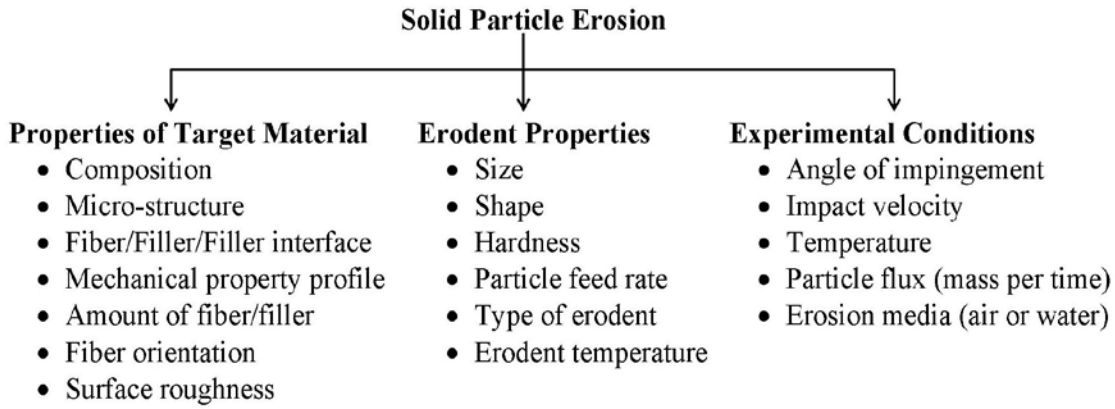


**Figure 2.3** Factors affecting erosive wear of polymers and composites

The erosion wear rates of the composites are found to be dependent on the impact velocity and impingement angle. Similarly, the type and physical characteristics of the erodent material play a key role in the erosion problem. Variations in erodent particle size and shape can cause fundamental changes in the erosion response of polymer composites. Transitions in wear mechanisms can often be attributed to a change in the shape, hardness or size of the erodents [193, 194]. If the eroding particles are blunt or spherical, then plastic deformation is favored. On the other hand, if the particles are sharp then cutting and brittle fragmentation are more likely.

The erodent fracture toughness may influence the erosive procedure if fragmentation of the erodent occurs during impact [195]. Moreover, when the erodent particles are at an elevated temperature (higher than the target surface temperature), they also dissipate a part of their thermal energy in addition to the

kinetic energy to the target material causing greater damage to the surface. Biswas and Satapathy [4] have reported extensively on the effect of erodent temperature on the erosion wear of a variety of epoxy based composites. The particle feed rate (i.e., the mass of impacting material per unit area per unit time) is another controlling parameter of the erosive wear rate.

The effects of experiment related parameters (impingement angle, impact velocity, erodent type, size, shape and hardness) and target related properties (strength, ductility, crystallinity, cross-link density, reinforcement content and arrangement) on the solid particle erosion have been reviewed by Barkoula and Karger-Kocsis [10]. Many researchers have evaluated the resistance of various types of polymers and their composites to SPE. The erosive wear behavior of fiber reinforced polymer (FRP) composite systems as a function of fiber content has been studied in the past [196-199]. Miyazaki et al. [196, 197] have examined the effect of fiber inclusion on the erosion behaviour by comparing erosion rate of an FRP with that of neat resin. Tilly and Sage [198] have also investigated the influence of erodent velocity, impact angle, particle size and weight of impacted abrasive for nylon, carbon fiber reinforced nylon and epoxy resin, polypropylene and glass fiber reinforced plastic. A crucial parameter for the design with composites is the fiber content, as it controls the mechanical and thermo-mechanical responses. Nevertheless, no definite rule is available to describe how the fiber content affects the erosion resistance of a composite. In this regard, an analytical approach was presented by Hovis et al. [199] which presumed that the erosion resistance of the multiphase material depends on the individual resistances of its constituents.

It is well known that the erosive wear of fiber reinforced polymer composites is usually higher than that of the unreinforced polymer matrix. It has also been reported that short fiber reinforced composites show a better resistance to erosion compared to unidirectional fiber reinforced composites. Hence different arrangements of fiber used for reinforcement in polymers, has got much

influence on the erosion behavior and performance. Erosion characteristics of polymers that have been reported in the literature include polystyrene [200], polypropylene [194, 201, 202], nylon [203], polyethylene [204], ultra high molecular weight polyethylene [205], poly-ether-ether-ketone [206, 207], polycarbonate and poly-methyl-methacrylate [208], epoxy [209-219], polyester [220], bismileimide [221], elastomers [222-224], rubber [225], polyurethane [226], polyaryletherketone [227], polyester [228-233], polyphenylenesulphide (PPS) [234, 235], polyetherimide [236-239], vinyl ester [240] and ABS/Polyamide6 [241]. Harsha et al. [227] reported the influence of impingement angles and impact velocities on solid particle erosion of various poly-aryl-ether-ketones and their composites with short fiber reinforcement. In another investigation, Barkoula and Karger-Kocsis [202] studied the effects of fiber content and relative fiber orientation on the SPE of glass fiber/polypropylene composites. A study by Tewari et al. [218] on the influence of impingement angle and fiber orientation concludes that unidirectional carbon and glass fiber reinforced epoxy composites show semi-ductile erosion behavior, with the maximum erosion rate occurring at $60^0$. In another study, Arjula and Harsha [242] have discussed the usefulness of the erosion efficiency parameter to identify various mechanisms in SPE. Few publications by Patnaik et al. [228-233] on erosion wear characteristics of glass-polyester composites filled with different particulate fillers suggest that in such hybrid composites, the rate of material loss due to SPE reduce significantly with the addition of hard particulate fillers into the matrix. This improvement in the wear resistance depends on both the type and the content of filler. They have also reviewed extensively on SPE wear characteristics of fiber and particulate filled polymer composites [11]. Panda et al. [243] studied the erosive wear analysis of glass fiber–epoxy reinforced AlN hybrid composites and more recently, Kaundal [190] made a critical review on role of process variables on the SPE of polymer composites.

Mohan et al. [244] analyzed the effect of incorporation of tungsten carbide (WC) powders on erosive wear behaviour in glass fabric-epoxy (G-E) composites. They also analyzed and discussed the results of erosive wear losses, impact angle, impact velocity and erosion rate of filled and unfilled G-E composites. The WC filled G-E composite exhibited a lower erosion rate as compared to that of unfilled ones. Bagci and Imrek [219] studied solid particle erosion behavior of a new composite material formed by adding boric acid particles to glass fibers and epoxy resin. Friction and wear behavior of the polyimide composites at elevated temperature under sliding and erosive conditions has been investigated by Zhao et al. [245]. Zhang et al. [246] investigated on the erosion characteristics of molded carbon fiber composites by sand erosion test using silica particles. They used finite element simulations of the particle erosion experiments, although highly simplified, to provide qualitative insight regarding the underlying mechanisms. Recently, Padhi and Satapathy [79, 247] have also reported on the erosion behaviour of blast furnace slag filled epoxy composites with and without glass fiber reinforcement. Besides, many other investigators have also reported extensively on responses of epoxy and PP based composites to erosive as well as other wear modes [201, 202, 248-251].

## 2.8 On Implementation of Design-of-Experiments and Artificial Neural Networks in Wear Analysis

Statistical methods have commonly been used for analysis, prediction and/or optimization of a number of engineering processes. Such methods enable the user to define and study the effect of every single condition possible in an experiment where numerous factors are involved. Solid particle erosion, for example, is a complex wear phenomenon in which a number of control factors collectively determine the performance output i.e. the erosion rate and there is enormous scope in it for implementation of appropriate statistical techniques for process optimization. But unfortunately, such studies have not been adequately reported so far. As already mentioned, wear processes in heterogeneous material systems like coatings and composites are complex phenomena involving a

number of operating variables and it is essential to understand how the wear characteristics are affected by different operating conditions. Although a large number of researchers have reported on properties, performance and wear characteristics of coatings and composites, neither the optimization of wear processes nor the influence of process parameters on wear rate has adequately been studied yet. Selecting the appropriate operating conditions is always a major concern as traditional experiment design would require many experimental runs to achieve satisfactory result. In any experimental research, since test procedures are generally expensive and time consuming, the need to satisfy the design objectives with the minimum possible number of tests is clearly an important requirement. In this context, Taguchi method suggested by Taguchi and Konishi [252, 253] provides the designer with a systematic and efficient approach for experimentation to determine near optimum settings of design parameters in terms of performance, time and cost. This method involves laying out the test conditions using specially constructed tables known as 'orthogonal arrays'.

Design-of-experiments (DOE) is a powerful analysis tool for modeling and analyzing the effect of control factors on performance output. During an experimental trial involving a number of process variables, the number of test runs required for full factorial design increases geometrically whereas the fractional factorial design is efficient and significantly reduces the time. This method is popular because of its simplicity, but this very simplicity has often led to unreliable results and inadequate conclusions. The fractional design might not contain the best design point. Moreover, the traditional multi-factorial experimental design is the *change one factor at a time* method. Under this method only one factor is varied, while all other factors are kept fixed at a specific set of conditions. To overcome these problems, Taguchi and Konishi [252] advocated the use of orthogonal arrays and Taguchi [253] devised a new experimental design that applied signal-to-noise ratio with orthogonal arrays to the robust design of products and processes. In this procedure, the effect of a factor is measured by average results and therefore, the experimental results can be reproducible.

This inexpensive and easy-to-operate experimental strategy based on Taguchi's parameter design has been adopted to study the effect of various parameters and their interactions in a number of engineering processes [254-259]. Phadke [254], Wu and Moore [255] and others [256-259] have applied this method to design various products and process parameters. Mahapatra et al. [260-263] have made optimization of parameter combinations in wire electrical discharge machining using this method. Patnaik et al. [228-230, 232, 264, 265] have also successfully employed this in erosion wear analysis of polymer composites. Pang et al. [266] introduced the application of Taguchi optimization methodology in optimizing the cutting parameters of end-milling process for machining the halloysite nanotubes (HNTs) with aluminium reinforced epoxy hybrid composite material under dry condition. Rubio et al. [267] reported the use of Taguchi's method in order to identify the best drilling setup of glass reinforced polyamide. They analyzed the effect of tool geometry, spindle speed and feed rate etc. on the thrust force, hole mean diameter and circularity error. Ramesh and Suresha [268] optimized the tribological parameters in abrasive wear of carbon-epoxy hybrid composites using Taguchi's orthogonal array. Vankanti and Ganta [269] optimized the process parameters namely, cutting speed, feed, point angle and chisel edge width in drilling of glass fiber reinforced polymer (GFRP) composites. Sahu et al. [162] have also made a tribo-performance analysis of plasma sprayed fly-ash/aluminium coatings using Taguchi's experimental design.

Artificial neural network (ANN), a technique inspired by the biological neural system has already been implemented to solve a wide variety of problems in diverse fields [270]. It was developed to simulate the strong learning, clustering and reasoning capacity of biological neurons. Using a well-trained ANN model, one can estimate predictive performance, pattern association and pattern classification. As aforementioned, the wear process is a complicated phenomenon lacking adequate mathematical description and therefore, a powerful method that combines the ANN technique and the Taguchi's design is proposed by many authors for better analysis and prediction of wear performance.

This proposed approach not only yields sufficient understanding of the effects of process parameters, but also produces an optimal parameter setting to ensure that the materials exhibit the best wear performance characteristics. The details of this ANN approach have been well documented by Kartalopoulos [270]. Zang and Friedrich [271] also made a detailed review on application of ANN to polymer composites whereas Kadi [272] made a review on modeling aspect of mechanical behavior of fiber-reinforced polymer composites. While Jiang et al. [273] have made a prediction on wear properties of composites, Gyurova et al. [274] have developed a model on the sliding wear and friction properties of polyphenylene sulfide composites using artificial neural networks. ANN has been suitably applied on wear analysis of different materials like polyamide 66 by Abdelbary et al. [275], $TiO_2$ reinforced polyester composites by Satapathy et al. [276] and pine wood dust filled epoxy composites by Kranthi and Satapathy [277], while Gyurova [278] made a detailed study on preliminary investigation of neural network techniques for prediction of tribological properties. Many others [79, 213, 247, 279-282] have also used ANN for wear rate prediction of a wide variety of materials under different test conditions.

## 2.9 Knowledge Gap in Earlier Investigations

The literature survey presented above reveals following knowledge gap in earlier investigations that help to set the objectives of this research work:

- A lot of research works have been carried out in the past on development and characterization of ceramic and metal based coatings using plasma spray coating route. But no attempt has so far been reported on the plasma spray deposition of glass micro-sphere coatings on metallic substrates.

- Reports are available in the literature on studies carried out on mechanical, thermal and electrical behaviour of glass micro-sphere filled polymer composites; but there exists hardly any report on their tribological characteristics. Moreover, most of the studies have considered hollow glass micro-spheres (HGM) and surprisingly no investigation has been reported on polymers filled with solid glass micro-spheres (SGM).

- Tribological studies reported in the past have been mostly focused on conventional engineering materials like metals/alloys and investigations on wear behavior of heterogeneous material systems like coatings and polymer composites have been relatively less.

- A possibility that premixing of ceramic particles with glass micro-spheres in preparation of overlay protective coatings could provide a synergism in terms of better coatability and improved mechanical properties has not been adequately addressed so far.

- Studies carried out worldwide on erosion behavior of plasma sprayed coatings and polymer composites have largely been experimental and use of statistical techniques in analyzing wear characteristics is rare.

- Taguchi method, in spite of being a simple, efficient and systematic approach to optimize designs for performance, quality and cost, is used only in a limited number of applications worldwide. Its implementation in parametric appraisal of wear processes has hardly been reported. Besides, there are only a few reports available on implementation of neural computation for analysis and prediction of tribo-performance of coatings and composites.

It is thus clear that the analysis of erosion wear response of coatings and composites has still remained a less studied area. It is felt that, a further study in this respect is needed both in view of scientific understanding and commercial importance.

## 2.10 Objectives of the Present Research

In view of the above, the present work is undertaken to investigate the solid particle erosion wear characteristics of plasma sprayed coatings and polymer based composites under multiple impact conditions. The specific objectives of this work are outlined as follows:

- To develop a series of plasma sprayed coatings of borosilicate glass micro-spheres (BGM), BGM pre-mixed with $Al_2O_3$ and BGM pre-mixed with $TiO_2$ in different weight proportions on metallic substrates.
- Fabrication of a new class of composites with different polymeric matrices (epoxy and polypropylene) filled with borosilicate glass micro-spheres.
- Physical, mechanical and micro-structural characterization of these coatings and composites.
- Experimental studies on erosion wear response of the prepared coatings and composites.
- Study on the effect of addition of $Al_2O_3$ / $TiO_2$ on the mechanical and erosion behaviour of glass micro-sphere coatings.
- Parametric appraisal of the erosion wear process using Taguchi's experimental design. Development of predictive equations for estimation of erosion rate based on Taguchi approach.
- Implementation of an artificial neural network (ANN) based prediction model for estimation of erosion rates under different test conditions.

**Chapter Summary**

This chapter has provided

- An exhaustive review of research works on various aspects of plasma sprayed coatings and polymer composites reported by previous investigators.
- The knowledge gap in earlier investigations.
- The objectives of the present research work.

The next chapter describes the materials and methods used for the development of coatings and the processing of the composites, the experimental planning, the Taguchi method and neural computation.

*****

Chapter 3

# MATERIALS AND METHODS

This chapter describes the materials and methods used for the processing of the coatings and composites under this investigation. It presents the details of the characterization and erosion tests which the coating and composite samples have been subjected to. This chapter also includes brief descriptions on the statistical techniques such as the Taguchi method and the artificial neural networks that are used for analysis in this investigation.

## 3.1 Materials

### 3.1.1 Glass Micro-spheres: *Primary coating and filler material*

This research is aimed at using solid glass micro-spheres in the development of wear resistant coatings and composites. For this, borosilicate glass microspheres (BGMs) of average size 100 μm (procured from NICE Ltd.) are the primary materials to be used in the present research. These microspheres are normally obtained by heating tiny droplets of dissolved sodium meta-silicate ($Na_2SiO_3$, commonly referred to as water glass or liquid glass) during ultrasonic spray pyrolysis process. Borosilicate glass is mainly composed of $SiO_2$ (70-80%), $B_2O_3$ (7-13%), small amounts of the alkalis such as 4-8% of $Na_2O$ and $K_2O$ and 2-7% of $Al_2O_3$. Table 3.1 provides some of its important properties.

### 3.1.2 Secondary Coating Materials: *To be premixed with glass micro-spheres*

- Aluminium Oxide ($Al_2O_3$)

  Aluminium oxide ($Al_2O_3$), an inorganic material and commonly referred to as alumina, can exist in several crystalline phases which all revert to the most stable hexagonal alpha phase at elevated temperatures. Alumina is the most cost effective and widely used material in the family of engineering ceramics. It is hard, wear resistant, has excellent dielectric properties, resistance to strong acid and alkali attack at elevated temperatures, high strength and

stiffness. With an excellent combination of properties and a reasonable price, it is no surprise that fine grain technical grade $Al_2O_3$ has a very wide range of applications.

**Table 3.1** Some important properties of glass microspheres [283]

| Characteristic Property | Values | |
|---|---|---|
| Density | 2.23 | $g/cm^3$ |
| Compressive strength | 248 | MPa |
| Tensile strength | 70 | MPa |
| Micro-hardness | 9.845 | GPa |
| Thermal conductivity | 0.15 | W/m-K |
| Coefficient of Thermal expansion | 32 | ppm/°C |
| Electrical conductivity | $0.109\times10^{-16}$ | S/cm |
| Volume Resistivity | 108-1013 | ohm-cm |
| Dielectric constant | 3.67 | at 1MHz |

- Titanium Dioxide ($TiO_2$)

  Titanium dioxide ($TiO_2$) powders with average particle size of 90-100 micron are supplied by Qualikems Ltd. It is the naturally occurring oxide form of titanium and occurs in nature as rutile, anatase or brookite. It is mainly sourced from ilmenite ore. This is the most widespread form of titanium dioxide bearing ore around the world. Rutile is the next most abundant form of titanium dioxide ore. The metastable anatase and brookite phases convert to rutile upon heating. Table 3.2 provides some of the important properties of titanium dioxide. Rutile $TiO_2$ has been used for this study.

**Table 3.2** Properties of $Al_2O_3$ and $TiO_2$ [284, 285]

| Characteristic Property | Values | | |
|---|---|---|---|
| | $Al_2O_3$ | $TiO_2$ | |
| Density | 3.89 | 4.197 | $g/cm^3$ |
| Compressive strength | 710 | 680 | MPa |
| Tensile strength | 250 | 367.5 | MPa |
| Micro-hardness | 6.82 | 6.13 | GPa |
| Thermal conductivity | 35 | 11.7 | W/m-K |
| Coefficient of thermal expansion | 8.1 | 8.6 | $ppm/^0C$ |

### 3.1.3 Matrix Material

Though metals, polymers and even ceramics serve as matrix materials for functional composites, polymer matrices are most commonly used because of cost efficiency, ease of fabricating complex parts with less tooling cost and they also have excellent room temperature properties when compared to metals and ceramic matrices. Polymer matrices can be either thermoplastic or thermoset in nature. Thermosets are formed due to an irreversible chemical transformation of the resin into an amorphous cross-linked polymer matrix. Due to huge molecular structures, thermoset resins provide good electrical and thermal insulation. They have low viscosity, which allow proper fiber wet out, excellent thermal stability and better creep resistance [286]. Normally, these resins can be formulated to give a wide range of properties upon the requirement [286].

Matrix Material-1 (Epoxy)

Commercially available common thermoset resins are epoxy, polyester, vinyl ester and phenolics. Among them, the epoxy resins are being widely used for many advanced composites due to their excellent adhesion to a wide variety of fibers, superior mechanical and electrical properties and good performance at elevated temperature. In addition to that they have low shrinkage upon curing and good chemical resistance. Due to several advantages over other thermoset polymers as mentioned above, epoxy (LY 556) is chosen as the matrix material for the present research work. It chemically belongs to the 'epoxide' family. Its common name is Bisphenol-A-Diglycidyl-Ether (commonly abbreviated to DGEBA or BADGE). Its molecular chain structure is shown in Figure 3.1. It provides a solvent free room temperature curing system when it is combined with the hardener tri-ethylene-tetramine (TETA) which is an aliphatic primary amine with commercial designation HY 951 (Figure 3.2). The LY 556 epoxy resin and the corresponding hardener HY 951 are procured from Ciba Geigy India Ltd. Table 3.3 provides some of the important properties of epoxy.

**Table 3.3** Some important properties of epoxy [284]

| **Characteristic Property** | **Values** | |
|---|---|---|
| Density | 1.1 | $g/cm^3$ |
| Compressive strength | 90 | MPa |
| Tensile strength | 58 | MPa |
| Micro-hardness | 0.085 | GPa |
| Thermal conductivity | 0.363 | W/m-K |
| Glass transition temperature | 104 | $^0C$ |
| Coefficient of Thermal expansion | 62.83 | $ppm/^0C$ |
| Electrical conductivity | $0.105 \times 10^{-16}$ | S/cm |
| Volume Resistivity | $10^{15}$ | ohm-cm |
| Dielectric constant | 3.98 | at 1MHz |

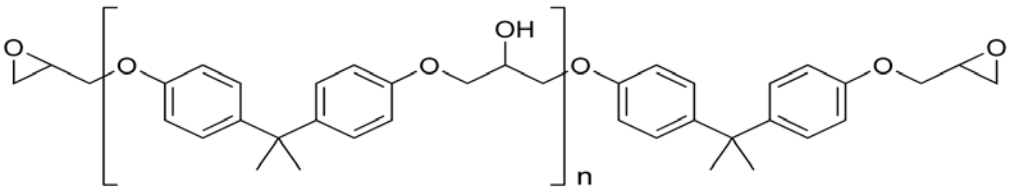


**Figure 3.1** Unmodified epoxy resin chain
(‘**n**’ denotes number of polymerized unit)

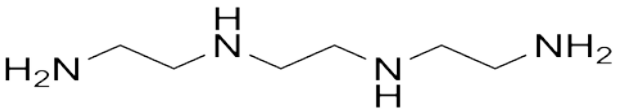


**Figure 3.2** Tri-ethylene-tetramine (hardener used for epoxy matrix)

Matrix Material-2 (Polypropylene)

Most widely used thermoplastic polymer, polypropylene (PP), is another matrix material used for the present investigation. Polypropylene of homo-polymer M110 grade shown in Figure 3.4 is chosen for the present research. Its molecular formula is $(C_3H_6)_n$, where n is the number of polymerized unit (Figure 3.3). It is used for its good mechanical performance, aesthetics, resistance to chemicals,

cost effectiveness and stability to heat and recyclability. Table 3.4 provides some important properties of polypropylene taken for this investigation.

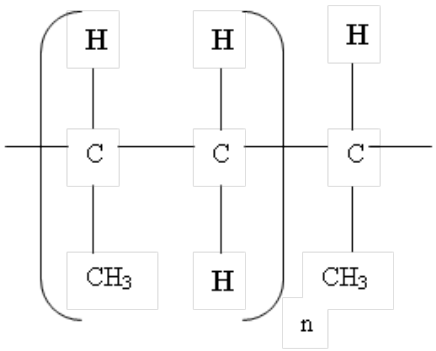


**Figure 3.3** Polypropylene chain (n is the number of polymerized unit)

**Table 3.4** Properties of homo-polymer M110 polypropylene [284]

| **Characteristic Property** | **Values** | |
|---|---|---|
| Density | 0.92 | $g/cm^3$ |
| Compressive strength | 82 | MPa |
| Tensile strength | 41 | MPa |
| Micro-hardness | 0.057 | GPa |
| Thermal conductivity | 0.1 | W/m-K |
| Glass transition temperature | -14.93 | $^0C$ |
| Coefficient of Thermal expansion | 31.144 | $ppm/^0C$ |
| Electrical conductivity | 2.3 | S/cm |

## 3.2 Deposition of the Coatings

### 3.2.1 Preparation of Substrates

Commercially available Al 6061 aluminium and AISI 1018 mild steel plates are chosen as the substrates and these are cut into rectangular pieces of dimension 120 x 60 x 4 mm. The elemental compositions of AISI 1018 mild and Al 6061 aluminium are shown in Tables 3.5 and 3.6 respectively. The specimens are grit blasted at a pressure of 3 $kg/cm^2$ using alumina grits having size of around 60 μm. During grit blasting, the average stand-off distance is kept constant at about 150 mm and the average roughness of the substrates obtained is 6.0-8.0 μm. The grit blasted specimens are cleaned in an ultrasonic cleaning unit and the weight

of each cleaned specimen is taken by using a precision electronic balance with ± 0.1 mg accuracy.

**Table 3.5** Elemental composition of AISI 1018 mild steel

| Element | Composition |
|---|---|
| Fe | 98.81-99.26% |
| C | 0.14-0.20% |
| Mn | 0.60-0.90% |
| P | 0.040% |
| S | 0.050% |

**Table 3.6** Elemental composition of Al 6061 aluminium

| Element | Composition |
|---|---|
| Al | 98% |
| Fe | 0.7% |
| Si | 0.4–0.8% |
| Cr | 0.04–0.35% |
| Mg | 0.8–1.2% |
| Ti | 0.15% |
| Cu | 0.15–0.4% |
| Mn | 0.15% |
| Zn | 0.25% |

**Table 3.7** Mixtures used for coating deposition

| S. No. | Coating Materials | Mixture Composition |
|---|---|---|
| 1 | BGM | BGM 100 wt % |
| 2 | BGM + $Al_2O_3$ | BGM 90 wt %, $Al_2O_3$ 10 wt % |
| 3 | BGM + $Al_2O_3$ | BGM 80 wt %, $Al_2O_3$ 20 wt % |
| 4 | BGM + $Al_2O_3$ | BGM 70 wt %, $Al_2O_3$ 30 wt % |
| 5 | BGM + $TiO_2$ | BGM 90 wt %, $TiO_2$ 10 wt % |
| 6 | BGM + $TiO_2$ | BGM 80 wt %, $TiO_2$ 20 wt % |
| 7 | BGM + $TiO_2$ | BGM 70 wt %, $TiO_2$ 30 wt % |

[*] *BGM: Borosilicate Glass Micro-spheres*

Spraying onto these specimens is carried out immediately after weighing. The glass micro-spheres and $Al_2O_3$ powders are thoroughly mixed in three different ratios by weight. Mixtures of glass micro-spheres and $TiO_2$ powder (again in three different ratios by weight) are also prepared in similar manner and are used as feed stock material in the present work (Table 3.7). The mixing is done in a rotary vibration mill and the mixtures are then dried prior to spraying.

### 3.2.2 Plasma Spraying

Plasma spray coating technique utilizes the exotic properties of the plasma medium to effect physical, chemical or metallurgical reactions to produce metallic and ceramic coatings for a variety of applications. In this work, the spraying is done using a 80 kW atmospheric plasma spray system (APS) working in the non-transferred arc mode (Figure 3.4) supplied by Metallizing Equipment Co. Pvt. Ltd. at Institute of Minerals and Materials Technology, Bhubaneswar, India. The plasma input power is varied from 8 to 24 kW by controlling plasma arc voltage and the arc current. Grit blasted aluminium and mild steel substrates are fixed on the substrate holder and deposition of coating is carried out at a constant powder feed rate of 25 g/min. The general arrangement of the plasma spraying equipment and schematic diagram of the spraying process are shown in Figures 3.5 and 3.6 respectively. The equipment consists of different units namely a plasma torch, a six axis robot, a mass flow controller, a robot controller, the control console, powder feeders, the power supply unit, the torch cooling system, hoses, cables, gas cylinders and accessories.

Argon is used as the primary plasmagen gas and helium as the secondary gas. The powders are deposited at constant spraying angle of $90^0$. The powder feeding is external to the gun. The operating parameters during coating deposition process are listed in Table 3.8 below. The pictorial view of some typical coating samples made for this study is also given in the Figure 3.7. The schematic sketch of a plasma sprayed coating showing the substrate, coating and the interfacial boundary is given in Figure 3.8.

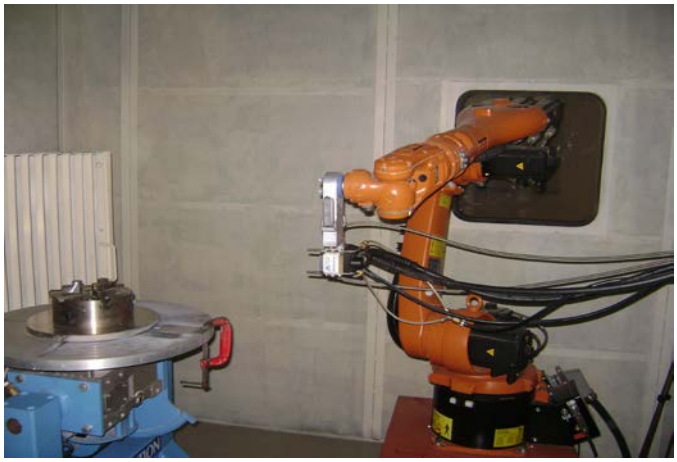

**Figure 3.4** Plasma spray set-up

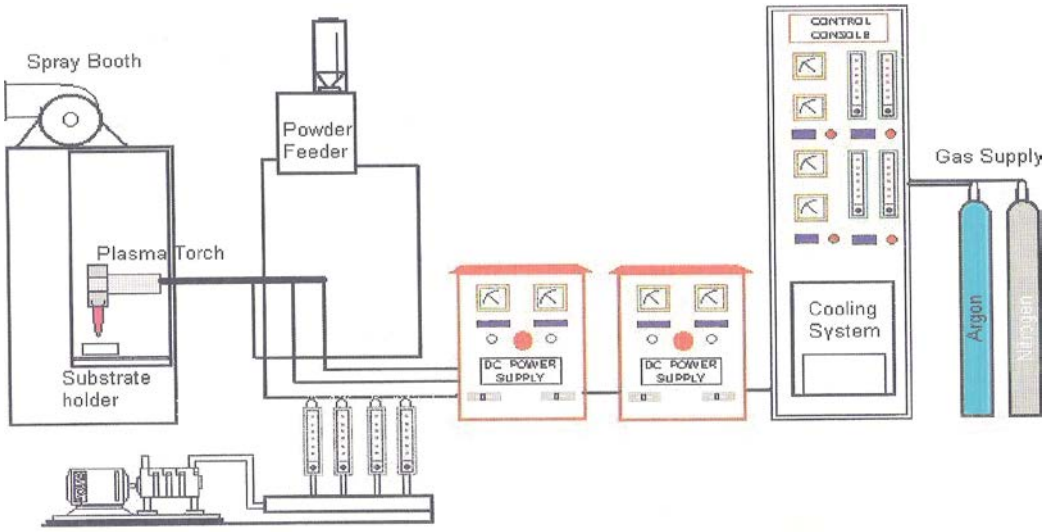


**Figure 3.5** General arrangement of the plasma spraying equipment

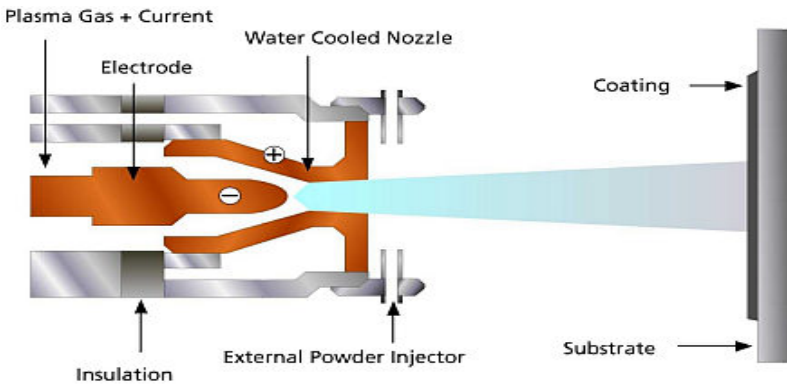


**Figure 3.6** Schematic diagram of the plasma spraying process

**Table 3.8** Operating parameters during coating deposition

| Operating Parameters | Values |
|---|---|
| Plasma Arc Current (amp) | **250-450** |
| Arc Voltage (volt) | **30, 40, 50, 60, 70** |
| Torch Input Power (kW) | **8, 12, 16, 20, 24** |
| Plasma Gas (Argon) Flow Rate (lpm) | **20** |
| Secondary Gas (He) Flow Rate (lpm) | **2** |
| Carrier Gas (Argon) Flow Rate (lpm) | **7** |
| Powder Feed Rate (g/min) | **25** |
| Torch to Base Distance TBD (mm) | **100** |

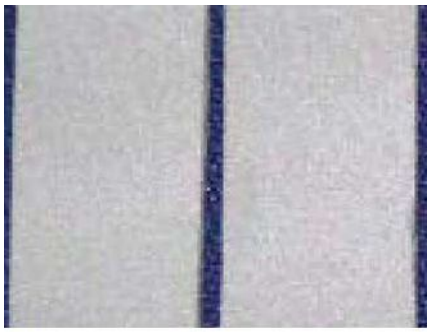

BGM Coatings

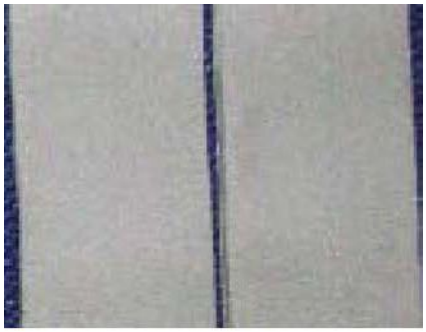

BGM+Alumina Coatings

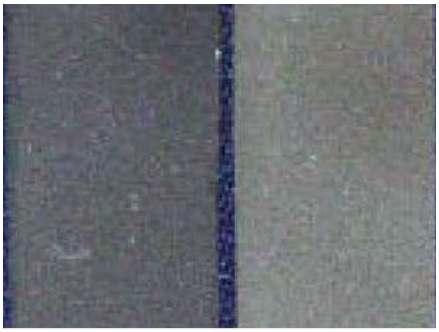

BGM+Titania Coatings

**Figure 3.7** Pictorial view of plasma sprayed coating samples

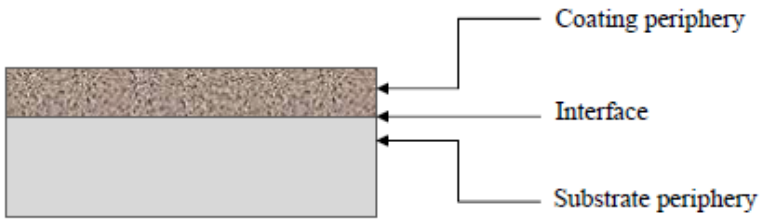


**Figure 3.8** Schematic view of the plasma sprayed coatings

### 3.3 Composite Fabrication

#### 3.3.1 Epoxy filled with glass micro-spheres (Epoxy-BGM Composites)

*Hand lay-up route*

Composite samples of various compositions are prepared by hand lay-up technique. Hand lay-up technique is the oldest and simplest technique for composite fabrication. The epoxy-BGM composites are prepared in the following steps (i) Uncured epoxy (LY556) and its corresponding hardener (HY 951) are mixed in a ratio of 10:1 by weight as per recommendation. (ii) Micro-sized BGM particles are mixed with the epoxy in different proportions. (iii) The uniformly mixed dough (epoxy filled with BGM) is then slowly decanted into the glass molds so as to get both disc type specimens (diameter 50 mm and thickness 3 mm) and rectangular slab specimens (length 200 mm, width 200 mm and thickness 3 mm), coated beforehand with wax and a uniform thin film of silicone-releasing agent. (iv) The castings are then left at room temperature for about 24 hours and then the glass molds are broken and the samples are released. From the composite slabs, rectangular/square/dog-bone shaped specimens are cut for different characterization tests. Composite samples of 4 different compositions with varying BGM content (Table 3.9) are made.

A schematic representation of glass micro-sphere filled epoxy composite is shown in Figure 3.9. It also presents a pictorial view of some of these composite samples prepared through this hand-layup technique.

**Table 3.9** Epoxy composites filled with glass microspheres

| S. No. | Composition |
|---|---|
| 1 | Epoxy + 0 wt % BGM |
| 2 | Epoxy + 10 wt % BGM |
| 3 | Epoxy + 20 wt % BGM |
| 4 | Epoxy + 30 wt % BGM |

*BGM: Borosilicate Glass Micro-spheres

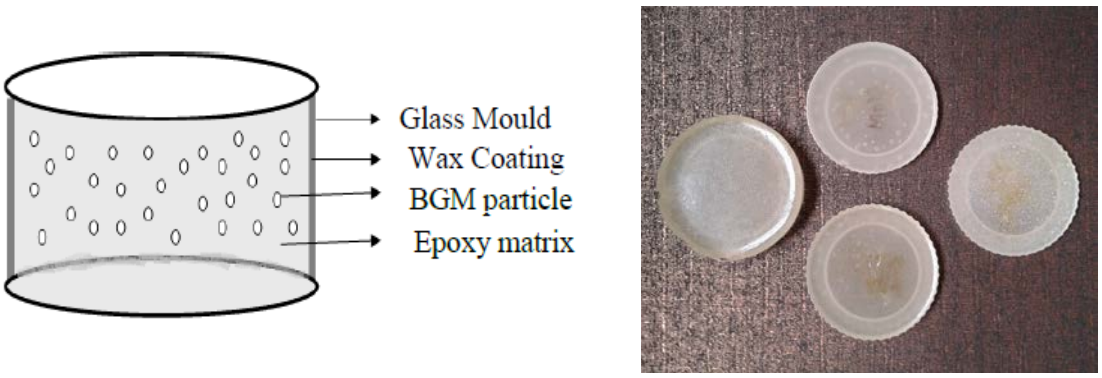


**Figure 3.9** Composite fabrication by hand lay-up process


**Figure 3.10** Injection molding machine

**Figure 3.11** Compression molding machine

### 3.3.2 Polypropylene filled with glass micro-spheres (PP-BGM Composites)

*Injection molding route*

An injection molding machine *Texair-40T*, shown in Figure 3.10, is used in the present work for fabrication of PP composite samples. Polypropylene granules mixed with different proportions of BGM particles (average size 100 micron) are heated to a temperature of 80°C in the preheater for three hours. Since polypropylene is hydrophobic (maximum absorption capacity is 0.01%), moisture will be on the surface only and during preheating process, this moisture on the surface gets evaporated. Polymeric raw materials are fed into the barrel through the hopper and this process is called screw refilling. After screw refilling process, plunger moves linearly backwards to maintain set back pressure in the barrel. Entire injection system is then moved towards mold cavity by means of guide ways as the injection nozzle is fed into the inlet of mold. Screw plunger in the barrel moves forward and pushes the material through three heaters (which is maintained at a temperature 225, 230 and $235^0$C respectively in the mold cavity). Mold cavity is completely filled with polypropylene-BGM mix (semi-solid state). 40 Ton of clamping force is applied and is held for some time till it completely solidifies. Mold is provided with water cooling system. It is opened and samples are ejected from mold by ejection pin. The above steps can also be done by setting machine in automatic mode or semiautomatic mode. Barrel is not to be emptied when heaters are on. As overheating of polypropylene causes evaporation, temperature is maintained below $250^0$C. Oiling is done before starting the machine. Injection pressure is set at 900 kg/cm$^2$ and the stroke length at 50 mm length. Nozzle temperature is set to 50% of heaters' temperature. Main parameters during the injection molding process are given in Table 3.10.

*Compression molding route*

Rheomix 600 batch mixer with chamber volume 90 cm$^3$ is used to melt and mix PP with BGM by the help of two rotors rotating in opposite direction. The temperature of the mixing chamber is set to $190^0$C and time of the mixing is 10

minutes. The temperature and time differ for different sets of matrix filler combination. As the mixing is over, the material is taken out from the chamber and after cooling it is cut into small pieces. These uniformly mixed PP-BGM composite pieces are then kept in a hot air oven for about an hour. These small pieces of materials are then taken out from the hot air oven and kept in compression molding die. The dimension of the die is 3 mm thickness and 200×200 mm in area. By using a hydraulic press, the material is pressed with a pressure of 150 kg/cm$^2$ for around three minutes. The temperature of the compression molding die is maintained at 190$^0$C with the help of heaters. After that it gets water cooled and the sheet is taken out from the die. Later the specimens of required shapes and dimensions are cut from the sheets for further experimentation. A picture of compression molding machine is shown in the Figure 3.11.

**Table 3.10** Main parameters during the injection molding

| | | |
|---|---|---|
| 1. | Clamping force | 40 Ton |
| 2. | Nozzle holding force | 3 Ton |
| 3. | Ejection force | 3 Ton |
| 4. | Mold open stroke | 250 mm |
| 5. | Screw diameter | 32 mm |
| 6. | Max. screw speed | 200 RPM |
| 7. | Screw stroke | 140-150 mm |
| 8. | Stroke volume | 112-135 cm$^3$ |
| 9. | Injection pressure | 550-660 bar |
| 10. | Injection rate | 75-90 g/sec |
| 11. | Heating capacity | 5.2 kW |
| 12. | Electrical system | 10.7 kW |
| 13. | Maximum hydraulic system pressure | 105 bar |
| 14. | Oil tank capacity | 140 litres |
| 15. | Cooling time | 2-4 min |
| 16. | Cycle time | 8 min |
| 17. | Melting temperature of composite(Unreinforced) | 170-190 $^0$C |
| 18. | Melting temperature of composite (Reinforced) | 210-230 $^0$C |
| 19. | Mold temperature | 30-40 $^0$C |
| 20. | Back pressure | 50 bar |
| 21. | The mixing quality | 95-98 % |

## 3.4 Coating Characterization

### 3.4.1 Coating Porosity

Measurement of porosity or the void fraction in the coating is done using the image analysis technique. The polished top coats are kept under a microscope (Neomate) equipped with a CCD camera (JVC, TK 870E). This system is used to obtain a digitized image of the object. The digitized image is transmitted to a computer equipped with VOIS image analysis software. The total area captured by the objective of the microscope or a fraction thereof can be accurately measured by the software. Hence the total area and the area covered by the pores are separately measured and the porosity of the surface under examination is determined.

### 3.4.2 Coating Thickness

Thicknesses of BGM based coatings on different substrates are measured on the coated cross-sections of the samples, using an Elcometer 456 thickness gauge (Figure 3.12). Five to six readings are taken at different points on each specimen and the average value is reported as the mean coating thickness.

### 3.4.3 Coating Adhesion Strength

To evaluate the coating adhesion strength, a horizontal table model universal testing machine PC-2000 Electronic Tenso-meter (Figure 3.13) is used. The test is conducted by the pull-out method in which two cylindrical specimens are taken. The face of one of the cylinders is plasma spray coated with the material under investigation. This coated face is glued with a resin (epoxy $900^0$C) to the face of the other uncoated cylindrical specimen. This uncoated face is to be grit blasted prior to the gluing. The assembly of the two cylinders is then subjected to gradual tensile load. The tensile strength i.e. the coating adhesion strength is calculated from the division of the maximum load applied at the rupture (i.e. failure occurs only at the coating-substrate interface) by the cross sectional area of the cylindrical specimen considered. The tensile loading arrangement during the pull out test is shown schematically in Figure 3.14. The test is performed as per ASTM C-633.

**Figure 3.12** Elcometer 456 thickness gauge

**Figure 3.13** PC-2000 Electronic Tenso-meter (Horizontal table model)

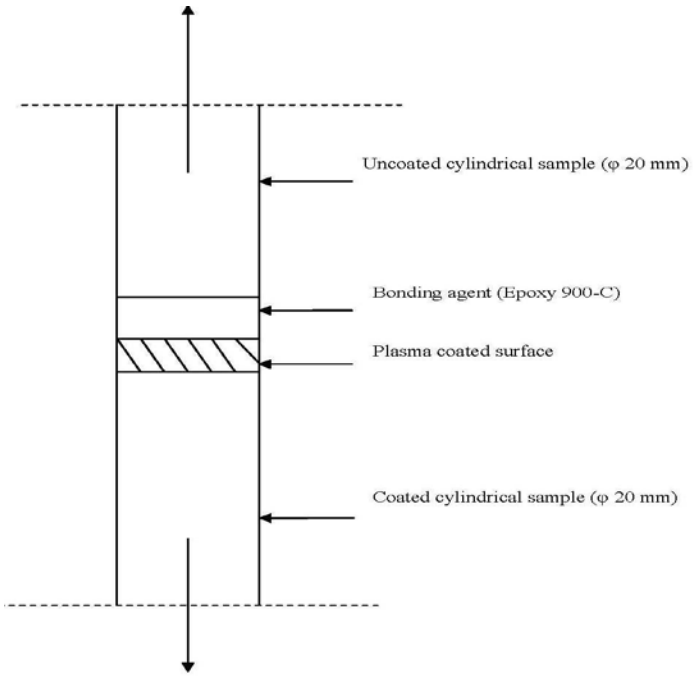


**Figure 3.14** Loading pattern during coating pull out test

### 3.4.4 Coating Deposition Efficiency

Deposition efficiency is defined as the ratio of the weight of coating deposited on the substrate to the weight of the expended feedstock. For various torch input power levels, the coating is deposited onto different rectangular specimens (which are previously weighed, numbered and noted) for a time period of one minute. The specimens are made of materials same as that of the substrates chosen for this work. After the spraying, the coated samples are weighed again and the difference of the weights of the coated and uncoated samples is calculated and is denoted as Gc. As mentioned previously, the weight of the coating material fed at a constant rate of 25 g/min for the entire duration of spraying is the weight of the expended feed stock denoted by Gp. Finally, the efficiencies of coating deposition for different substrates at different torch input power are found using the following equation [287]:

$$\eta_{deposition} = ( Gc / Gp) \times 100 \ \% \quad \textbf{(3.1)}$$

### 3.4.5 Scanning Electron Microscopy

Specimens of size 5×5 mm are sliced from the uneroded and eroded samples for microscopic observation. The top surfaces of the specimens are observed under scanning electron microscope JEOL JSM-6480LV (Figure 3.15), by using the secondary electron imaging. To enhance the electrical conductivity of the samples, a thin film of platinum is vacuum-evaporated onto them before the photo-micrographs are taken.

### 3.4.6 X-Ray Diffraction (XRD) Studies

The coatings are examined for the identification of the crystalline phases with a Philips X-Ray Diffractometer, shown in Figure 3.16. The X-ray diffractograms are taken using Cu Kα radiation.

### 3.4.7 Micro-hardness

Micro-hardness measurement of the metallographically polished coating specimens is made using a Leitz Micro-hardness Tester equipped with a monitor and a microprocessor based controller (Figure 3.17). A diamond indenter, in the

form of a right pyramid with a square base and an angle $136^0$ between opposite faces, is forced into the coated surface under a load F. The two diagonals *X* and *Y* of the indentation left on the surface of the material after removal of the load are measured and their arithmetic mean *L* is calculated. In the present study, the load considered *F* = 0.493 N for a loading time of 20 seconds and Vickers hardness number is calculated using the following equation:

$$H_V = 0.1889 \frac{F}{L^2} \quad \textbf{(3.2)}$$

Where, $L = \frac{X + Y}{2}$

Here, *F* is the applied load (N), *L* is the diagonal of square impression (mm), *X* is the horizontal length (mm) and *Y* is the vertical length (mm). About six to seven readings are taken for each sample on different optically distinguishable points and the average value is reported as the mean coating hardness. It is then converted and expressed in terms of SI units (GPa).

### 3.5 Composite Characterization

#### 3.5.1 Density and Volume Fraction of Void

The theoretical density of composite materials in terms of weight fraction can easily be obtained as for the following equations given by Agarwal and Broutman [288]:

$$\rho_{ct} = \frac{1}{(W_p/\rho_p) + (W_m/\rho_m)} \quad \textbf{(3.3)}$$

Where, *W* and $\rho$ represent the weight fraction and density respectively. The suffix *p* and *m* represent particulate filler material and matrix material respectively.

The actual density ($\rho_{ce}$) of the composite, however, can be determined experimentally by simple water immersion technique. The volume fraction of voids ($V_v$) in the composites is calculated using the following equation:

$$V_v = \frac{\rho_{ct} - \rho_{ce}}{\rho_{ct}} \quad \textbf{(3.4)}$$


**Figure 3.15** Scanning electron microscope


**Figure 3.16** X-ray diffractometer

**Figure 3.17** Leitz micro-hardness tester

### 3.5.2 Tensile Strength

The dog-bone type specimens with end tabs are commonly used for tensile test. ASTM-D3039-76 standard test method is employed for tensile test of composite specimens. The test is performed using the universal testing machine (UTM) Instron 1195 (Figure 3.18) at a cross-head speed of 10 mm per minute. Each test is repeated three times on different composite specimens of same composition and the average of the three results is recorded as the mean value of the tensile strength. The pictorial view of the composite specimens and the loading arrangement for tensile test are shown in Figures 3.19 and 3.20 (a) respectively.

### 3.5.3 Flexural Strength

The short beam shear (SBS) tests are performed on the composite samples at room temperature to evaluate the value of flexural strength. It is a 3-point bend test, which generally promotes failure by inter-laminar shear. The SBS test is conducted as per standard ASTM: D5379/D5379M using the same UTM. The dimension of each specimen is 60 ×10 × 3 mm. Span length of 40 mm and the cross head speed of 10 mm/min are maintained. The loading arrangement is shown in Figure 3.20 (b). The flexural strength (*FS*) of any composite specimen is determined using the following equation:

$$F \cdot S = \frac{3Pl}{2bt^2} \qquad \textbf{(3.5)}$$

Where, $l$ is the span length of the sample, $P$ is the load applied; $b$ and $t$ are the width and thickness of the specimen respectively.

### 3.5.4 Impact Strength

The pendulum impact testing machine confirming to ASTM: D256 ascertains the notch impact strength of the material by shattering the specimen with a pendulum hammer, measuring the spent energy and relating it to the cross section of the specimen. The machine is adjusted such that the blade on the free-hanging pendulum just barely contracts the specimen (zero position). The specimens are clamped in a square support and are struck at their central point by a hemispherical bolt of diameter 5 mm.


**Figure 3.18** Instron 1195 universal testing machine

**Figure 3.19** Composite samples for tensile test


**Figure 3.20 (a)** Loading arrangement for tensile test


**Figure 3.20 (b)** Loading arrangement for flexural strength test

### 3.5.5 Effective Thermal Conductivity

Unitherm™ Model 2022 thermal conductivity tester is used to measure the thermal conductivity of various materials, which include polymers, glasses, ceramics, rubbers, composites, metals and other materials with medium to low thermal conductivity. In the present work, this instrument is used to measure the room temperature effective thermal conductivity of the composite specimens. Disc type specimens (diameter = 50 mm, thickness = 3 mm) are used for this purpose. This test is conducted in accordance with ASTM E-1530 standards. The pictorial view of the Unitherm™ Model 2022 tester is given in Figure 3.21.

**Figure 3.21** Unitherm™ Model 2022 tester

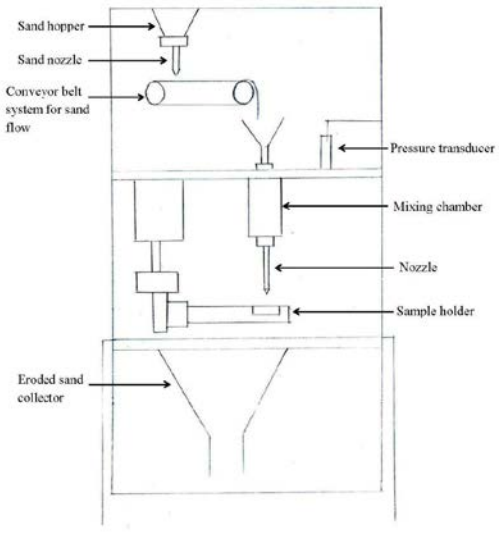


**Figure 3.22 (a)** Schematic diagram of erosion test rig

**Figure 3.22 (b)** Solid particle erosion test set-up

### 3.6 Erosion Wear Behaviour

Erosion wear trials are carried out as per ASTM G 76 using an air jet type erosion test rig. The setup mainly consists of an air compressor, an air-particle mixing chamber and an accelerating chamber. The schematic diagram and the pictorial view of the erosion set up are given in Figures 3.22 (a) and (b) respectively. This test rig employs a 30 mm long nozzle of 3 mm bore. This nozzle size permits a wider range of particle types to be used in the course of testing, allowing better simulations of real erosion conditions. The mass flow rate is measured by conventional method. Particles are fed from a simple hopper under gravity into the groove. This setup is capable of creating reproducible erosive situations for assessing erosion wear resistance of the coating and composite samples under this investigation. In the present study, dry silica sand particles of different sizes (i.e. 50, 100, 150 and 200 μm) are used as erodent. Prior to erosion trials in the test rig, the samples are cleaned with acetone and weighed. Erosion process is carried out on each sample for a period of 10 minutes with different impact velocities (32, 40, 48 and 56 m/s) at different angles of impingement ($30^0$ to $90^0$). Velocity of impact is measured using the standard double disc method [187]. Then the samples are weighed again to determine the weight loss due to the impact of dry silica sand particles in order to evaluate the erosion wear rate in every single test run. The erosion rate is defined as the weight loss of the specimen due to erosion divided by the weight of the erodent causing the loss. The process is repeated till the erosion rate attains a constant value called steady state erosion rate.

### 3.7 Process Optimization and Taguchi Method

Statistical methods are commonly used in engineering and related studies to improve the quality of a product or process. Such methods enable the user to define and study the effect of every single condition possible in an experiment where numerous factors are involved. Solid particle erosion is such a process in which a number of control factors collectively determine the performance output, i.e., the erosion rate. In this context, Taguchi experimental design

happens to be a powerful analysis tool for modeling and analyzing the influence of control factors on the performance output. This method achieves the integration of design of experiments (DOE) with the parametric optimization of the process yielding the desired results. The orthogonal array (OA) indicates a set of well-balanced (minimum test runs) experiments. Taguchi's method uses a statistical measure of performance called signal-to-noise ratio (S/N), which is the logarithmic function of desired output to serve as objective functions for optimization. The ratio depends on the qualitative characteristics/attributes of the product/process variables to be optimized. The three categories of S/N ratios normally used are smaller-the-better (SB), higher-the-better (HB) and nominal-the-best (NB) as given by the Eqs. 3.6, 3.7 and 3.8 respectively. In the present case, the S/N ratio for minimum erosion rate falling under smaller-the-better norm can be calculated as logarithmic transformation of the loss function by using Eq. 3.6.

Smaller the better characteristics $$\frac{S}{N} = -10\log\frac{1}{n}\left(\sum y^2\right) \quad \textbf{(3.6)}$$

Higher the better characteristics $$\frac{S}{N} = -10\log\frac{1}{n}\left(\sum\frac{1}{y^2}\right) \quad \textbf{(3.7)}$$

Nominal the best characteristics $$\frac{S}{N} = -10\log\frac{1}{n}\left(\sum\frac{\bar{Y}}{S_Y^2}\right) \quad \textbf{(3.8)}$$

The most important stage in the design of experiments (DOE) lies in the proper selection of the control factors. Therefore, a large number of factors are initially included so that non-significant variables can be identified at the earliest opportunity. In Taguchi's experimental design, some selected parameters influencing the performance output are considered in determining the experimental schedule as per the prescribed orthogonal arrays. In the present

work, $L_{16}$ orthogonal arrays are taken for the erosion wear experiments of coating and composite samples.

### 3.8 Artificial Neural Network

Artificial Neural Network (ANN) is a technique inspired by the network of biological neurons and has already been used to solve a wide variety of problems in tribology [271, 272, 289, 290]. It was developed to simulate the strong learning, clustering and reasoning capacity of biological neurons. With a strong learning capability and use of parallel computation and non-linear mapping, neural networks can be successfully applied for identifying several non-linear systems and control problems. The back propagation ANN can be used to train multiple layered feed-forward networks with differential transfer functions to develop a functional model. Using a well-trained ANN model, one can estimate predictive performance, pattern association and pattern classification. As already mentioned, the erosion process is a complicated phenomenon lacking adequate mathematical description and therefore, in this analysis, an integrated method has been proposed that combines Taguchi's design approach with the ANN for parametric analysis and prediction of wear performance of the coatings and composites. It not only gives a clear understanding of the effects of process parameters but also develops optimal parameter settings to ensure that the coatings and composites exhibit the best performance characteristics in regard to erosion wear.

ANN is a technique that involves database training to predict input-output evolutions. Basically this technology is suitable for some complex, nonlinear and multi-dimensional problems because it is able to imitate the learning capability of human beings. This means that the network can learn directly from the examples without any prior formulae about the nature of the problem and generalize by itself some knowledge, which could be applied for new cases. A neural network is a system composed of many cross-linked simple processing units called 'neurons'. The network generally consists of three parts connected in

series: input layer, hidden layer and output layer. The coarse information is accepted by the input layer and processed in the hidden layer. Finally the results are exported via the output layer [291]. The details of this methodology are described by Rajasekaran and Pai [292].

**Chapter Summary**

This chapter has provided:

- The descriptions of materials used in the experiments
- The details of deposition and characterization of the coatings
- The details of fabrication and characterization of the composites
- The description of solid particle erosion wear test
- An explanation of the Taguchi experimental design and neural computation

The next chapter presents the physical, mechanical and micro-structural characterization of the plasma sprayed coatings under this study.

*****

Chapter 4

Results and Discussion - I

# COATING CHARACTERIZATION

This chapter reports on various physical and mechanical characteristics of the glass micro-sphere coatings under this investigation. Plasma sprayed coatings of borosilicate glass micro-spheres (BGMs) pre-mixed with $Al_2O_3$ and separately with $TiO_2$ in different weight proportions are deposited on aluminium and mild steel substrates using a 80 kW atmospheric plasma spray system at the Institute of Minerals and Materials Technology, Bhubaneswar, India. Coating deposition is done at different power levels (8 kW-24 kW) i.e. input power to the DC plasma torch in the spray system. Characterization of these coatings in regard to their physical and mechanical properties is done. The results of various characterization tests are presented and discussed in this chapter.

## 4.1 Characterization of Coating Material

The particle size distribution of BGMs (before plasma spraying) is characterized using LASER particle size analyzer of Malvern Instruments make.

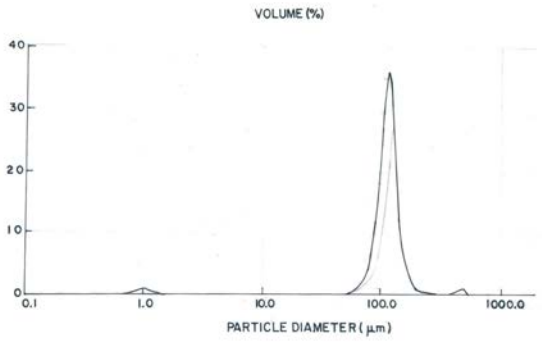


**Figure 4.1 (a)** Particle size analysis of borosilicate glass micro-spheres

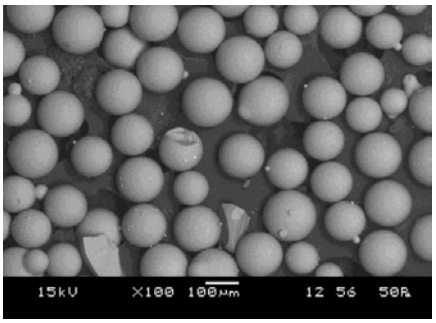


**Figure 4.1 (b)** SEM micrographs of BGM powder prior to coating

Figure 4.1 (a) shows the particle size distribution of the BGMs used in this research. It can be seen that, majority of particles are in the range of 98-100 μm. SEM micrograph of BGMs in feedstock prior to coating is shown in Figure 4.1 (b). It is observed that the particles are circular in shape.

## 4.2 Characterization of Coatings

Coating Thickness

To assess the deposition of coating on the substrates, coating thickness is measured on the polished cross-sections of the samples, using an Elcometer 456 thickness gauge. Figures 4.2 (a) and (b) illustrate the variation of thickness values with torch input power for the BGM and 'BGM + $Al_2O_3$' coatings on mild steel and aluminium substrates respectively. Similarly, Figures 4.3 (a) and (b) show the same for the BGM and 'BGM + $TiO_2$' coatings on mild steel and aluminium substrates respectively. Each data point on the curves is the average of five or six readings taken on different locations on the coated surface. It is evident from these curves that with increase in torch input power the thickness of the coating increases irrespective of the composition of the coating material. But beyond 20 kW a slight drop in the mean coating thickness is recorded invariably for all the samples which is possibly due to the vaporization of coating material at higher power level.

The thicknesses of the coatings are found to be varying in between 61 μm to 220 μm for mild steel substrates and 56 μm to 200 μm for aluminium substrates with different proportions of $Al_2O_3$ with BGM as the power level changes gradually from 8 kW to 24 kW. The feed material with 30 wt% $Al_2O_3$ powder resulted in thicker coating, with a maximum thickness of 220 μm at 20 kW power level on mild steel substrate. Whereas in case of aluminium substrate the maximum thickness obtained is 200 μm. Similarly, the thickness is found to be varying in between 61 μm to 232 μm for mild steel substrates and 56 μm to 208 μm for aluminium substrates with different amount of $TiO_2$ mixed with BGM with increase in torch input power. The feed material with 30 wt% $TiO_2$ powder gives thicker coating, with a maximum thickness of 232 μm on mild steel substrate and 208 μm on aluminium substrate at 20 kW power level.

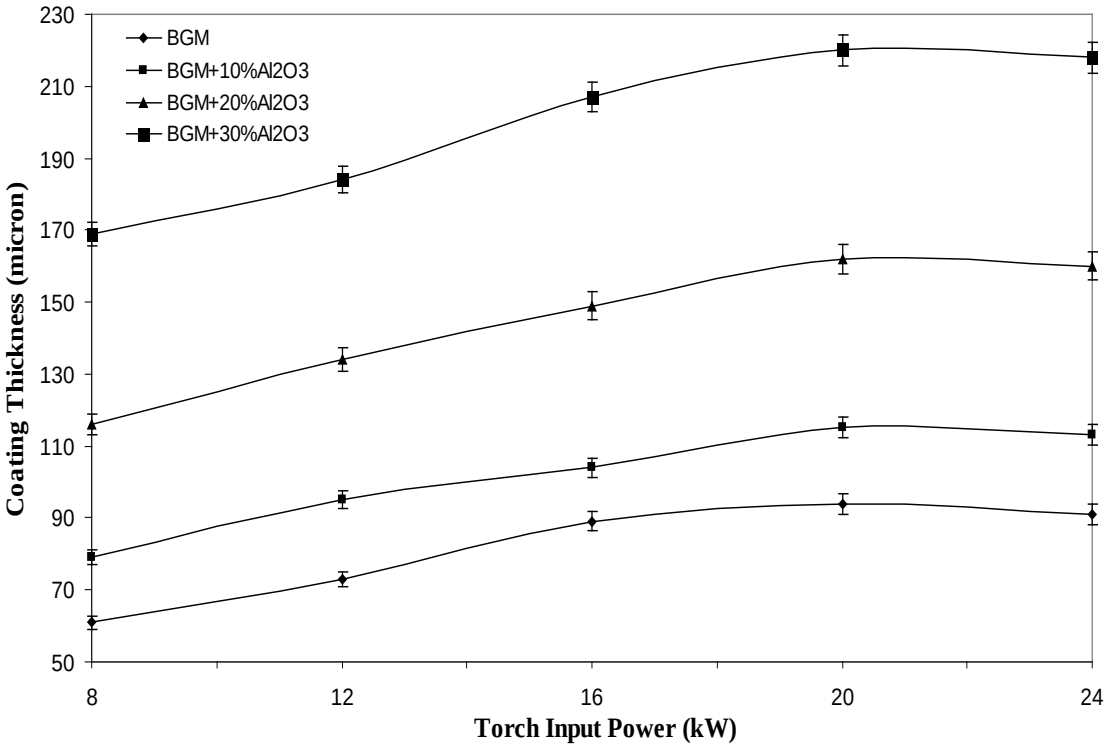


(a) For mild steel substrates

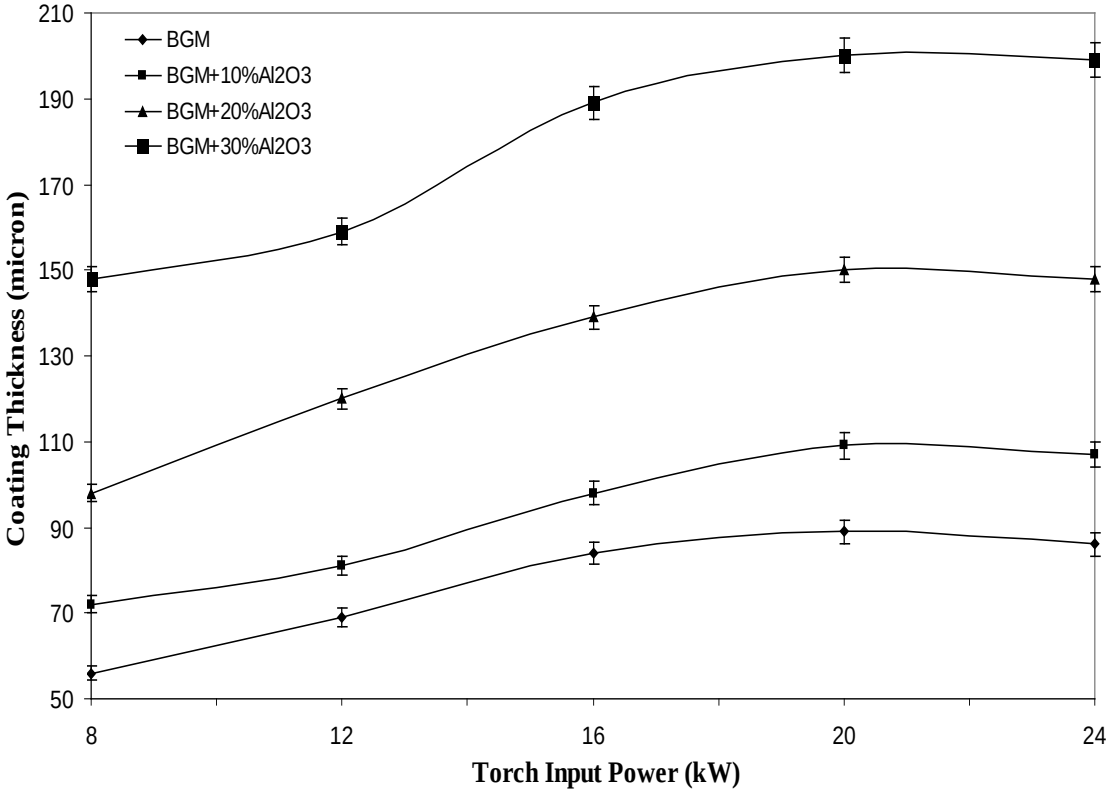


(b) For aluminium substrates

**Figure 4.2** Variation of coating thickness for BGM and BGM-$Al_2O_3$ with torch input power

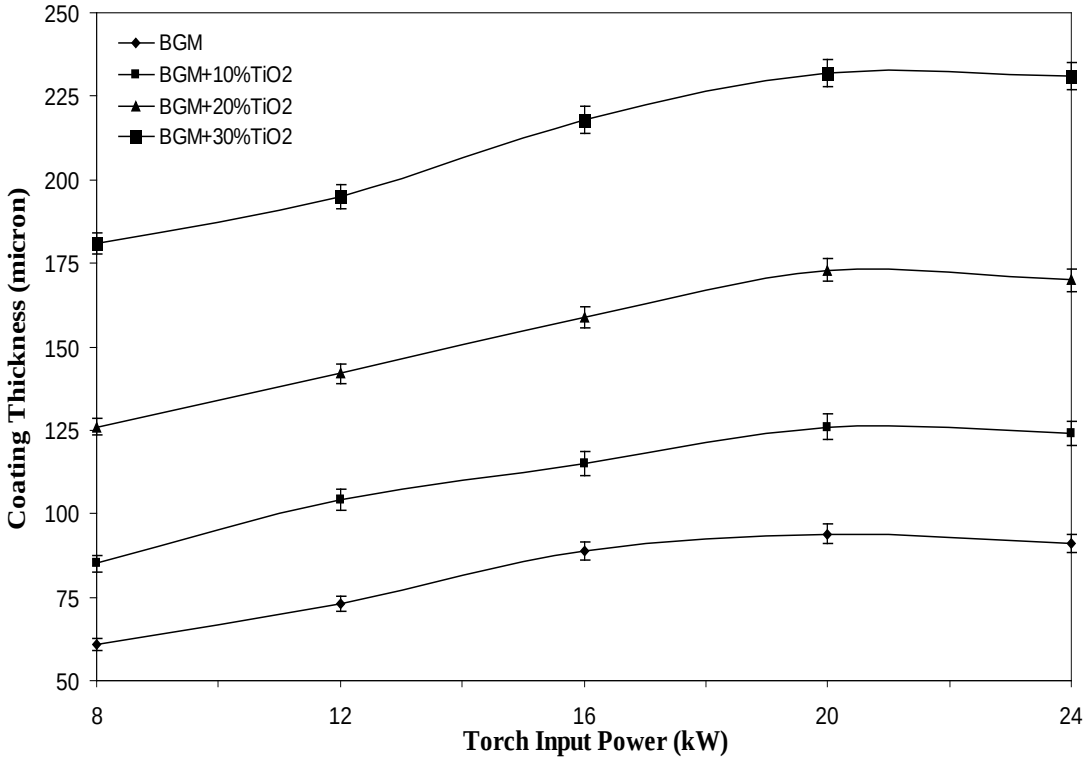


(a) For mild steel substrates

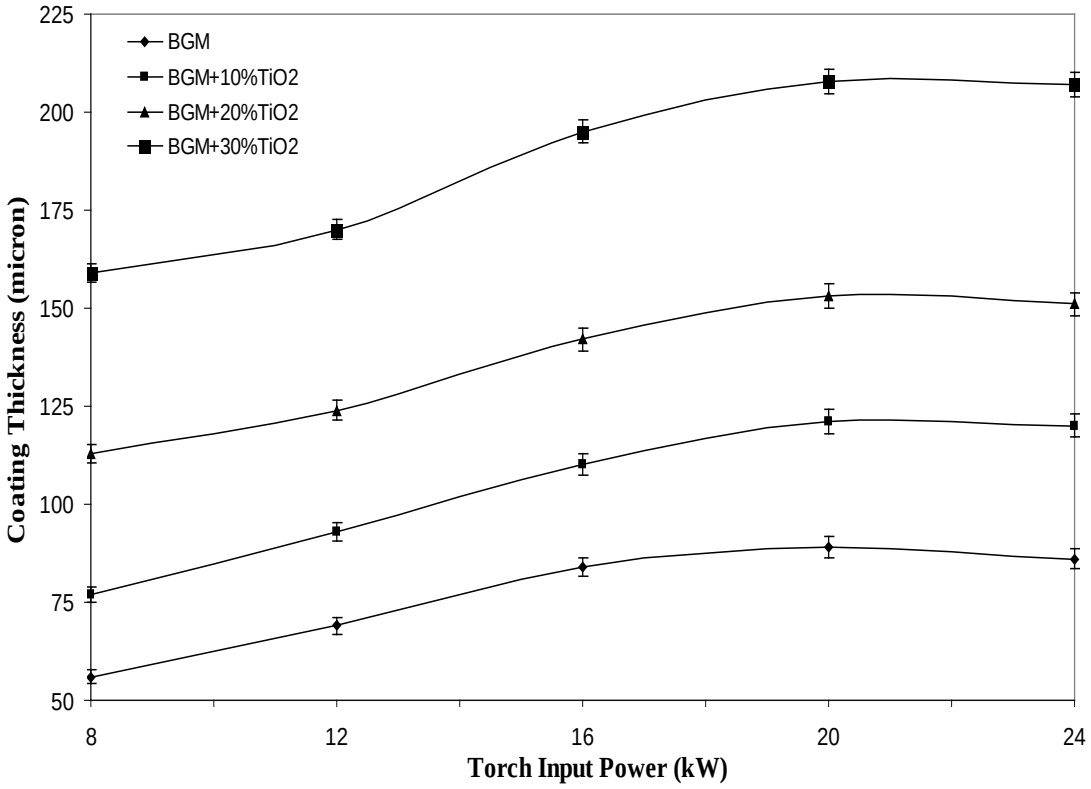


(b) For aluminium substrates

**Figure 4.3** Variation of coating thickness for BGM and BGM-$TiO_2$ with torch input power

It is known that for oxide coatings developed by atmospheric plasma spraying (APS) technique, particle deposition is largely influenced by the torch input power [293]. With the increase in power level, the plasma density increases leading to rise in enthalpy of the plasma jet and thereby the temperature of the particles (coating material) residing within the jet. Hence at higher torch input power, better melting of the feed material during the in-flight traverse through the plasma results in better inter-particle bonding which subsequently gives rise to a higher rate of coating deposition. Similar results and trends have been observed also by many previous investigators for fly ash and red mud coatings on metals [1, 3, 294].

Coating Deposition Efficiency

Deposition efficiency of coatings made within the scope of this investigation is evaluated because it is an important factor that determines the cost effectiveness of both the coating product and the process. Deposition efficiency depends on many factors that include the input power to the plasma torch, particle size range, heat capacity of the powder being sprayed, material properties such as melting point and the torch to base distance (TBD) etc. [2, 46]. For a given TBD and a specific coating material, torch input power appears to be an important factor for the deposition efficiency. The deposition efficiency is a measure of the fraction of the fed powder that is deposited on the substrate. Deposition efficiency values of BGM, 'BGM + $Al_2O_3$' and 'BGM + $TiO_2$' coatings made at different operating powers (on mild steel and aluminium substrates) are presented in Figures 4.4 (a, b) and 4.5 (a, b) respectively.

In case of mild steel substrate, deposition efficiency of 38.65% is recorded as the highest for coating of 'BGM + 30 wt% $Al_2O_3$' at 20 kW torch input power. Again, 36.46% of deposition efficiency is obtained in case of the aluminium substrate under similar spraying conditions. Similarly, for 'BGM + $TiO_2$' mixture with different weight proportions, the coating deposition efficiency on both mild steel and aluminium substrates are also evaluated and plotted. In case of mild steel substrate the highest deposition efficiency of 41.85% is obtained at 20 kW torch input power and with 30 wt% of $TiO_2$ in the mixture, whereas on aluminium substrate, a maximum deposition efficiency of 39.98% is recorded for the similar spraying conditions. It is further evident from the graphs in

Figures 4.4 (a, b) and 4.5 (a, b) that the coating deposition efficiency is higher for the 'BGM + $TiO_2$' deposition on mild steel substrate than that on the aluminium substrate at the highest torch input power.

For coatings of glass micro-spheres premixed with $Al_2O_3$, it is interesting to note that the deposition efficiency improves with the increase in $Al_2O_3$ content in the feedstock and the torch input power. Similar trend is observed in case of coatings of BGMs premixed with $TiO_2$ as well. It is found that the deposition efficiency presents a sigmoid-type evolution with the increase in torch input power. As the power level increases, the net available energy in the plasma jet increases leading to a better in-flight particle melting and hence to higher probability for the molten particles to flatten. The deposition efficiency reaches a plateau for the highest power levels due to the plasma jet temperature increasing which in turn increases both the particle vaporization ratio and the plasma jet viscosity.

This study reveals that efficiency of coating deposition is significantly influenced by the input power to the torch. In fact, plasma spray deposition efficiency of a given material depends on its melting point, heat capacity, rate of heat dissipation at coating-substrate interface, particle size of the sprayed powder etc. [46]. At lower power level, the plasma jet temperature is not high enough to melt the entire feed powder (particles) that enters the plasma jet. As the power level is increased, plasma temperature and enthalpy increases, thus melting a larger fraction of the feed material. The spray efficiency therefore increases with increase in input power to the plasma torch. However, beyond a certain power level of the torch, temperature of the plasma becomes high enough leading to vaporization or dissociation of the particles that causes a slight drop in deposition efficiency. This tendency is generally observed in deposition of a wide range of plasma sprayed ceramic and cermet coatings [46]. However, the operating power above which no further increase of deposition efficiency is noticed depends on the nature of the feed material i.e. powder and its particle size, thermal conductivity, in-situ phase transformations etc.

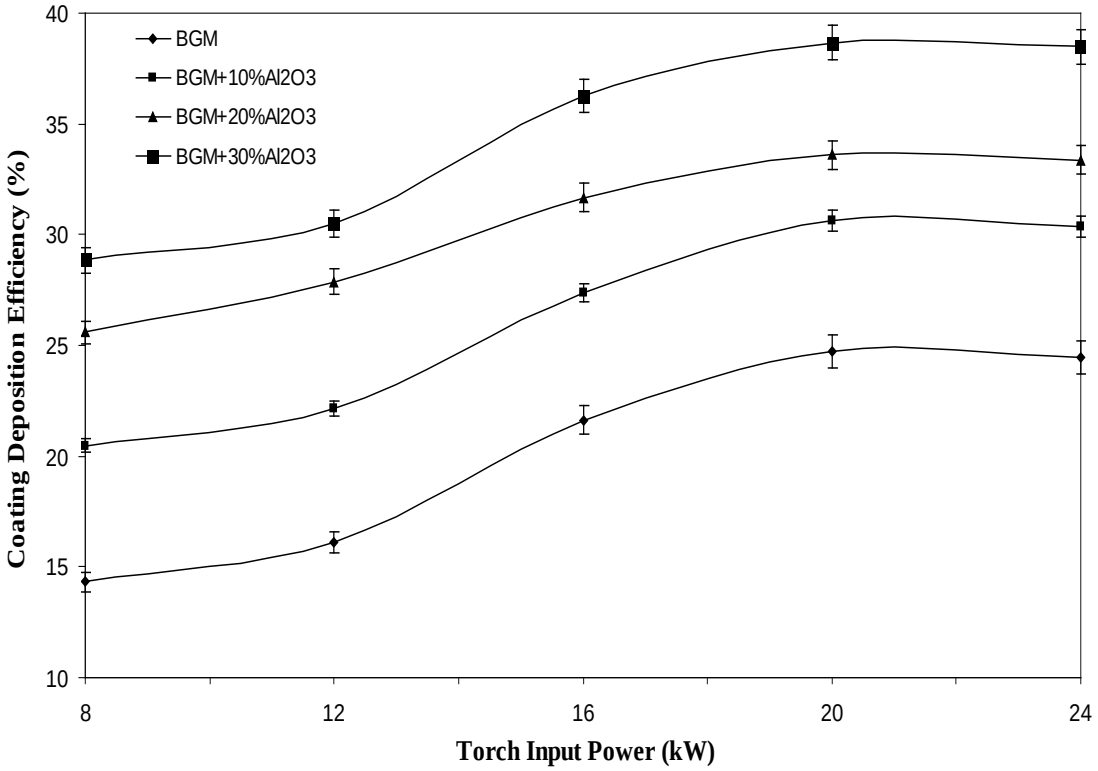


(a) For mild steel substrates

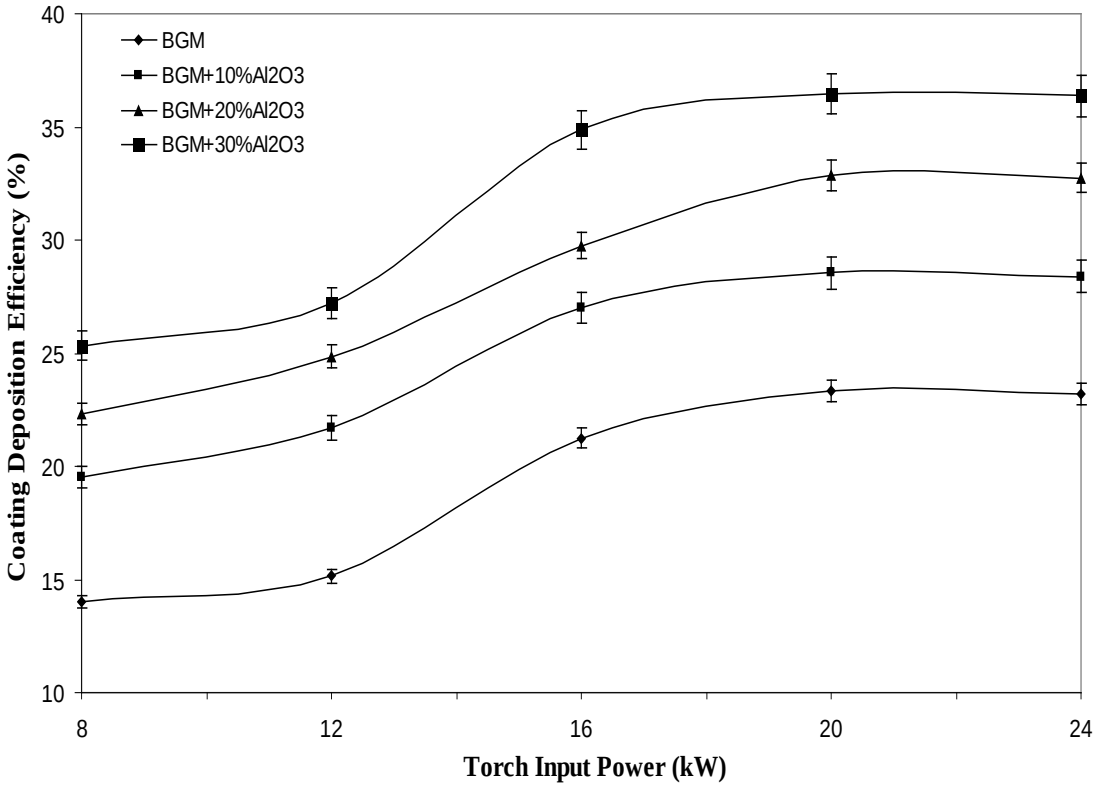


(b) For aluminium substrates

**Figure 4.4** Variation of coating deposition efficiency for BGM and BGM-$Al_2O_3$ with torch input power

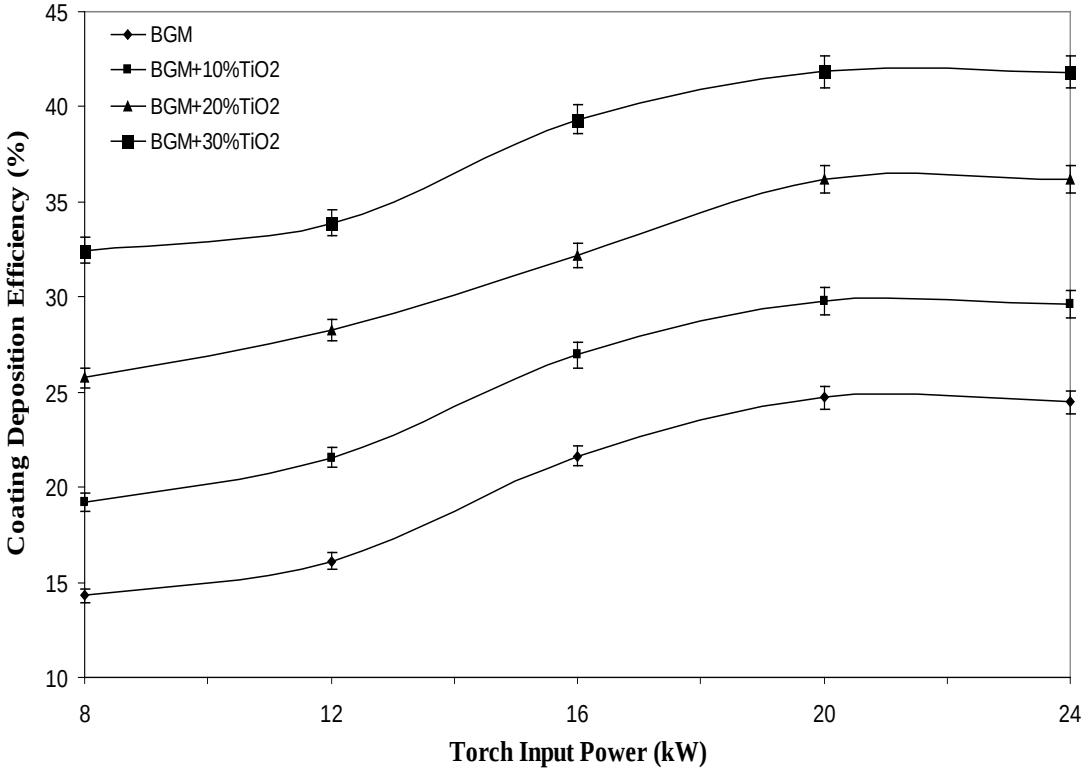


(a) For mild steel substrates

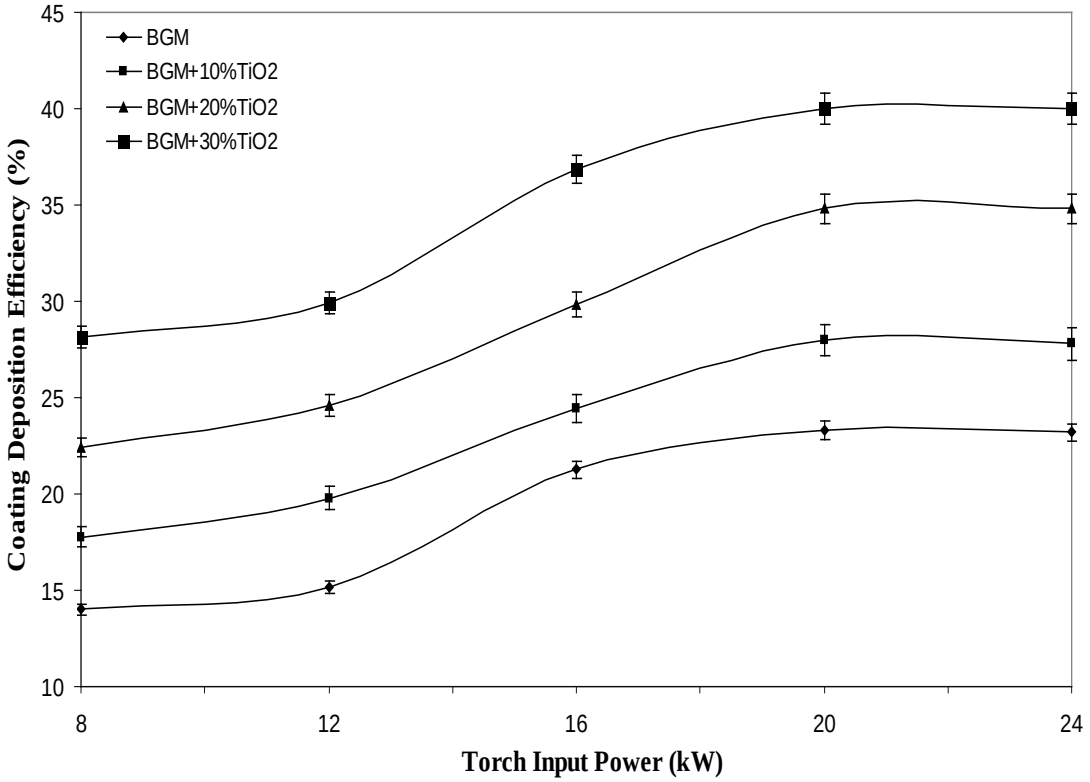


(b) For aluminium substrates

**Figure 4.5** Variation of coating deposition efficiency for BGM and BGM-$TiO_2$ with torch input power

Coating Adhesion Strength

Coating adhesion tests have been carried out by many investigators in the past with various coatings. It has been stated that, the fracture mode is adhesive if it takes place at the coating-substrate interface and that the measured adhesion value is the value of practical adhesion, which is strictly an interface property, depending exclusively on the surface characteristics of the adhering phase and the substrate surface condition [295, 296]. From the microscopic point of view, adhesion is due to physico-chemical surface forces (Vander-walls, Covalent, Ionic etc.), which are established at the coating-substrate interface [297] and corresponds to the work of adhesion. From the mechanical point of view, strength of adherence can be estimated by the force corresponding to interfacial fracture and is macroscopic in nature.

In the present investigation, to evaluate the coating adhesion strength, test is conducted by the pull out method following ASTM C-633 test standards. It is found that, in all the samples, fracture occurred at the coating-substrate interface. The variations of adhesion strength with operating power level are shown in Figures 4.6 (a, b) and 4.7 (a, b) for 'BGM + $Al_2O_3$' and for 'BGM + $TiO_2$' coatings respectively. Each pull out test is repeated three times and the average of three test runs is taken as the data point. From the figures, it is clear that the adhesion strength varies with operating power of the plasma torch. The strength also differs from substrate to substrate and depends on the composition of the coating materials as well.

From the Figures 4.6 (a) and (b), it is clear that the adhesion strength varies appreciably with operating power (8-24 kW) of the plasma torch and the maximum adhesion strength is obtained at 20 kW. Maximum adhesion strengths of about 32 MPa and 33 MPa are recorded with 'BGM + 30 wt% $Al_2O_3$' powder for the mild steel and aluminium substrates respectively. The Figures 4.7 (a) and (b) also show almost similar trends as those obtained in case of 'BGM + $Al_2O_3$' coatings. Among all the coated samples, 'BGM + 30 wt% $TiO_2$' coating made at 20 kW on mild steel and aluminium substrates exhibited the maximum adhesion strengths of about 34 MPa and 35 MPa respectively. A drop in coating adhesion

strength is noticed for all coatings deposited at an operating power beyond 20 kW.

The variational trend of coating adhesion strength with torch input power is explained as follows: initially, when the operating power level is gradually increased from 8 kW onwards, the melting fraction and velocity of the particles also increase. Therefore, there is better splashing and mechanical interlocking of molten particles on the substrate surface leading to an increase in adhesion strength [298]. But, at higher power level (beyond 20 kW), the amount of fragmentation and vaporization of the particles are likely to increase. There is also a greater chance of smaller particles (during in-flight traverse through the plasma) to fly off during spraying. This has resulted in poor adhesion strength of the coatings. During in-flight traverse through the plasma, particles would melt either partially or fully depending on the temperature and the flame residence time of that particular particle. The fully molten particles take the form of spherical droplets and the partially molten ones reduce in size. Moreover, at higher operating power, due to high temperature and high enthalpy, more particles are fragmented into smaller particles. These smaller particles tend to fly off during spraying [3, 44, 294]

Coating Porosity

Measurement of porosity or the void fraction in the coating is done using the image analysis technique. The results are tabulated in Table 4.1. In this investigation it is observed that porosity in the BGM based coatings lie in the range of 6-9%. The lowest porosity is recorded to be 6.19% for 'BGM + 30 wt% $Al_2O_3$'coatings and 5.21% for 'BGM + 30 wt% $TiO_2$' coatings, both at 16 kW power.

It is also noticed that with addition of both $Al_2O_3$ and $TiO_2$ to glass micro-spheres in the feed stock the percentage of pores can be reduced. This reduction is relatively more for $TiO_2$ than for $Al_2O_3$. In conventional plasma sprayed ceramic coatings, porosity of about 3-10% is generally observed [3, 46, 294, 299]. Thus the values obtained in the coatings under this study are well within the acceptable range.

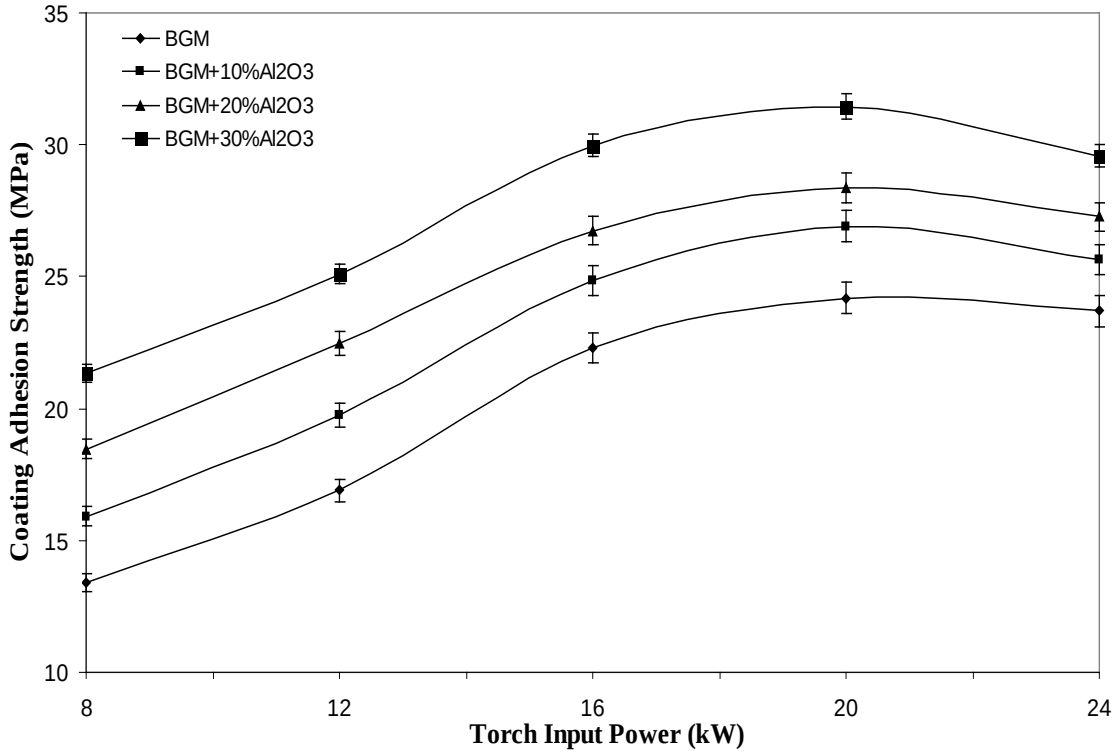


(a) For mild steel substrates

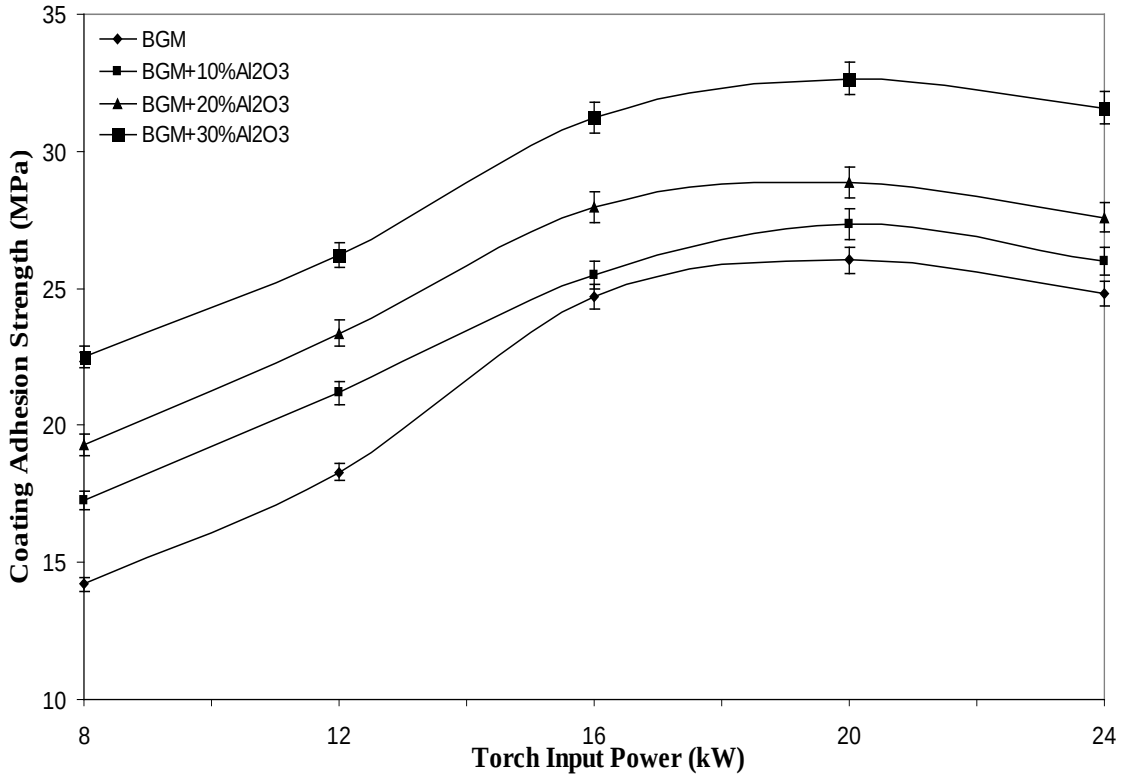


(b) For aluminium substrates

**Figure 4.6** Variation of coating adhesion strength for BGM and BGM-$Al_2O_3$ with torch input power

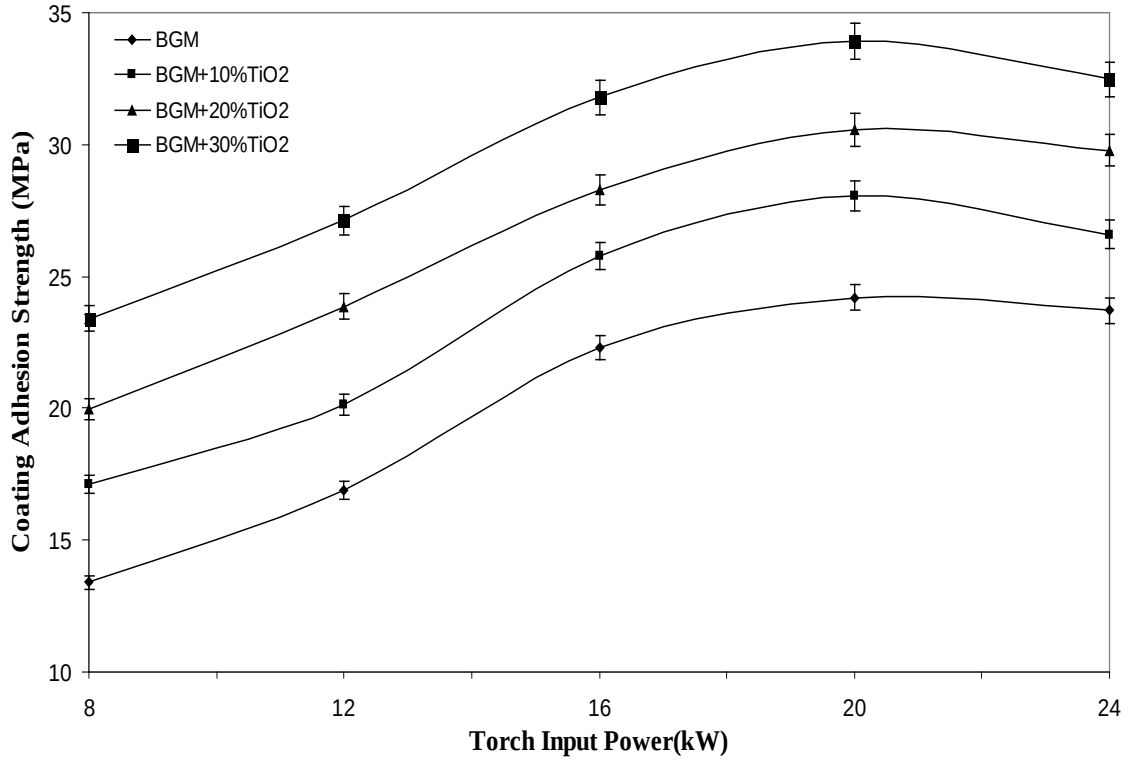


(a) For mild steel substrates

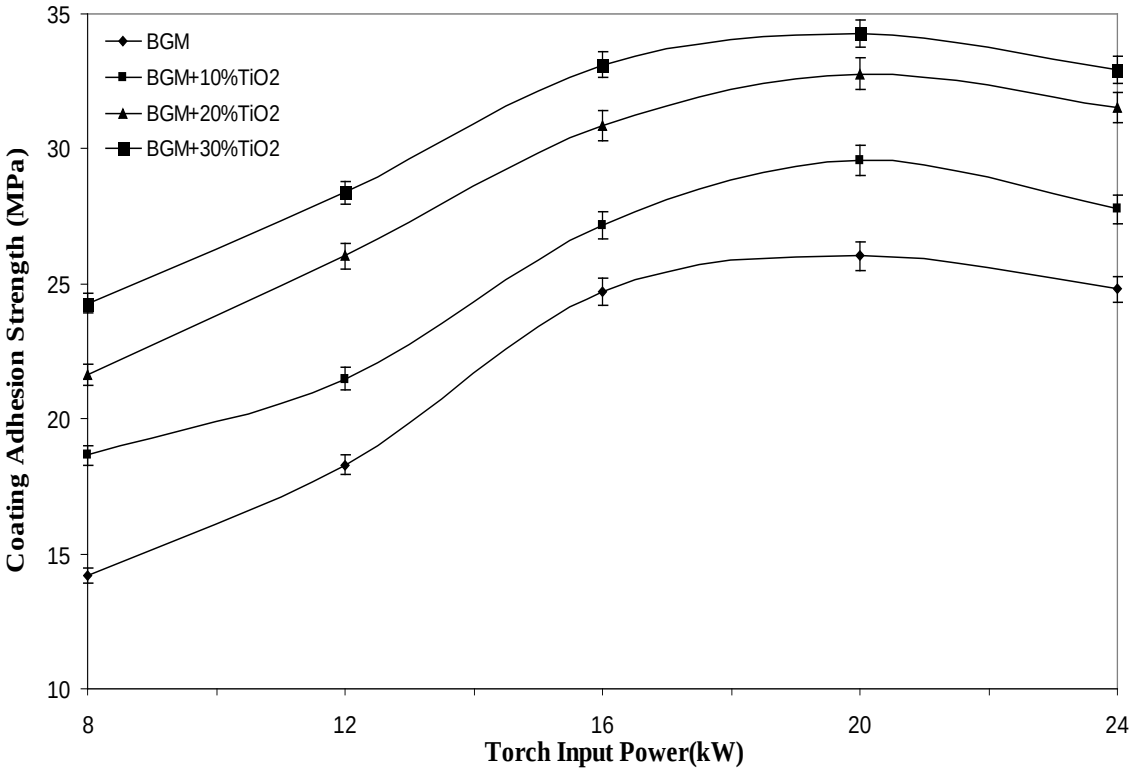


(b) For aluminium substrates

**Figure 4.7** Variation of coating adhesion strength for BGM and BGM-$TiO_2$ with torch input power

**Table 4.1** Coating porosity at different torch input power for different feed materials

| Coating Material | Porosity (%) | | | | |
|---|---|---|---|---|---|
| | **8 kW** | **12 kW** | **16 kW** | **20 kW** | **24 kW** |
| BGM | 8.39 | 7.76 | 6.95 | 7.65 | 7.87 |
| BGM + 10 wt% $Al_2O_3$ | 7.84 | 7.33 | 6.58 | 7.34 | 7.51 |
| BGM + 20 wt% $Al_2O_3$ | 7.63 | 6.99 | 6.37 | 7.10 | 7.35 |
| BGM + 30 wt% $Al_2O_3$ | 7.39 | 6.67 | 6.19 | 6.78 | 7.61 |
| BGM + 10 wt% $TiO_2$ | 6.71 | 6.43 | 5.45 | 6.39 | 6.60 |
| BGM + 20 wt% $TiO_2$ | 6.57 | 5.84 | 5.31 | 6.25 | 6.40 |
| BGM + 30 wt% $TiO_2$ | 6.35 | 5.71 | 5.21 | 5.56 | 6.27 |

[*] *BGM: Borosilicate Glass Micro-spheres*

The variation of coating porosity with torch input power can be explained as follows: during spraying the coating materials melt and travel at high speed and these molten species hit the substrate with a reasonably high impact velocity. On impact, they get flattened and adhere to the surface forming big splats. If the inter-lamellar bonding between these splats is strong and the area of contact between the lamellae is more, then it leads to less amount of porosity. Therefore, although there is decrease in coating thickness, a dense coating is formed. Similar trend of increase in porosity with coating thickness has also been observed by Sarikaya [300] in case of alumina coatings.

X-Ray Diffraction Analysis

To identify the major phases after plasma spraying, the X-ray diffractograms are taken on some of chosen coating samples using a Phillips X-ray Diffractometer with Ni-filtered Cu Kα radiation. Figures 4.8, 4.9 and 4.10 are the typical XRDs obtained for BGM, 'BGM + $Al_2O_3$' and 'BGM + $TiO_2$' coatings. It is seen that the major oxide phases present in the coatings are silica ($SiO_2$) and boron oxides ($B_2O$, $B_2O_3$).

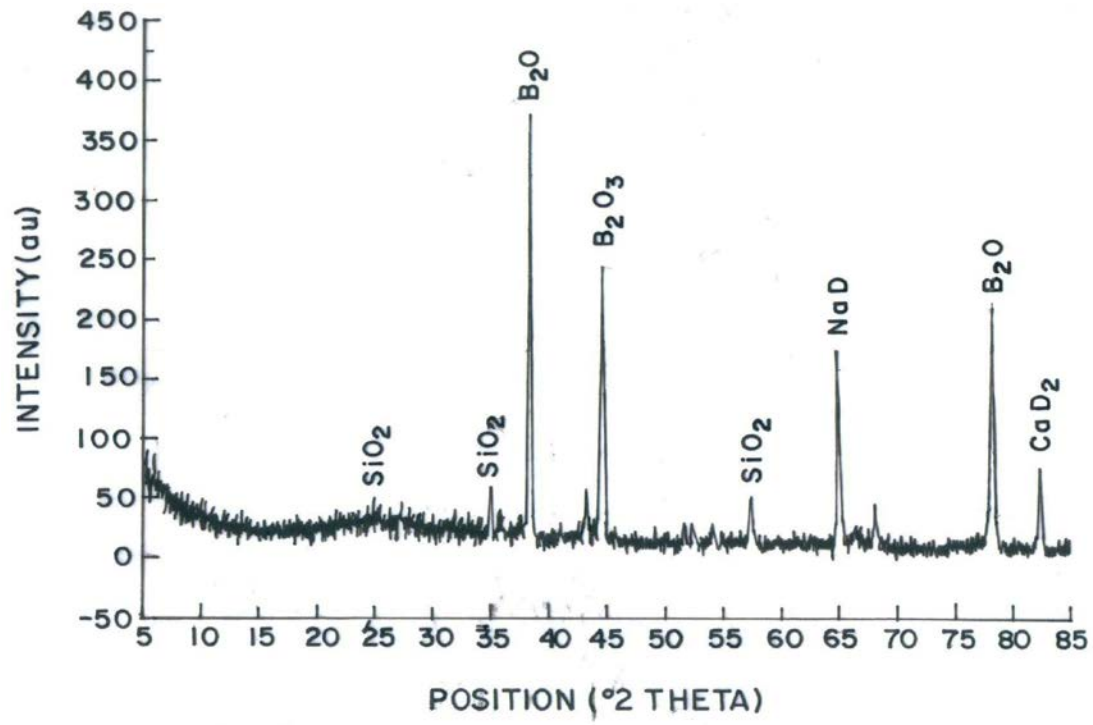


**Figure 4.8** X-ray diffractogram of the BGM coating

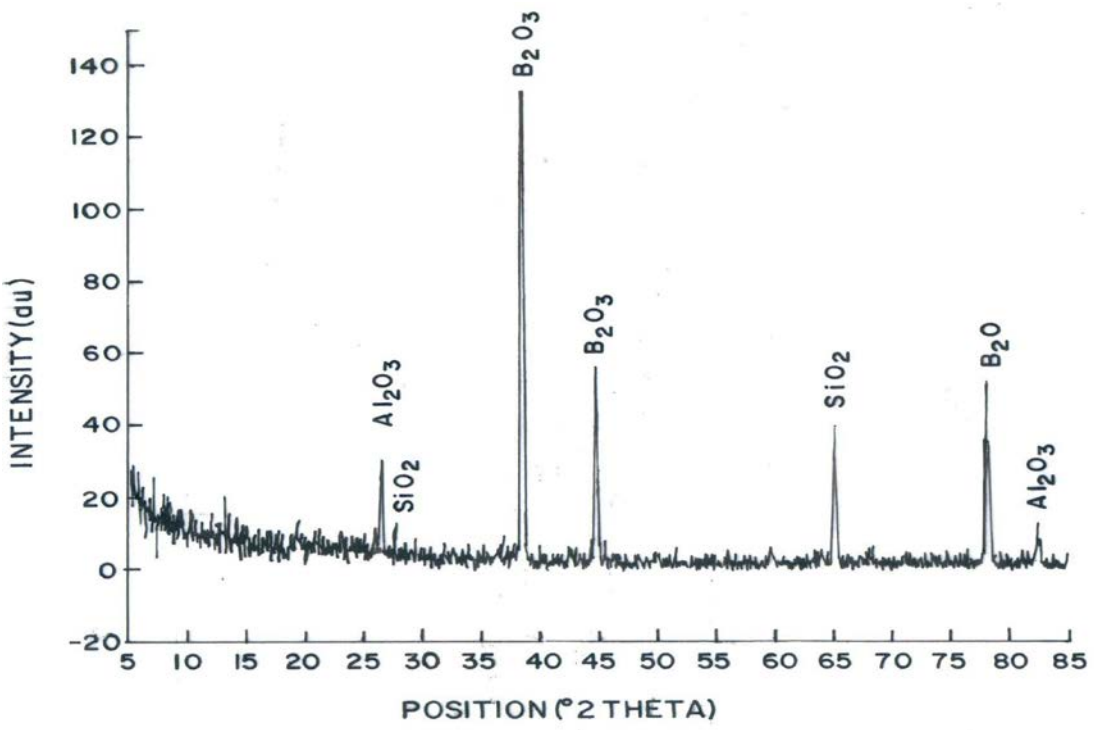


**Figure 4.9** X-ray diffractogram of the BGM-$Al_2O_3$ coating

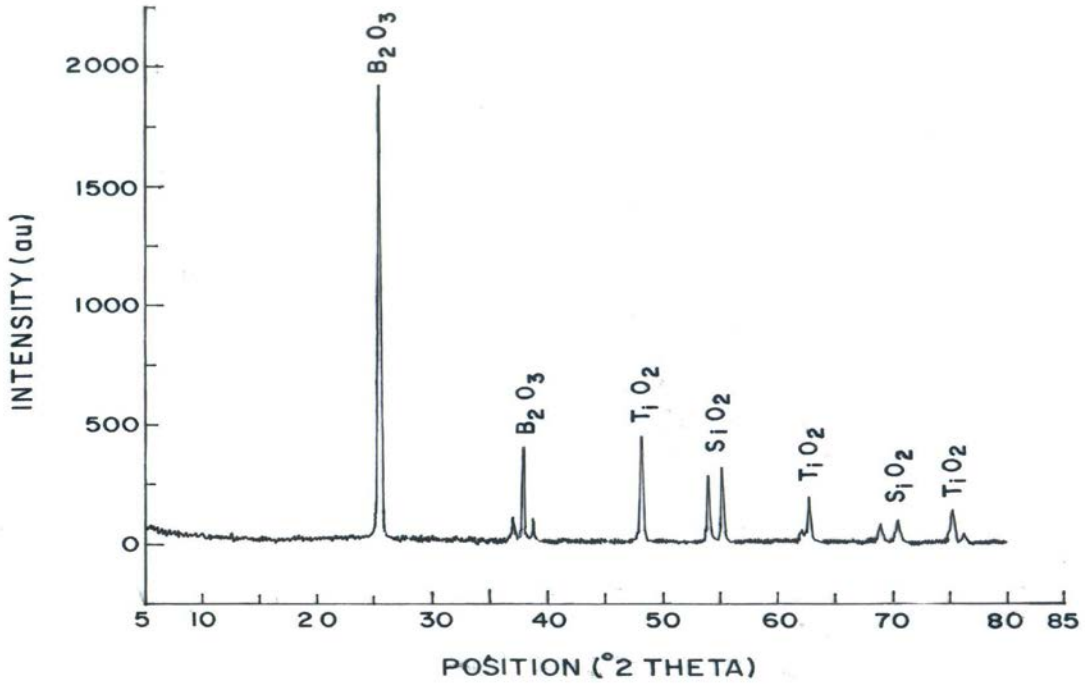


**Figure 4.10** X-ray diffractogram of the BGM-$TiO_2$ coating

**Table 4.2** Coating micro-hardness at different torch input power for different feed materials

| Coating Material | Micro-hardness (GPa) | | | | |
|---|---|---|---|---|---|
| | **8 kW** | **12 kW** | **16 kW** | **20 kW** | **24 kW** |
| BGM | 9.92 | 10.12 | 11.23 | 11.67 | 11.42 |
| BGM + 10 wt% $Al_2O_3$ | 9.55 | 9.81 | 10.98 | 11.41 | 11.12 |
| BGM + 20 wt% $Al_2O_3$ | 9.41 | 9.74 | 10.89 | 11.29 | 11.02 |
| BGM + 30 wt% $Al_2O_3$ | 9.27 | 9.59 | 10.65 | 11.13 | 10.89 |
| BGM + 10 wt% $TiO_2$ | 9.25 | 9.53 | 10.67 | 11.06 | 10.80 |
| BGM + 20 wt% $TiO_2$ | 8.91 | 9.22 | 10.41 | 10.84 | 10.51 |
| BGM + 30 wt% $TiO_2$ | 8.42 | 8.77 | 9.88 | 10.38 | 10.07 |

[*] *BGM: Borosilicate Glass Micro-spheres*

Coating Micro-hardness

Micro-hardness measurement of the metallographically polished coating specimens is made using a Leitz Micro-hardness Tester equipped with a monitor and a microprocessor based controller. Different phases on the coating body bear different hardness values and the average of these values is recorded as the mean hardness of the coating. Each data point therefore is the mean of at least six or seven such readings taken on optically distinguishable phases. The values of coating micro-hardness for different coating materials at different torch input power are shown in Table 4.2. Such variations in coating hardness with input power level have also been reported by previous investigators. [1, 294]

For the glass micro-sphere coatings, the value of coating micro-hardness is found to increase from 9.92 GPa to 11.42 GPa as the torch input power increases from 8 kW to 24 kW. It is also observed that there is slight variation in the bulk hardness of the coatings with the addition of either $Al_2O_3$ or $TiO_2$ to glass micro-spheres in the feed stock. Influence of torch input power in terms of improvement of coating hardness is clearly seen from the results presented in the table.

**Chapter Summary**

This chapter has provided:

- The physical and mechanical characterization of the plasma sprayed coatings of BGM, 'BGM + $Al_2O_3$' and 'BGM + $TiO_2$' on mild steel and aluminium substrates.
- The relative effects of coating material composition and plasma torch input power on various coating characteristics.
- The identification of various phases in the coatings made of materials of different compositions.

The next chapter presents the solid particle erosion characteristics of plasma sprayed glass micro-sphere based coatings.

*****

Chapter 5

Results and Discussion - II

# EROSION WEAR RESPONSE OF PLASMA SPRAYED GLASS MICRO-SPHERE COATINGS

In this chapter solid particle erosion wear characteristics of plasma sprayed BGM, 'BGM + $Al_2O_3$' and 'BGM + $TiO_2$' coatings have been presented. These are investigated experimentally following a test schedule based on the Taguchi technique which is used to acquire the erosion test data in a controlled way. This chapter reports the wear rates obtained from these erosion trials and presents a critical analysis of the test results. Further, predictions of erosion rate under different test conditions following an ANN approach are presented. Correlations among various control factors influencing the erosion rate have also been proposed for predictive purpose. Possible wear mechanisms are identified from the scanning electron microscopy of the eroded surfaces.

## 5.1 Morphology of Coating Surfaces

The morphology of the coated surfaces before and after erosion wear was observed using scanning electron microscopy (SEM) and the micrographs are shown in Figure 5.1. Figures 5.1 (a) and (b) show the features of the uneroded surface of the coating deposited at 20 kW power level in which regions of fully-molten and semi-molten particles are seen. No sizable cracks are noticed on the coating surface; however, some cavities are observed. Particle distribution seems to be uniform along the coating surface. Figures 5.1 (c, d) present the SEM images of eroded surfaces of glass micro-sphere coatings on Al substrates. These micrographs show features like cracks and craters on the worn surface indicating the surface damage due to erosion by silica sand particles. As a result of repeated impact of high velocity erodent particles there is formation of grooves of different sizes. The impact also causes the initiation and subsequent propagation of cracks on the surface as shown. These occurrences collectively lead to the

removal of material by dislodgement of worn particles from the coating surface and the mass loss of the coatings can be attributed to this.

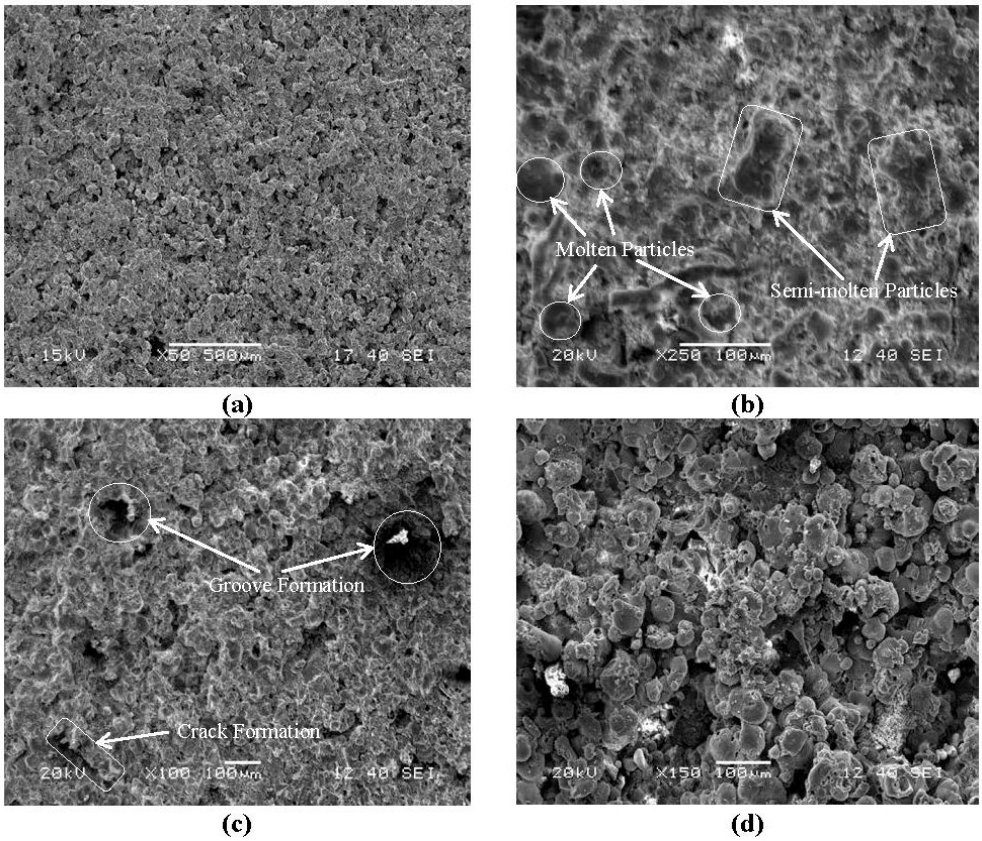


**Figure 5.1** SEM micrographs of uneroded (5.1 a, b)/eroded (5.1 c, d) surfaces of the BGM coatings

SEM micrographs of uneroded and eroded surfaces for the plasma sprayed 'BGM + $Al_2O_3$' coatings deposited at torch input power of 20 kW are shown in Figures 5.2 (a, b) and Figures 5.2 (c, d) respectively. Microstructures obtained are typical of a plasma sprayed surface consisting of splats, which are irregular shaped with distinguished boundaries. A considerable amount of molten and semi molten particles are observed for the uneroded samples. The particles injected into the plasma stream get heated to temperatures much above the melting point of the materials and the molten drops are propelled through the plasma jet. Figures 5.2 (c, d) show SEM micrographs of eroded surfaces of 'BGM + $Al_2O_3$' coatings. As a result of repeated impact of high velocity erodent particles there is formation of grooves of different sizes. However, there is no sign of cracks seen on these micrographs.

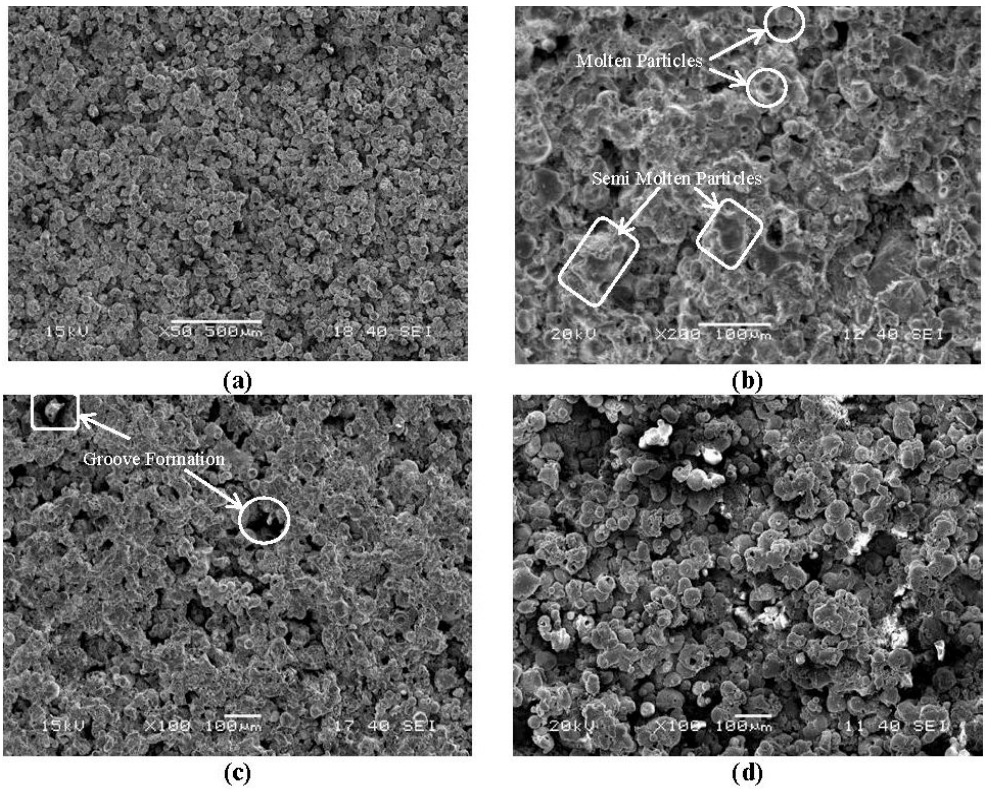


**Figure 5.2** SEM micrographs of uneroded (5.2 a, b) and eroded (5.2 c, d) surfaces of the BGM+$Al_2O_3$ coatings

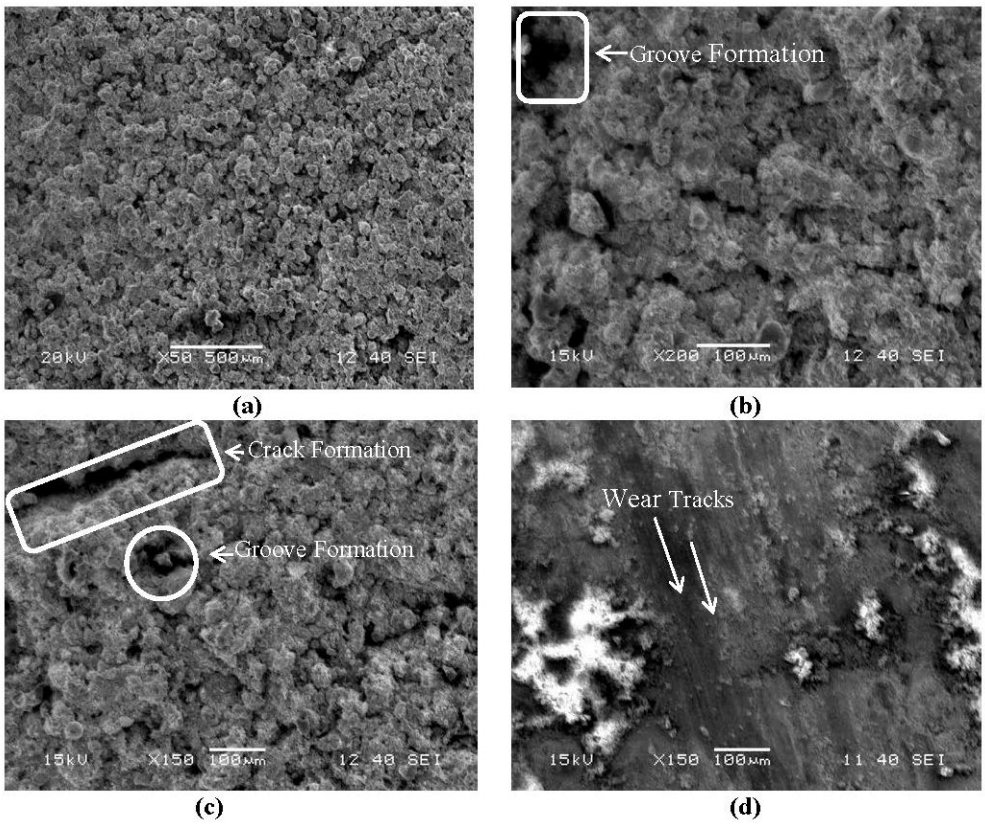


**Figure 5.3** SEM micrographs of uneroded (5.3 a) and eroded (5.3 a, b, c) surfaces of the BGM+$TiO_2$ coatings

SEM micrographs of uneroded and eroded surfaces for the plasma sprayed 'BGM + $TiO_2$' coatings deposited at torch input power of 20 kW are shown in Figure 5.3 (a) and Figures 5.3 (b, c, d) respectively. These microstructures also reveal splats, which are irregular shaped with distinguished boundaries. A considerable amount of molten and semi molten particles are observed on the uneroded coating sample (Figure 5.3 (a)). Figures 5.3 (b, c, d) show SEM micrographs of eroded surfaces of 'BGM + $TiO_2$' coatings. Repeated impact of hard silica sand particles has caused initiation and subsequent propagation of cracks on the surface as shown in Figure 5.3 (c). Figures 5.3 (b) and (c) also show features like grove and crack formation. The magnifications, however, are different for different micrographs. These occurrences collectively lead to the removal of material by dislodgement of worn particles from the coating surface. Wear tracks are often formed on the coating surface as shown in Figure 5.3 (d).

### 5.2 Erosion Test Results and Taguchi Analysis

The erosion wear rates of BGM coatings obtained for all the 16 test runs along with the corresponding signal-to-noise ratio are presented in Table 5.1. Each data point (value of erosion rate) is in fact the average of three replications. This ratio, often abbreviated SNR or S/N is a measure used in science and engineering that compares the level of a desired signal to the level of background noise. It is defined as the ratio of signal power to the noise power, often expressed in decibels. From this table, the overall mean for the S/N ratio of the wear rate is found to be -23.8644 db. This is done using the software MINITAB-14 specifically used for design of experiment applications. The S/N ratio response analysis presented in Table 5.2 indicates the hierarchical order of the control factors as impact velocity (A), impingement angle (B), erodent size (C) and erodent temperature (D) in decreasing order according to their relative significance on the erosion rate. The effects of control factors on erosion rate are graphically shown in Figure 5.4. In this figure, the variation of S/N ratio for every single individual control factor (A, B, C and D) is shown. It also indicates that the erodent temperature (D) has negligible effect on the wear rate. It is evident from Figure 5.4 and the response table, that as far as the erosion rate is concerned, the factor combination $A_1$, $B_1$, $C_1$ and $D_2$ will give the minimum erosion rate for glass micro-sphere coatings.

**Table 5.1** Experimental design using $L_{16}$ orthogonal array and the wear test results for BGM coatings

| Test Run | Impact Velocity (A) m/sec | Impingement Angle (B) degree | Erodent Size (C) µm | Erodent Temperature (D) $^{o}$C | Erosion Rate (ER) mg/kg | S/N Ratio db |
|---|---|---|---|---|---|---|
| 1 | 32 | 30 | 50 | 30 | 8.56667 | -18.6562 |
| 2 | 32 | 45 | 100 | 60 | 10.62868 | -20.5296 |
| 3 | 32 | 60 | 150 | 90 | 13.49236 | -22.6018 |
| 4 | 32 | 90 | 200 | 120 | 16.75004 | -24.4803 |
| 5 | 40 | 30 | 100 | 90 | 12.50006 | -21.9382 |
| 6 | 40 | 45 | 50 | 120 | 14.06929 | -22.9654 |
| 7 | 40 | 60 | 200 | 30 | 19.85718 | -25.9584 |
| 8 | 40 | 90 | 150 | 60 | 17.48883 | -24.8552 |
| 9 | 48 | 30 | 150 | 120 | 14.92867 | -23.4804 |
| 10 | 48 | 45 | 200 | 90 | 15.53333 | -23.8253 |
| 11 | 48 | 60 | 50 | 60 | 16.25003 | -24.2171 |
| 12 | 48 | 90 | 100 | 30 | 19.46154 | -25.7835 |
| 13 | 56 | 30 | 200 | 60 | 17.99984 | -25.1054 |
| 14 | 56 | 45 | 150 | 30 | 18.08336 | -25.1456 |
| 15 | 56 | 60 | 100 | 120 | 19.33333 | -25.7261 |
| 16 | 56 | 90 | 50 | 90 | 21.28575 | -26.5618 |

**Table 5.2** S/N ratio response table for erosion rate of BGM coatings

| Level | A | B | C | D |
|---|---|---|---|---|
| 1 | -21.57 | -22.30 | -23.10 | -23.89 |
| 2 | -23.93 | -23.12 | -23.49 | -23.68 |
| 3 | -24.33 | -24.63 | -24.02 | -23.73 |
| 4 | -25.63 | -25.42 | -24.84 | -24.16 |
| Delta | 4.07 | 3.13 | 1.74 | 0.49 |
| **Rank** | **1** | **2** | **3** | **4** |

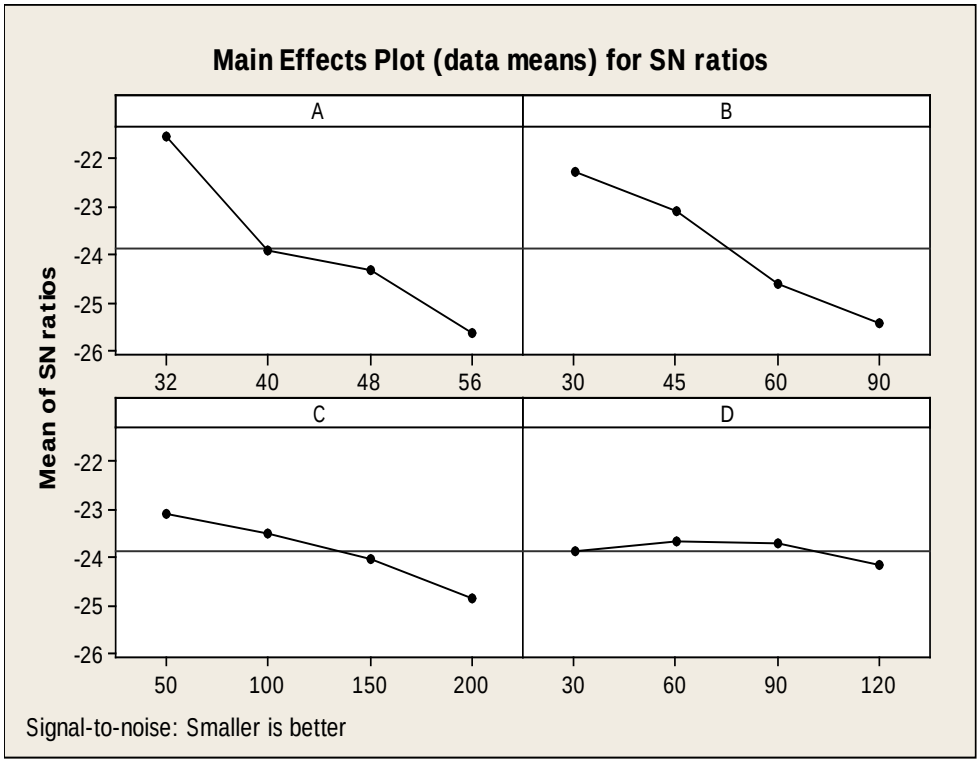


**Figure 5.4** Effect of control factors on erosion rate for BGM coatings

The results of erosion experiments carried out according to the predetermined design on BGM coatings premixed with $Al_2O_3$ and $TiO_2$ particles are presented in Table 5.3. This table provides the experimental erosion rate along with the signal-to-noise ratio for each individual test run. The overall mean of the S/N ratios for 'BGM + $Al_2O_3$' coating is found to be -24.3731 db and for 'BGM + $TiO_2$' coating is found to be -25.2253 db.

The S/N ratio response analyses are presented in Tables 5.4 and 5.5 for 'BGM + $Al_2O_3$' and 'BGM + $TiO_2$' coatings respectively. These tables show the hierarchical order of the control factors as impact velocity (A), impingement angle (B), erodent size (C), feed stock composition (E) and erodent temperature (D) in decreasing order according to their significance on the erosion rate for both the coatings. It can thus be concluded that the erodent temperature (D) has negligible effect on the wear rate.

**Table 5.3** Experimental design using $L_{16}$ orthogonal array and the wear test results for 'BGM + $Al_2O_3$' and 'BGM + $TiO_2$' coatings

| Test Run | A | B | C | D | E | BGM + $Al_2O_3$ | | BGM + $TiO_2$ | |
|---|---|---|---|---|---|---|---|---|---|
| | | | | | | ER | S/N Ratio | ER | S/N ratio |
| 1 | 32 | 30 | 50 | 30 | 0 | 8.56667 | -18.6562 | 8.56667 | -18.6562 |
| 2 | 32 | 45 | 100 | 60 | 10 | 11.65643 | -21.3313 | 13.05603 | -22.3162 |
| 3 | 32 | 60 | 150 | 90 | 20 | 14.23695 | -23.0683 | 16.30952 | -24.2488 |
| 4 | 32 | 90 | 200 | 120 | 30 | 17.04751 | -24.6332 | 19.14727 | -25.6421 |
| 5 | 40 | 30 | 100 | 90 | 30 | 13.34126 | -22.5039 | 15.12634 | -23.5947 |
| 6 | 40 | 45 | 50 | 120 | 20 | 15.56129 | -23.8409 | 17.11569 | -24.6679 |
| 7 | 40 | 60 | 200 | 30 | 10 | 20.98768 | -26.4393 | 21.99968 | -26.8483 |
| 8 | 40 | 90 | 150 | 60 | 0 | 18.81183 | -25.4886 | 20.78683 | -26.3558 |
| 9 | 48 | 30 | 150 | 120 | 10 | 16.23178 | -24.2073 | 18.17823 | -25.1910 |
| 10 | 48 | 45 | 200 | 90 | 0 | 16.53376 | -24.3674 | 18.37653 | -25.2853 |
| 11 | 48 | 60 | 50 | 60 | 30 | 17.43003 | -24.8260 | 19.00493 | -25.5773 |
| 12 | 48 | 90 | 100 | 30 | 20 | 20.46321 | -26.2195 | 22.77321 | -27.1485 |
| 13 | 56 | 30 | 200 | 60 | 20 | 19.00984 | -25.5796 | 21.41234 | -26.6133 |
| 14 | 56 | 45 | 150 | 30 | 30 | 19.14336 | -25.6404 | 21.84363 | -26.7865 |
| 15 | 56 | 60 | 100 | 120 | 0 | 20.44331 | -26.2110 | 22.46531 | -27.0302 |
| 16 | 56 | 90 | 50 | 90 | 10 | 22.27585 | -26.9567 | 24.10505 | -27.6422 |

***Note :*** *Factor A : Impact Velocity (m/sec), Factor B: Impingement Angle (degree)*
*Factor C : Erodent Size (µm), Factor D : Erodent Temperature ($^oC$)*
*Factor E : $Al_2O_3$/ $TiO_2$ Content in the feedstock (wt%)*
*ER : Erosion Rate (mg/kg), S/N Ratio : Signal to Noise Ratio (db)*
*BGM: Borosilicate glass micro-sphere*

**Table 5.4** S/N ratio response table for erosion rate of 'BGM + $Al_2O_3$' coatings

| Level | A | B | C | D | E |
|---|---|---|---|---|---|
| 1 | -21.92 | -22.74 | -23.57 | -24.24 | -23.68 |
| 2 | -24.57 | -23.80 | -24.07 | -24.31 | -24.73 |
| 3 | -24.91 | -25.14 | -24.60 | -24.22 | -24.68 |
| 4 | -26.10 | -25.82 | -25.25 | -24.72 | -24.40 |
| Delta | 4.17 | 3.09 | 1.68 | 0.50 | 1.05 |
| **Rank** | **1** | **2** | **3** | **5** | **4** |

**Table 5.5** S/N ratio response table for erosion rate of 'BGM + $TiO_2$' coatings

| Level | A | B | C | D | E |
|---|---|---|---|---|---|
| 1 | -22.72 | -23.51 | -24.14 | -24.86 | -24.33 |
| 2 | -25.37 | -24.76 | -25.02 | -25.22 | -25.50 |
| 3 | -25.80 | -25.93 | -25.65 | -25.19 | -25.67 |
| 4 | -27.02 | -26.70 | -26.10 | -25.63 | -25.40 |
| Delta | 4.30 | 3.18 | 1.96 | 0.77 | 1.34 |
| **Rank** | **1** | **2** | **3** | **5** | **4** |

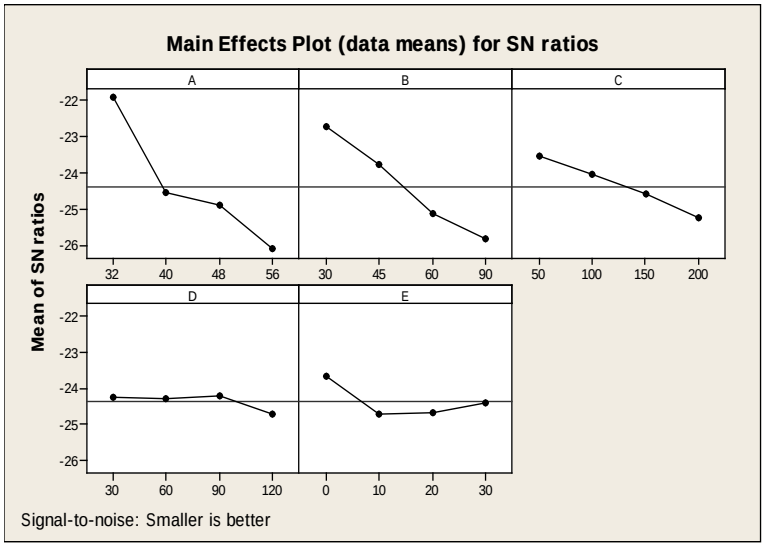


**Figure 5.5** Effect of control factors on erosion rate for 'BGM + $Al_2O_3$'coatings

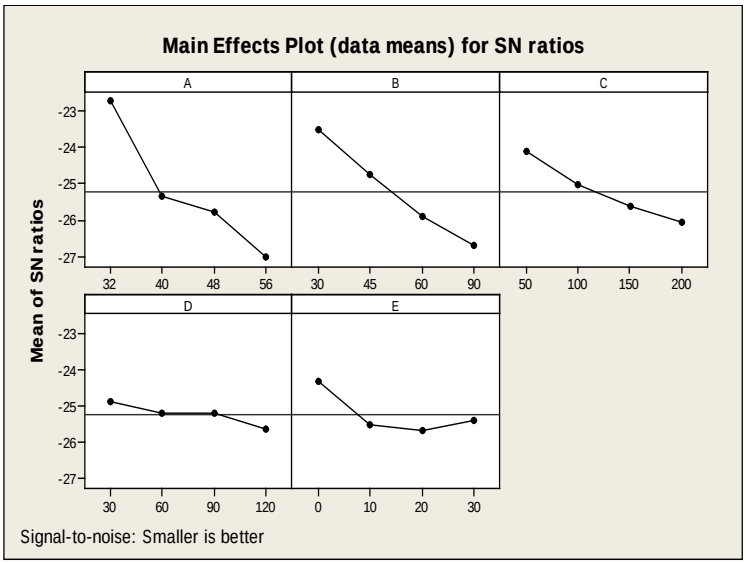


**Figure 5.6** Effect of control factors on erosion rate for 'BGM + $TiO_2$'coatings

Figures 5.5 and 5.6 illustrate the effect of control factors on erosion rate for 'BGM + $Al_2O_3$' and 'BGM + $TiO_2$' coatings respectively. Analysis of the results leads to the conclusion that factor combination of $A_1$ (Impact velocity), $B_1$ (Impingement angle), $C_1$(Erodent size), $D_3$ (Erodent temperature) and $E_1$ (Alumina content in the feedstock) gives minimum erosion rate (Figure 5.5) for 'BGM + $Al_2O_3$' coatings and factor combination $A_1$ (Impact velocity), $B_1$ (Impingement angle), $C_1$(Erodent size), $D_1$ (Erodent temperature) and $E_1$ (Titania content in the feedstock) gives minimum erosion rate (Figure 5.6) for 'BGM + $TiO_2$' coatings.

### 5.3 Confirmation Experiment

The confirmation experiment is the final test in the design-of-experiment process. The purpose of the confirmation experiment is to validate the conclusions drawn during the analysis phase. It is performed by considering a new arbitrary set of factors other than the optimal factor setting to evaluate the erosion rate. For this investigation $A_2B_3C_4D_1$, $A_2B_3C_4E_2$ and $A_2B_4C_3E_3$ for BGM, 'BGM + $Al_2O_3$' and 'BGM + $TiO_2$' coatings respectively are chosen as the arbitrary sets considering which a prediction equation can be formulated using Taguchi's approach to estimate S/N ratio for erosion rate as [301]:

$$\overline{\eta_1} = \overline{T} + \left(\overline{A_2} - \overline{T}\right) + \left(\overline{B_3} - \overline{T}\right) + \left(\overline{C_4} - \overline{T}\right) + \left(\overline{D_1} - \overline{T}\right) \quad \textbf{(5.1)}$$

$$\overline{\eta_2} = \overline{T} + \left(\overline{A_2} - \overline{T}\right) + \left(\overline{B_3} - \overline{T}\right) + \left(\overline{C_4} - \overline{T}\right) + \left(\overline{E_2} - \overline{T}\right) \quad \textbf{(5.2)}$$

$$\overline{\eta_3} = \overline{T} + \left(\overline{A_2} - \overline{T}\right) + \left(\overline{B_4} - \overline{T}\right) + \left(\overline{C_3} - \overline{T}\right) + \left(\overline{E_3} - \overline{T}\right) \quad \textbf{(5.3)}$$

| | |
|---|---|
| $\overline{\eta_1}, \overline{\eta_2}, \overline{\eta_3}$ | Predicted average for BGM, 'BGM + $Al_2O_3$' and 'BGM + $TiO_2$' coatings respectively |
| $\overline{T}$ | Overall experimental average |
| $\overline{A}, \overline{B}, \overline{C}, \overline{D}, \overline{E}$ | Mean response for factors |

By combining like terms, the equations reduce to

$$\overline{\eta_1} = \overline{A_2} + \overline{B_3} + \overline{C_4} + \overline{D_1} - 3\overline{T} \quad \textbf{(5.4)}$$

$$\overline{\eta_2} = \overline{A_2} + \overline{B_3} + \overline{C_4} + \overline{E_2} - 3\overline{T} \quad \textbf{(5.5)}$$

$$\overline{\eta_3} = \overline{A_2} + \overline{B_4} + \overline{C_3} + \overline{E_3} - 3\overline{T} \quad \textbf{(5.6)}$$

**Table 5.6** Results of the confirmation experiments for erosion rate

| | Optimal Control Parameters | | | | | |
|---|---|---|---|---|---|---|
| | BGM Coatings | | BGM+$Al_2O_3$ Coatings | | BGM+$TiO_2$ Coatings | |
| | Pred. | Exp. | Pred. | Exp. | Pred. | Exp. |
| Level | $A_2B_3C_4D_1$ | $A_2B_3C_4D_1$ | $A_2B_3C_4E_2$ | $A_2B_3C_4E_2$ | $A_2B_4C_3E_3$ | $A_2B_4C_3E_3$ |
| S/N ratio for erosion rate (db) | -25.6902 | -25.9921 | -26.4393 | -26.9207 | -27.3377 | -28.2514 |
| Percentage Error | 1.16 % | | 1.78 % | | 3.20 % | |

For these chosen combinations of factors, the S/N ratios for BGM, 'BGM + $Al_2O_3$' and 'BGM + $TiO_2$' coatings are found to be -25.6902, -26.4393 and -27.3377 db respectively. Further, an experiment is also conducted taking the same factor combination and the test results are compared with value obtained from the predictive Equations 5.4, 5.5 and 5.6. The comparison of the experimental and the predicted results along with the associated error percentage are given in Table 5.6. Errors of 1.16, 1.78 and 3.20 % in S/N ratios are recorded for erosion rates of BGM, 'BGM + $Al_2O_3$' and 'BGM + $TiO_2$' coatings respectively. The errors can be further reduced if the number of measurements is increased. The proposed correlations are thus capable of predicting erosion rate to a reasonable accuracy.

### 5.4 Wear Rate Estimation using Predictive Equation

The solid particle erosion wear rate of the coated sample can also be predicted using a nonlinear regressive predictive equation showing the relationship

between the erosion rate and the individual control factors. This correlation is developed statistically using the standard software SYSTAT 7. In order to express the erosion rate in terms of a nonlinear regressive mathematical equation, the following form is suggested:

$$ER = k_0 + k_1 \times A + k_2 \times B + k_3 \times C + k_4 \times D + k_5 \times E \quad \textbf{(5.7)}$$

Here, ER is the performance output term i.e. the erosion rate in mg/kg and $k_i$ (i = 0, 1, 2, 3, 4, 5) are the model constants. A is the impact velocity (m/sec), B is the impingement angle (degree), C is the erodent size (micron) and D is the erodent temperature ($^0$C) and E is the $Al_2O_3$/ $TiO_2$ content in the feedstock (wt%).

By using the software, the values of all of the constants are calculated and the final nonlinear regression expressions for the BGM, 'BGM + $Al_2O_3$' and 'BGM + $TiO_2$' coatings are obtained by the Equations 5.8, 5.9 and 5.10 respectively.

$$ER = -2.516 + 0.263 \times A + 0.091 \times B + 0.016 \times C - 0.002 \times D \quad \textbf{(5.8)}$$

$$ER = -2.72 + 0.282 \times A + 0.091 \times B + 0.016 \times C + 0 \times D + 0.014 \times E \quad \textbf{(5.9)}$$

$$ER = -4.042 + 0.317 \times A + 0.099 \times B + 0.019 \times C + 0.003 \times D + 0.039 \times E \quad \textbf{(5.10)}$$

The correctness of the calculated constants is confirmed because very high correlation coefficients ($r^2$) of 0.996, 0.995 and 0.996 for the BGM, 'BGM + $Al_2O_3$' and 'BGM + $TiO_2$' coatings respectively are obtained for Equation (5.7); therefore, the models are quite suitable for further analysis. A comparison between the wear rate obtained from experimental results and the predictive equations for all three coating types are shown in Table 5.7, which indicates that the percentage error associated with the predicted values with respect to the experimental one varies in the range of 0 to 12 %.

**Table 5.7** Comparison of experimental and predicted values for erosion rate

| BGM | | | BGM + $Al_2O_3$ | | | BGM + $TiO_2$ | | |
|---|---|---|---|---|---|---|---|---|
| **ER Exp.** | **ER Pred.** | **% Error** | **ER Exp.** | **ER Pred.** | **% Error** | **ER Exp.** | **ER Pred.** | **% Error** |
| 8.56667 | 9.371 | 9.389 | 8.56667 | 9.487 | 10.743 | 8.56667 | 9.122 | 6.482 |
| 10.62868 | 11.475 | 7.962 | 11.65643 | 12.139 | 4.140 | 13.05603 | 13.027 | 0.222 |
| 13.49236 | 13.58 | 0.649 | 14.23695 | 14.444 | 1.454 | 16.30952 | 15.942 | 2.253 |
| 16.75004 | 17.05 | 1.790 | 17. 04751 | 18.114 | 6.256 | 19. 14727 | 20.342 | 6.256 |
| 12.50006 | 12.154 | 2.768 | 13.34126 | 13.31 | 0.234 | 15. 12634 | 14.948 | 1.179 |
| 14.06929 | 12.659 | 10.023 | 15.56129 | 13.735 | 11.736 | 17.11569 | 15.183 | 11.291 |
| 19.85718 | 18.923 | 4.704 | 20.98768 | 19.56 | 6.802 | 21.99968 | 20.858 | 5.189 |
| 17.48883 | 18.474 | 5.633 | 18.81183 | 19.15 | 1.798 | 20.78683 | 20.578 | 1.004 |
| 14.92867 | 14.998 | 0.464 | 16.23178 | 16.086 | 0.898 | 18. 17823 | 17.744 | 2.388 |
| 15.53333 | 17.223 | 10.877 | 16.53376 | 18.111 | 9.540 | 18. 37653 | 19.699 | 7.196 |
| 16.25003 | 16.248 | 0.124 | 17.43003 | 17.496 | 0.379 | 19.00493 | 19.414 | 2.152 |
| 19.46154 | 19.838 | 1.934 | 20.46321 | 20.886 | 2.066 | 22.77321 | 22.854 | 0.354 |
| 17.99984 | 18.022 | 0.123 | 19.00984 | 19.282 | 1.432 | 21.41234 | 21.44 | 0.129 |
| 18.08336 | 18.647 | 3.116 | 19.14336 | 19.987 | 4.407 | 21.84363 | 22.275 | 1.974 |
| 19.33333 | 19.032 | 1.558 | 20.44331 | 20.132 | 1.523 | 22.46531 | 21.91 | 2.471 |
| 21.28575 | 21.022 | 1.239 | 22.27585 | 22.202 | 0.332 | 24.10505 | 24.23 | 0.518 |

***Note:*** *ER: Erosion Rate (mg/kg)*

*BGM: Borosilicate glass micro-sphere*

## 5.5 ANN Based Prediction

As mentioned earlier, artificial neural network (ANN) is a technique that involves database training to predict input-output evolutions. In this attempt to simulate the erosion wear process and to predict the erosion rate for BGM, 'BGM + $Al_2O_3$' and 'BGM + $TiO_2$' coatings under different operating conditions, certain input parameters are taken each of which is characterized by one neuron in the input layer of the ANN structure. Different ANN structures with varying number of neurons in the hidden layer are tested at constant cycles, learning rate, error tolerance, momentum parameter, noise factor and slope parameter. Based on least error criterion, three ANN structures (one structure for each coating type) shown in Tables 5.8, 5.9 and 5.10 are selected for training of the input-output data for different types of coatings.

**Table 5.8** Input parameters for training (BGM coatings)

| Input Parameters for Training | Values |
|---|---|
| Error tolerance | 0.003 |
| Learning rate (β) | 0.002 |
| Momentum parameter (α) | 0.002 |
| Noise factor (NF) | 0.001 |
| Number of epochs | 1,00,00,000 |
| Slope parameter (£) | 0.6 |
| Number of hidden layer neurons (H) | 7 |
| Number of input layer neurons (I) | 4 |
| Number of output layer neurons (O) | 1 |

**Table 5.9** Input parameters for training ('BGM + $Al_2O_3$' coatings)

| Input Parameters for Training | Values |
|---|---|
| Error tolerance | 0.003 |
| Learning rate (β) | 0.002 |
| Momentum parameter (α) | 0.002 |
| Noise factor (NF) | 0.001 |
| Number of epochs | 1,00,00,000 |
| Slope parameter (£) | 0.6 |
| Number of hidden layer neurons (H) | 7 |
| Number of input layer neurons (I) | 5 |
| Number of output layer neurons (O) | 1 |

**Table 5.10** Input parameters for training ('BGM + $TiO_2$' coatings)

| Input Parameters for Training | Values |
|---|---|
| Error tolerance | 0.003 |
| Learning rate (β) | 0.002 |
| Momentum parameter (α) | 0.002 |
| Noise factor (NF) | 0.001 |
| Number of epochs | 1,00,00,000 |
| Slope parameter (£) | 0.6 |
| Number of hidden layer neurons (H) | 9 |
| Number of input layer neurons (I) | 5 |
| Number of output layer neurons (O) | 1 |

The optimized three-layer neural network used in these simulations is shown in Figures 5.7, 5.8 and 5.9 which are for the three different types of coatings taken in this study. A software package NEURALNET for neural computing based on back propagation algorithm is used as the prediction tool for erosion wear rate of the coatings under various test conditions.

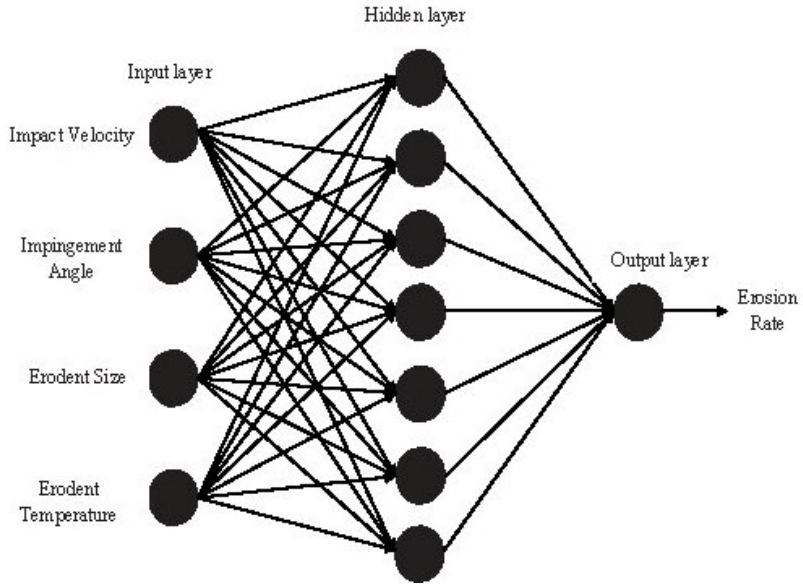


**Figure 5.7** Three layer neural network (BGM coatings)

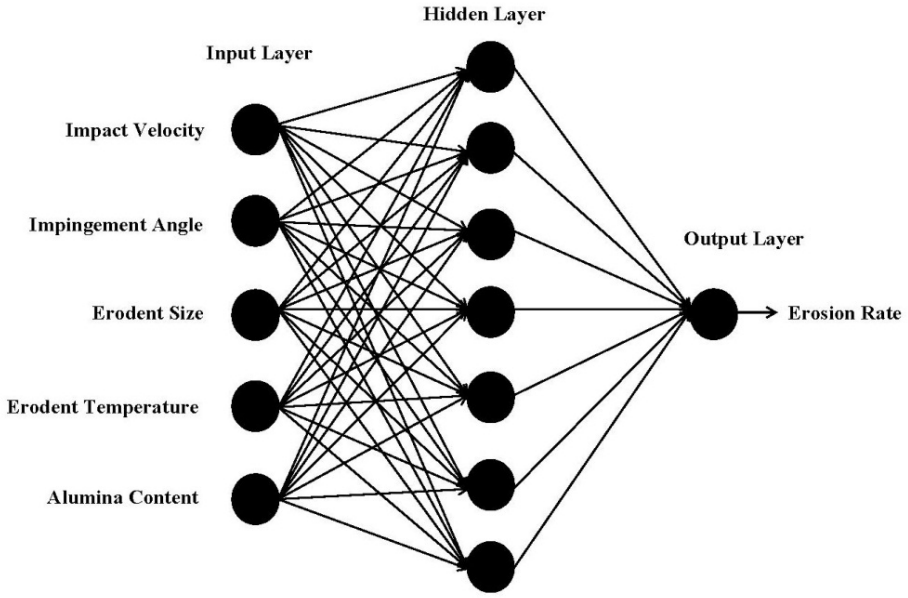


**Figure 5.8** Three layer neural network ('BGM + $Al_2O_3$' coatings)

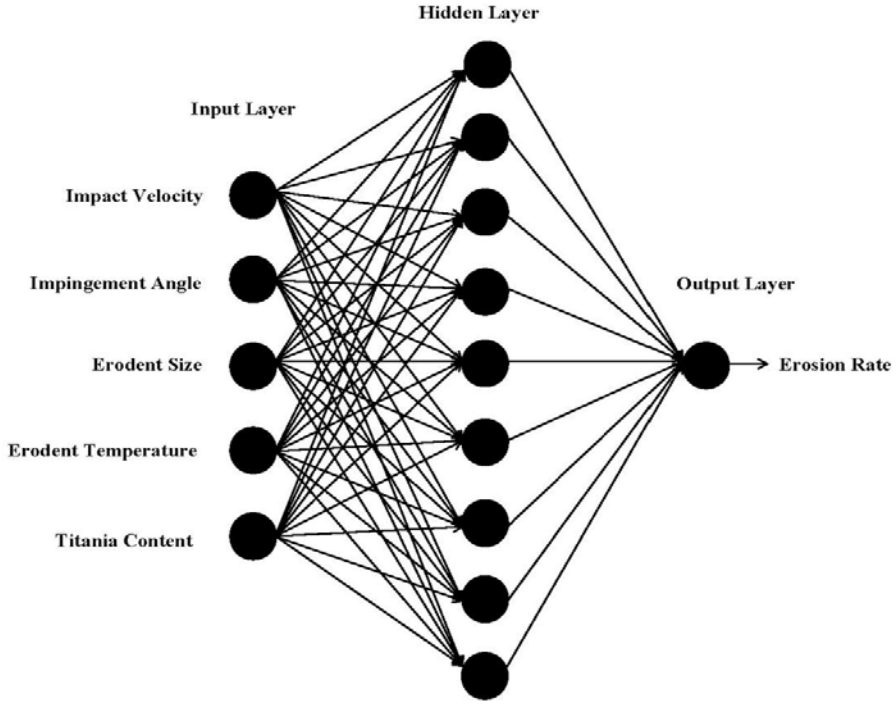


**Figure 5.9** Three layer neural network ('BGM + $TiO_2$' coatings)

The ANN predictive results of erosion wear rate for all the 16 test conditions and for all the coating combinations are shown and compared with the corresponding experimental values along with the associated percentage errors in Table 5.11. It is observed that the errors lie in the range of 0-10%, which establishes the validity of the neural computation. The errors, however, can still be reduced and the quality of predictions can be further improved by enlarging the data sets and optimizing the construction of the neural network.

A well-trained ANN is expected to be very helpful for the analysis of erosion wear characteristics of any given coating and permits to study quantitatively the effect of each of the considered input parameters on the wear rate. The range of any chosen parameter can be beyond the actual experimental limits, thus offering the possibility to use the generalization property of ANN in a large parameter space. In the present investigation, this possibility has been explored by selecting the most significant factor i.e. the impact velocity in a range from 25 to 75

m/sec. Sets of predictions for erosion wear rate of BGM, 'BGM + $Al_2O_3$' and 'BGM + $TiO_2$' coatings at different impact velocities are evolved and the predicted evolutions for different impingement angles and erodent sizes are presented in Figures 5.10, 5.11 and 5.12 respectively. It is interesting to see that the erosion rate presents either a linear or an exponential type evolution with the impact velocity.

**Table 5.11** Percentage error between experimental results and ANN predictions

| **BGM** | | | **BGM + $Al_2O_3$** | | | **BGM + $TiO_2$** | | |
|---|---|---|---|---|---|---|---|---|
| **ER Exp.** | **ER ANN** | **% Error** | **ER Exp.** | **ER ANN** | **% Error** | **ER Exp.** | **ER ANN** | **% Error** |
| 8.56667 | 8.7379 | 1.9987 | 8.56667 | 9.0548 | 5.6980 | 8.56667 | 9.2277 | 7.6812 |
| 10.62868 | 11.6231 | 9.3560 | 11.65643 | 11.7859 | 1.1107 | 13.05603 | 13.4704 | 3.1738 |
| 13.49236 | 14.3790 | 6.5714 | 14.23695 | 13.254 | 6.9042 | 16.30952 | 16.0329 | 1.6961 |
| 16.75004 | 16.8280 | 0.4654 | 17. 04751 | 18.4587 | 8.2779 | 19. 14727 | 19.3998 | 1.3189 |
| 12.50006 | 12.0978 | 3.2180 | 13.34126 | 13.3369 | 0.0326 | 15. 12634 | 15.4844 | 2.3671 |
| 14.06929 | 12.8433 | 8.7139 | 15.56129 | 14.589 | 6.2481 | 17.11569 | 16.3429 | 4.5151 |
| 19.85718 | 18.1766 | 8.4633 | 20.98768 | 21.4589 | 2.2452 | 21.99968 | 20.8326 | 5.3049 |
| 17.48883 | 18.1392 | 3.7187 | 18.81183 | 18.1495 | 3.5208 | 20.78683 | 20.0772 | 3.4138 |
| 14.92867 | 15.4408 | 3.4305 | 16.23178 | 15.5895 | 3.9569 | 18. 17823 | 17.9658 | 1.1686 |
| 15.53333 | 16.1932 | 4.2480 | 16.53376 | 16.4859 | 0.2894 | 18. 37653 | 19.1823 | 4.3848 |
| 16.25003 | 16.2124 | 0.2315 | 17.43003 | 17.2458 | 1.0569 | 19.00493 | 19.3803 | 1.9751 |
| 19.46154 | 19.5264 | 0.3332 | 20.46321 | 21.5487 | 5.3045 | 22.77321 | 21.6862 | 4.7732 |
| 17.99984 | 17.7275 | 1.5130 | 19.00984 | 18.865 | 0.7619 | 21.41234 | 20.7916 | 2.8989 |
| 18.08336 | 19.0410 | 5.2956 | 19.14336 | 20.0014 | 4.4821 | 21.84363 | 21.4276 | 1.9046 |
| 19.33333 | 20.8075 | 7.6250 | 20.44331 | 20.221 | 1.0874 | 22.46531 | 22.6418 | 0.7856 |
| 21.28575 | 21.4066 | 0.5677 | 22.27585 | 24.3568 | 9.3417 | 24.10505 | 24.3157 | 0.8739 |

***Note:*** *ER: Erosion Rate (mg/kg)*

*BGM: Borosilicate glass micro-sphere*

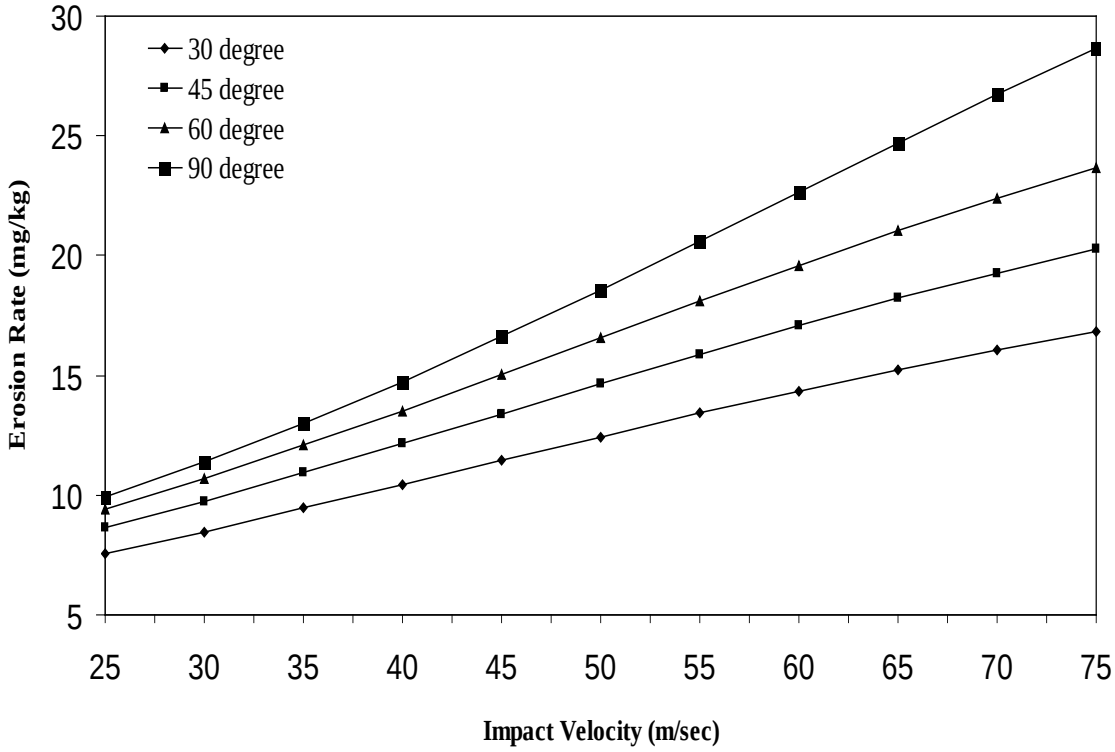


**(a)**

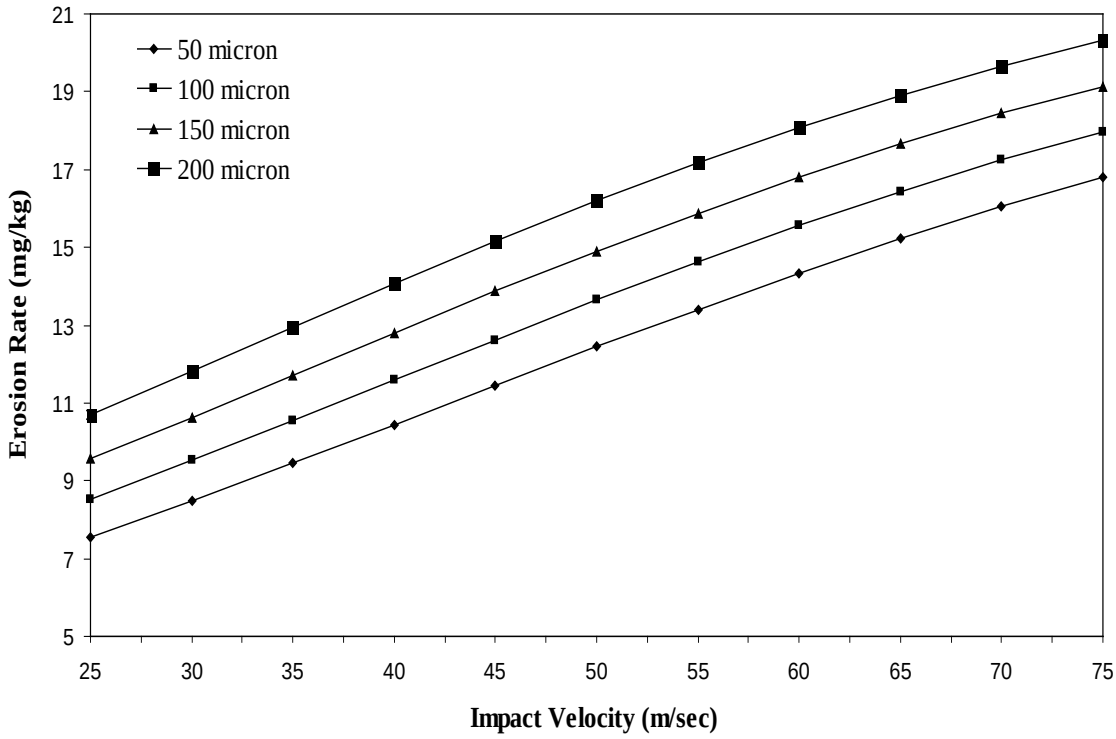


**(b)**

**Figure 5.10** Effect of impact velocity on erosion rate for different (a) impingement angle (b) erodent size for BGM coatings

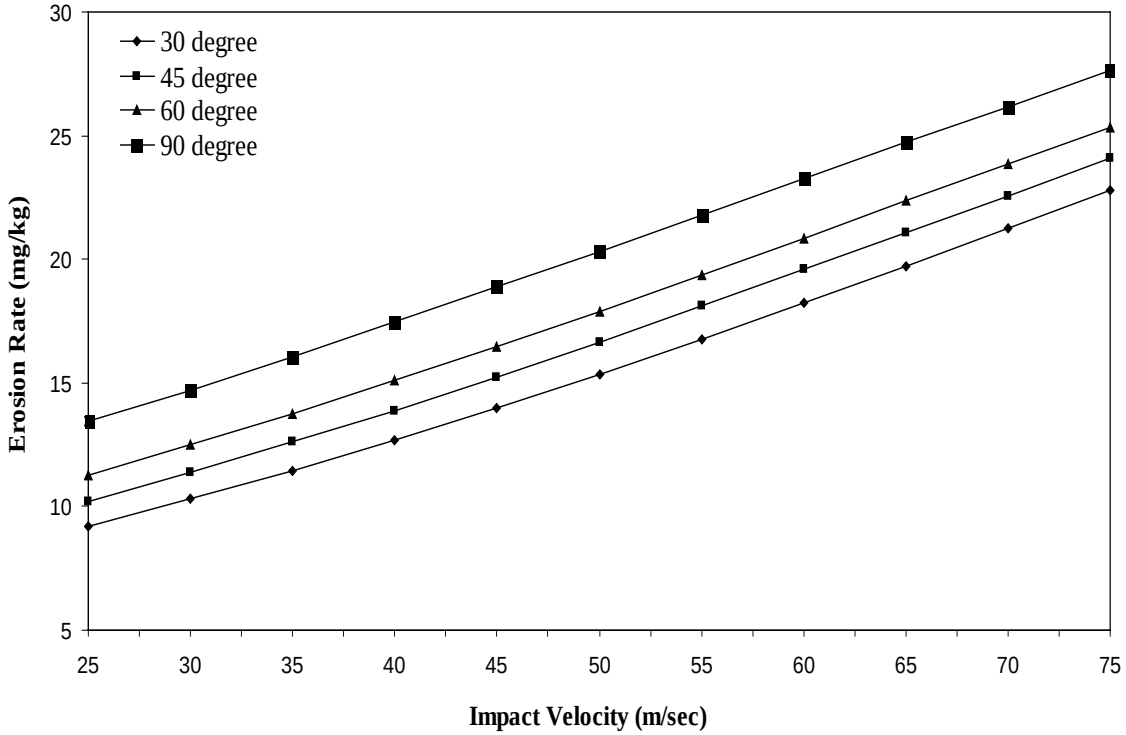


**(a)**

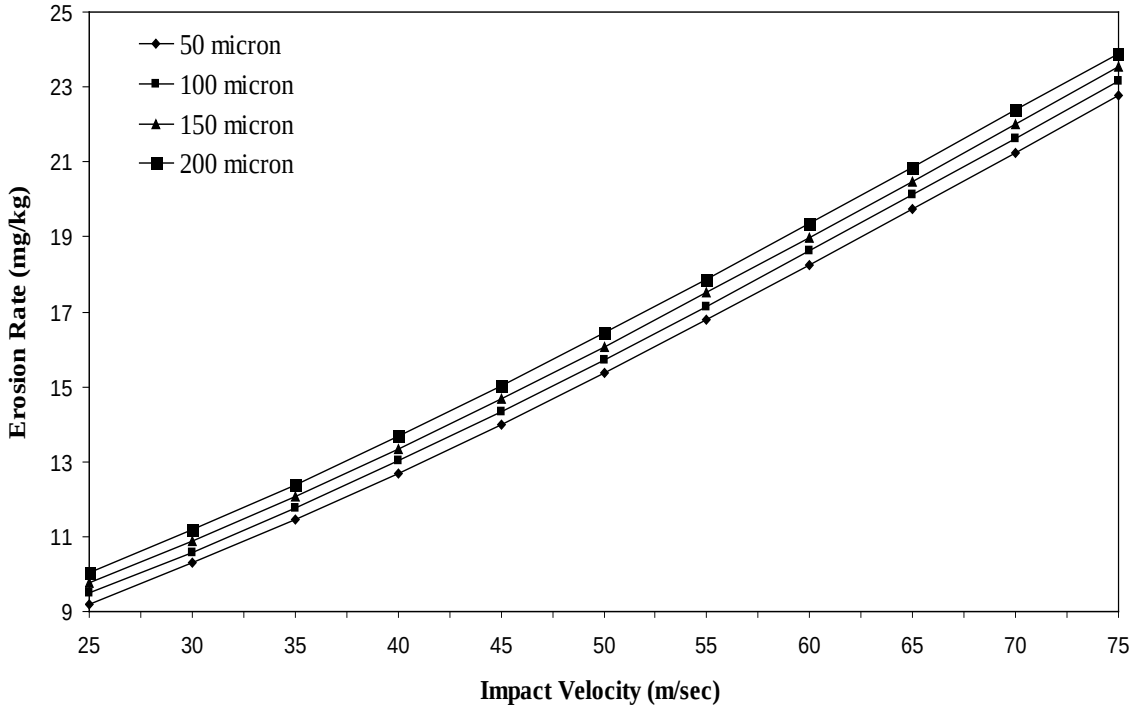


**(b)**

**Figure 5.11** Effect of impact velocity on erosion rate for different (a) impingement angle (b) erodent size for 'BGM + $Al_2O_3$' coatings

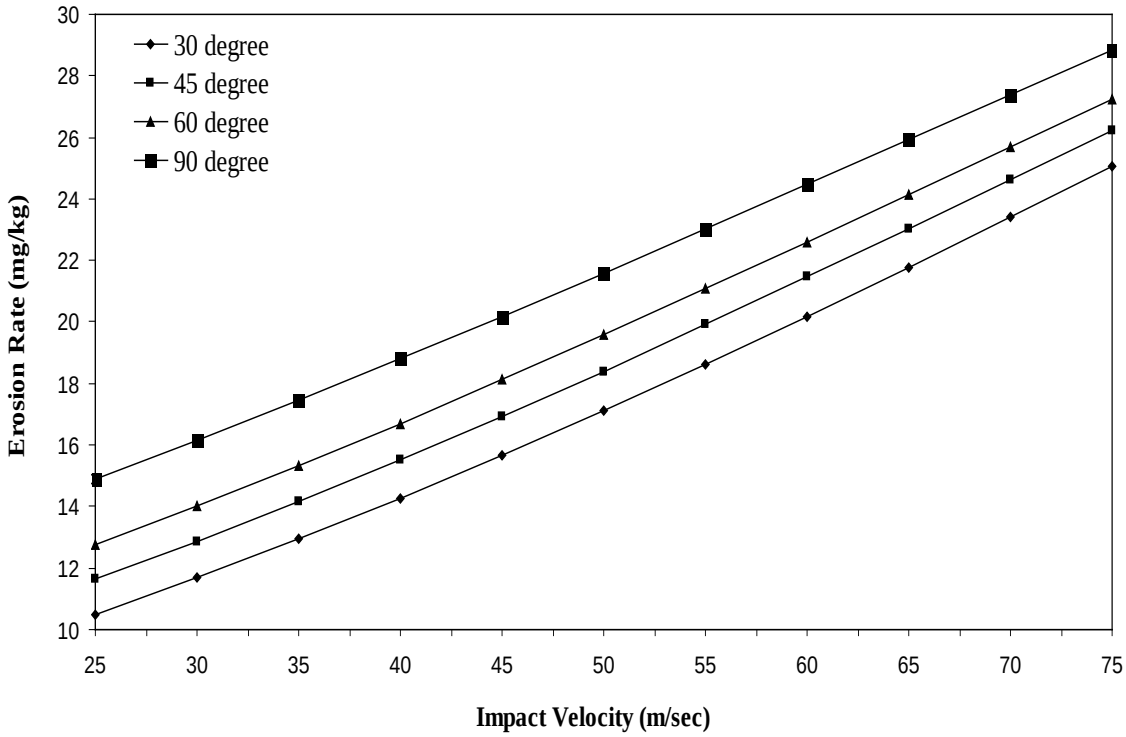


**(a)**

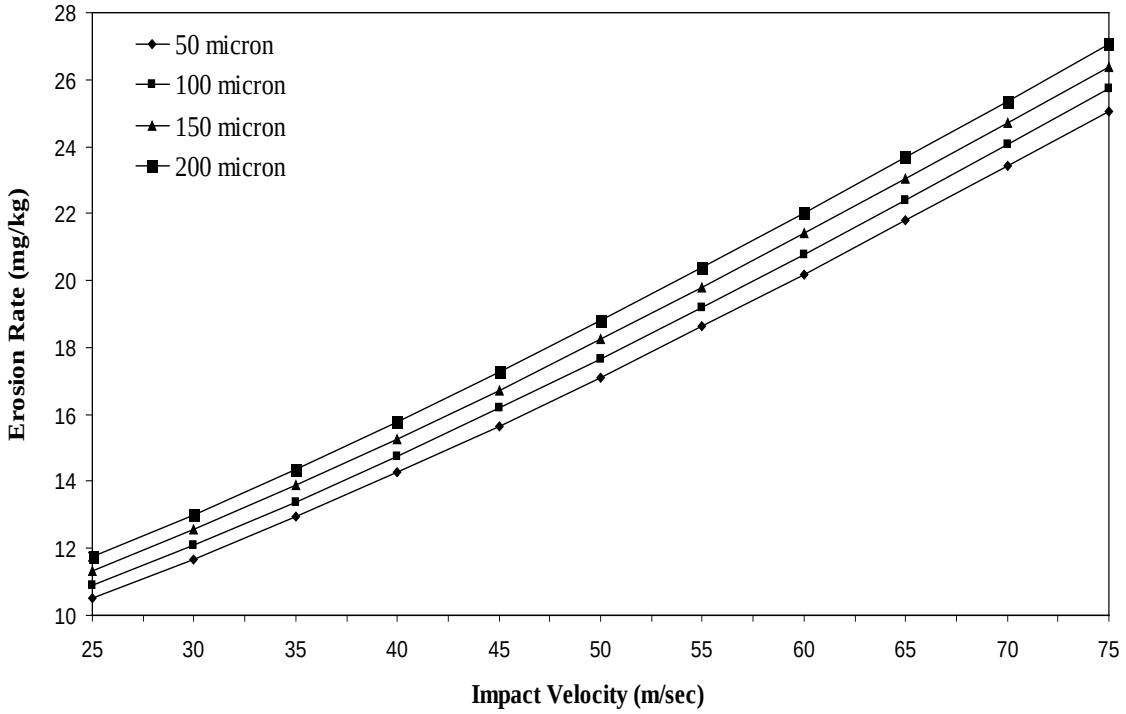


**(b)**

**Figure 5.12** Effect of impact velocity on erosion rate for different (a) impingement angle (b) erodent size for 'BGM + $TiO_2$' coatings

Similar observations have also been reported by previous investigators for other plasma sprayed ceramic coatings [1, 302-304]. As the impact velocity of the erodent increases, the kinetic energy carried by it also increases. This causes transfer of greater amount of energy to the target coating surface upon impact and leads to higher material loss due to erosion wear. It has also been reported in the past that impact velocity happens to be an important test variable in any erosion test and can easily overshadow changes in other variables such as erodent size, impingement angle etc. [304]. Erosion rate (ER) depends on velocity ($V$) by a power law, given as $ER = k.V^n$, where $k$ is a material constant. However, the exponent $n$ is reported to be material independent and is governed by test conditions including particle characteristics and the erosion test apparatus [305-307].

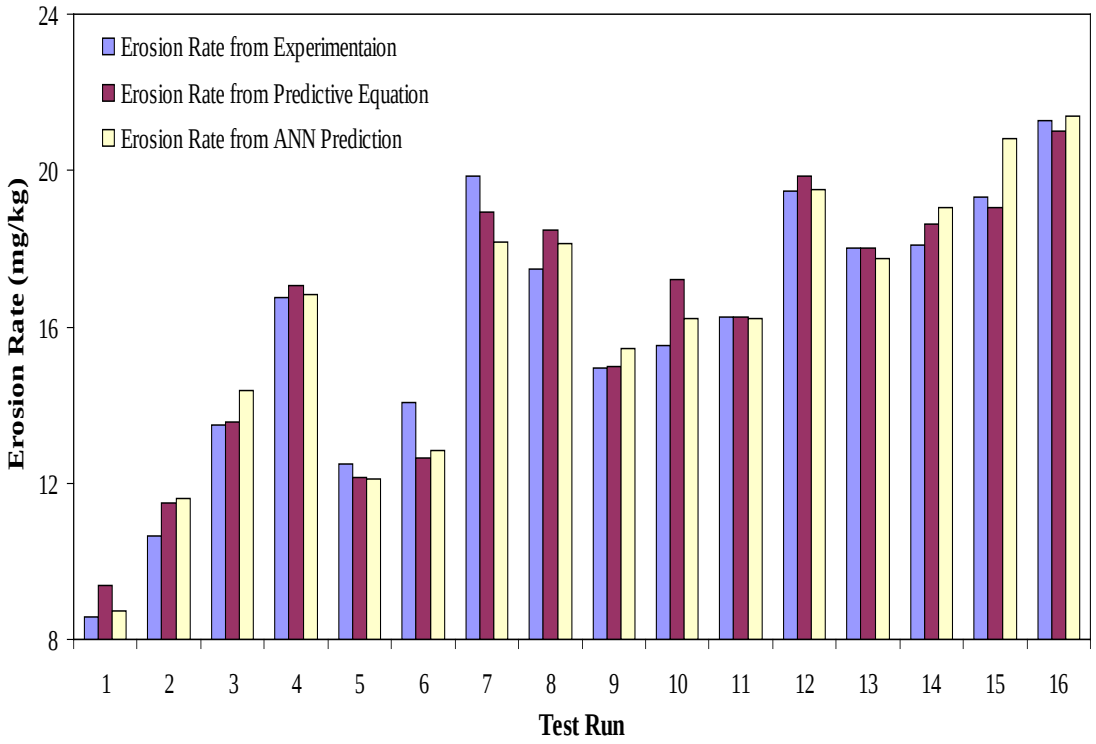


**Figure 5.13** Comparison of erosion rates of BGM coatings obtained from different methods

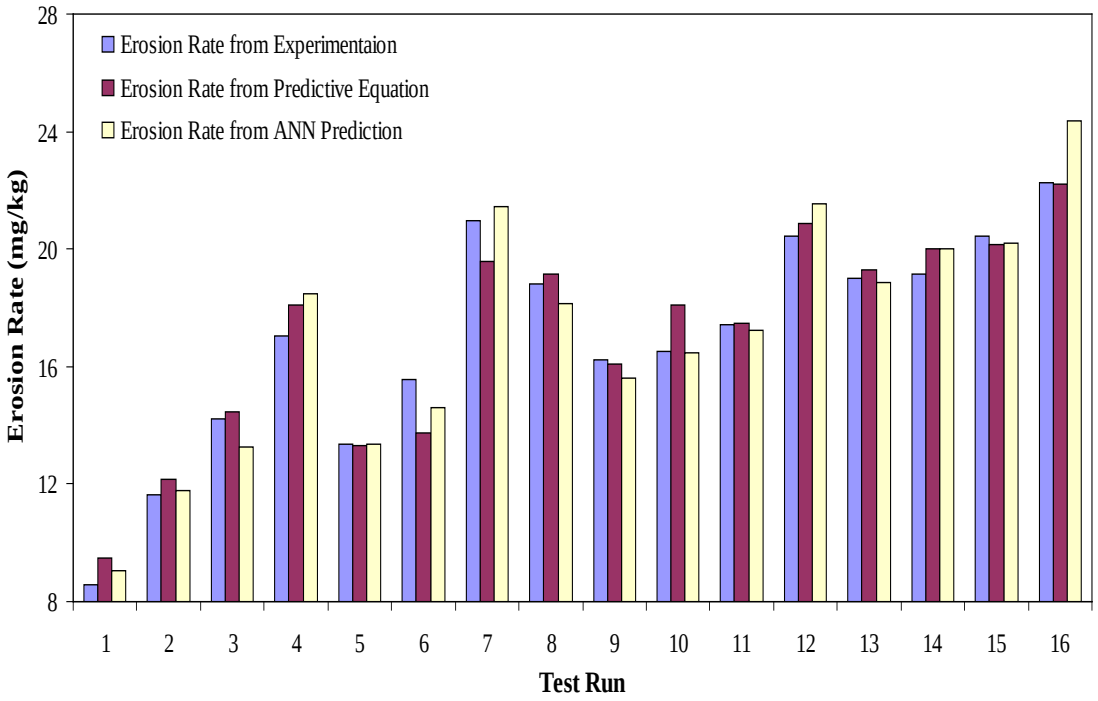


**Figure 5.14** Comparison of erosion rates of 'BGM + $Al_2O_3$' coatings obtained from different methods

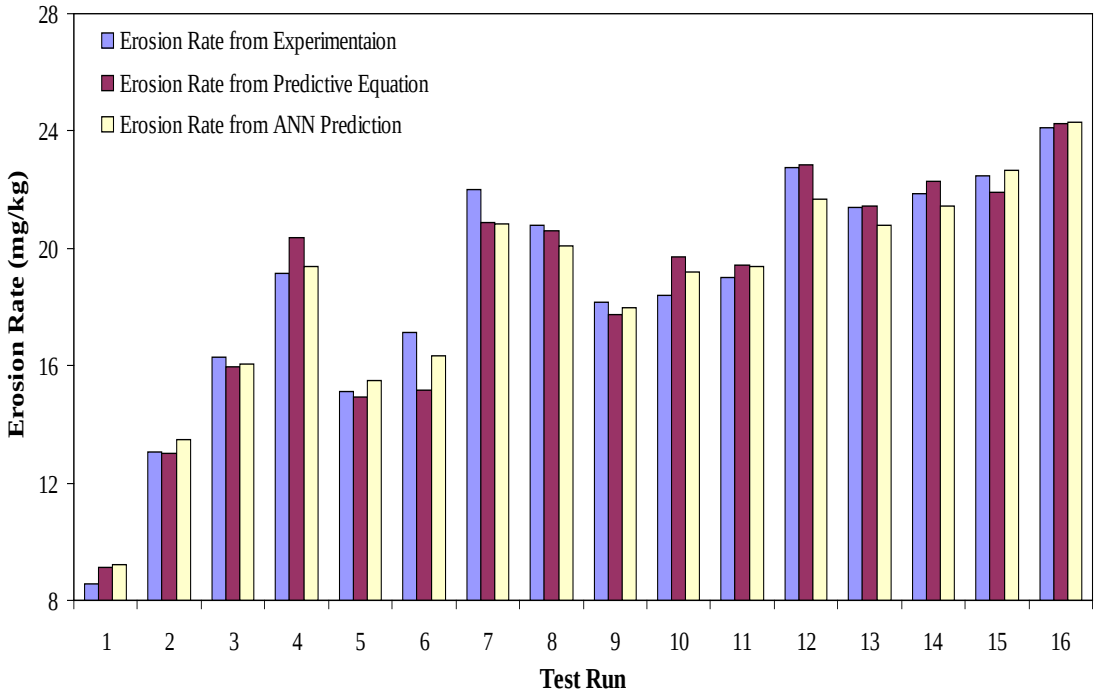


**Figure 5.15** Comparison of erosion rates of 'BGM + $TiO_2$' coatings obtained from different methods

Comparison of the measured erosion rates of BGM, 'BGM + $Al_2O_3$' and 'BGM + $TiO_2$' coatings with those obtained using the two prediction models proposed in this work are presented in Figures 5.13, 5.14 and 5.15 respectively. While the errors associated with the ANN predictions lie in the range of 0-10 %, the same for results obtained from the proposed correlation lie in the range of 0-12%. Thus it can be concluded that the results obtained from the predictive model based on ANN are relatively closer to the measured values of erosion rates. However, both the ANN and the predictive equations are equally useful for wear rate prediction in similar situations.

**Chapter Summary**

This chapter has provided a critical analysis of the test results related to the solid particle erosion characteristics of BGM, 'BGM + $Al_2O_3$' and 'BGM + $TiO_2$' coatings using Taguchi experimental design. Significant control factors affecting the erosion rate have been identified through successful implementation of this technique. Impact velocity and impingement angle in declining sequence are found to be significant for minimizing the erosion rate.

The experimental results suggest the potential of glass micro-spheres to be used as a wear resistant coating material for deposition on metallic substrates. The research presented in this chapter further illustrates that the use of a neural network model to simulate experiments with parametric design strategy is effective, efficient and helps to predict the solid particle erosion response of glass micro-sphere based coatings under different test conditions within and beyond the experimental domain. The predicted and the experimental values of erosion wear rate exhibit good agreement and validate the remarkable prediction capability of a well-trained neural network for this kind of processes.

The next chapter presents the physical and mechanical properties of the glass micro-sphere filled polymer composites.

*****

Chapter 6

Results and Discussion - III

# COMPOSITE CHARACTERIZATION

This chapter reports the measured values of the physical and mechanical properties of borosilicate glass micro-sphere (BGM) filled epoxy (EP) and polypropylene (PP) composites considered in this study. The results of various characterization tests are presented and the effects of glass micro-spheres on the modified composite properties are discussed.

## 6.1 Physical Characterization of the Composites

Density and Void Fraction

Density is a material property which is of prime importance in several weight sensitive applications. Thus, in many such applications, polymer composites are found to replace conventional metals and materials primarily for their low densities. Density of a composite essentially depends on the relative proportion of matrix and the reinforcing materials. There is always a difference between the measured and the theoretical density values of a composite due to the presence of voids and pores. These voids significantly affect some of the mechanical properties and even the performance of composites in the workplace. Higher void contents usually mean lower fatigue resistance, greater susceptibility to water penetration and weathering [288]. The information about the amount of void content is desirable for estimation of the quality of the composites. In the present research work, the theoretical and measured densities of BGM filled epoxy and PP composites are reported along with the corresponding volume fraction of voids in Table 6.1. The difference between the theoretical and measured density is a measure of voids and pores present in the composites. It is observed that, by the addition of glass micro-spheres, the density of the composites gradually increases. It is obvious as the density of glass micro-spheres is higher than that of the polymers taken in this work. As the filler

content in the composite increases from 0 to 30 wt %, the volume fraction of voids is also found to increase proportionately. Similar observations have been reported earlier by previous researchers [209, 230, 308, 309].

**Table 6.1** Measured and theoretical densities along with the void fractions of the composites

| S. No. | Composition | Theoretical Density ($gm/cm^3$) | Measured Density ($gm/cm^3$) | Void Fraction (%) |
|---|---|---|---|---|
| 1 | EP + 0 wt% BGM | 1.100 | 1.098 | 0.18 |
| 2 | EP + 10 wt% BGM | 1.159 | 1.151 | 0.69 |
| 3 | EP + 20 wt% BGM | 1.224 | 1.212 | 0.98 |
| 4 | EP + 30 wt% BGM | 1.297 | 1.279 | 1.39 |
| 5 | PP + 0 wt% BGM | 0.920 | 0.918 | 0.21 |
| 6 | PP + 10 wt% BGM | 1.134 | 1.125 | 0.79 |
| 7 | PP + 20 wt% BGM | 1.198 | 1.181 | 1.41 |
| 8 | PP + 30 wt% BGM | 1.282 | 1.259 | 1.79 |

** EP: Epoxy, PP: Polypropylene, BGM: Borosilicate Glass Micro-sphere*

It is understandable that a good composite should have fewer voids [310]. However, presence of void is unavoidable in composite making particularly through hand lay-up route. The composites under the present investigation possess very less voids (maximum ≈ 2%) and can thus be termed as good composites.

### 6.2 Mechanical Characterization of the Composites

Evaluation of strength and other mechanical properties of any new composite is essential from research as well as functionality point of view. Various authors have earlier characterized mechanical properties of different polymeric materials on different occasions [311-318]. In the present work, a wealth of property data has been generated by conducting different characterization tests under

controlled laboratory conditions to evaluate various mechanical characteristics of the composites fabricated for this work. The property values are presented in Table 6.2.

**Table 6.2** Mechanical properties of the composites

| Composition | Tensile Strength (MPa) | Tensile Modulus (GPa) | Flexural Strength (MPa) | Impact Energy ($KJ/m^2$) | Mean Hardness (GPa) |
|---|---|---|---|---|---|
| EP + 0% BGM | 58 | 3.6 | 28.76 | 18.5 | 0.085 |
| EP + 10% BGM | 57.54 | 3.62 | 27.03 | 21.7 | 0.229 |
| EP + 20% BGM | 56.79 | 3.70 | 26.22 | 26.3 | 0.448 |
| EP + 30% BGM | 55.29 | 3.76 | 25.87 | 28.9 | 0.587 |
| PP + 0% BGM | 41 | 1.75 | 31.72 | 20.2 | 0.057 |
| PP + 10% BGM | 40.2 | 1.84 | 30.48 | 23.3 | 0.247 |
| PP + 20% BGM | 39.4 | 1.92 | 29.16 | 28.7 | 0.498 |
| PP + 30% BGM | 38.3 | 1.98 | 27.98 | 31.2 | 0.663 |

** EP: Epoxy, PP: Polypropylene, BGM: Borosilicate Glass Micro-sphere*

Micro-hardness

Hardness is considered as one of the most important factors that govern the wear resistance of any material. In the present work, micro-hardness values of the epoxy and PP based composites filled with BGM particles are measured and the test results presented in Table 6.2 are shown graphically in Figure 6.1. It is evident that with addition of glass micro-spheres, micro-hardness of the composites are improved irrespective of the matrix type and this improvement is a function of the filler content. As far as the comparison between the epoxy and PP composites is concerned, the PP based composites exhibit superior micro-hardness values than the epoxy composites. The hardness values have been found to have improved invariably for all the composites with addition of glass microspheres and it is obvious as the intrinsic hardness of glass is higher than those of the resin materials. Among all the composites under this investigation, the maximum hardness value is recorded for PP reinforced with 30 wt% BGM (0.663 GPa) and this value is about 11 times the hardness of neat PP. Increase in composite hardness with incorporation of glass micro-spheres has previously been reported also by Mishra [283].

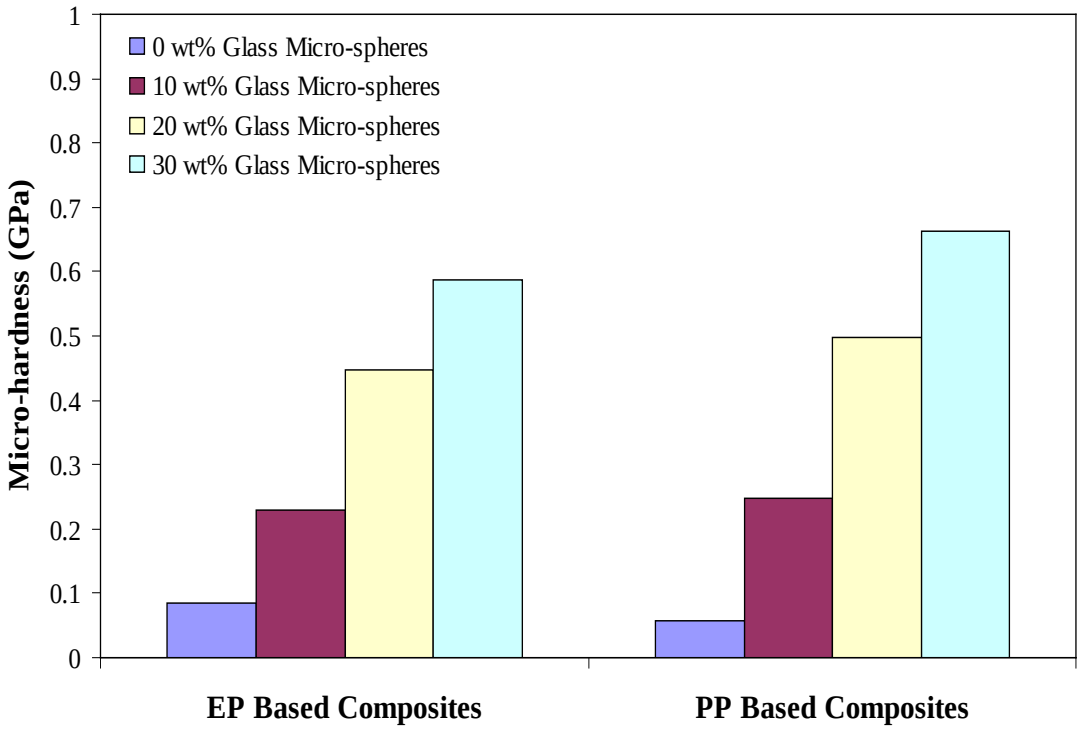


**Figure 6.1** Micro-hardness of glass micro-sphere filled composites

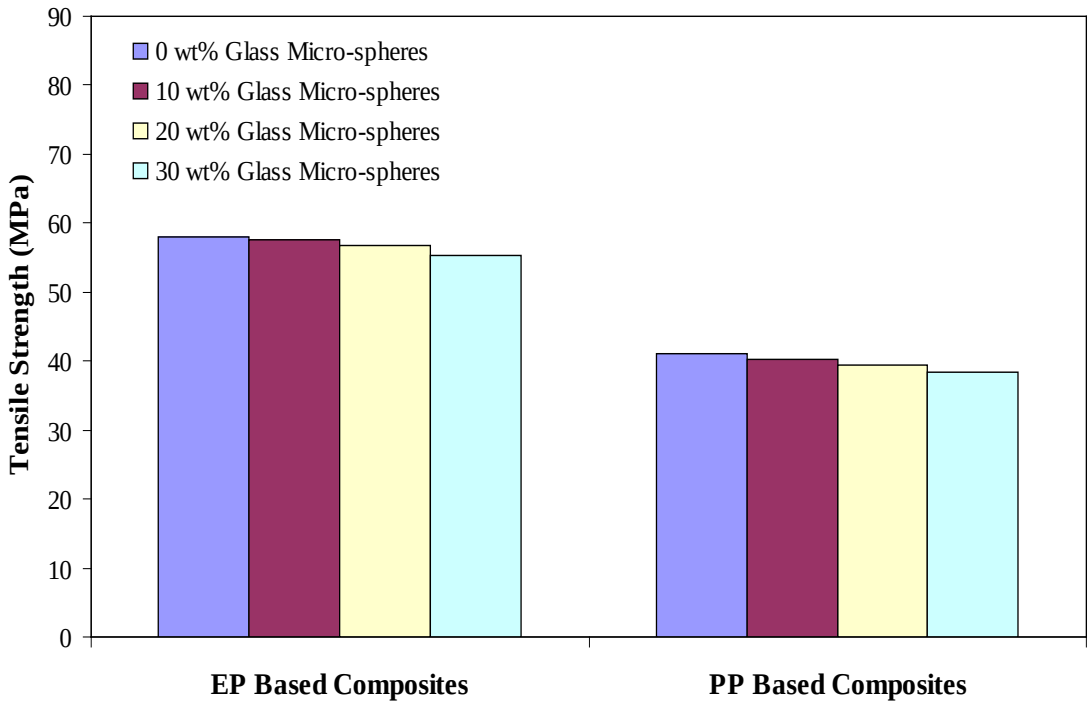


**Figure 6.2** Tensile strength of glass micro-sphere filled composites

Tensile Strength

The variation of tensile strength with BGM content for both the epoxy and PP based composites is presented in Figure 6.2. It is found that with increase in BGM content from 0 to 30 wt%, the tensile strengths of both the epoxy as well as polypropylene based composites decrease. However, this decrement is very marginal. The reduction in tensile strength with filler addition may be due to the fact that chemical bond strength between filler particles and the matrix body is weak to transfer the tensile load and due to the increase in void percentage in the composites with increase in filler content.

Figure 6.3 presents the variation of tensile modulus with BGM content for both the epoxy and PP based composites. The tensile moduli of the composite samples are found to be increasing as the BGM content in composites increase from 0 to 30 wt%. This reduces the strain rate; but with both the tensile strength and strain decreasing, it seems that a synergistic effect takes place which ultimately leads to a small increment in modulus.

Flexural Strength

Composite materials used in structures are prone to fail in bending and therefore development of new composites with improved flexural characteristics is essential. In the present work, the variation of flexural strength of epoxy and PP based composites with BGM content is shown. Marginal decrement in flexural strength is recorded for all the composite samples with the incorporation of BGM particles (Figure 6.4). The reduction in flexural strength of the composites with filler content may be attributed to poor interfacial bonding, particle to particle interaction, voids and the non-uniformity in dispersion of glass micro-spheres in the polymer matrix.

Decrease in tensile and flexural strength in particulate composites has been a common phenomenon as reported by a large number of investigators in the past [5, 59, 61, 63, 68, 69, 72, 74, 75, 319]. Most of them have attributed this reduction to factors like improper wetting and the irregular shape of the particulate fillers.

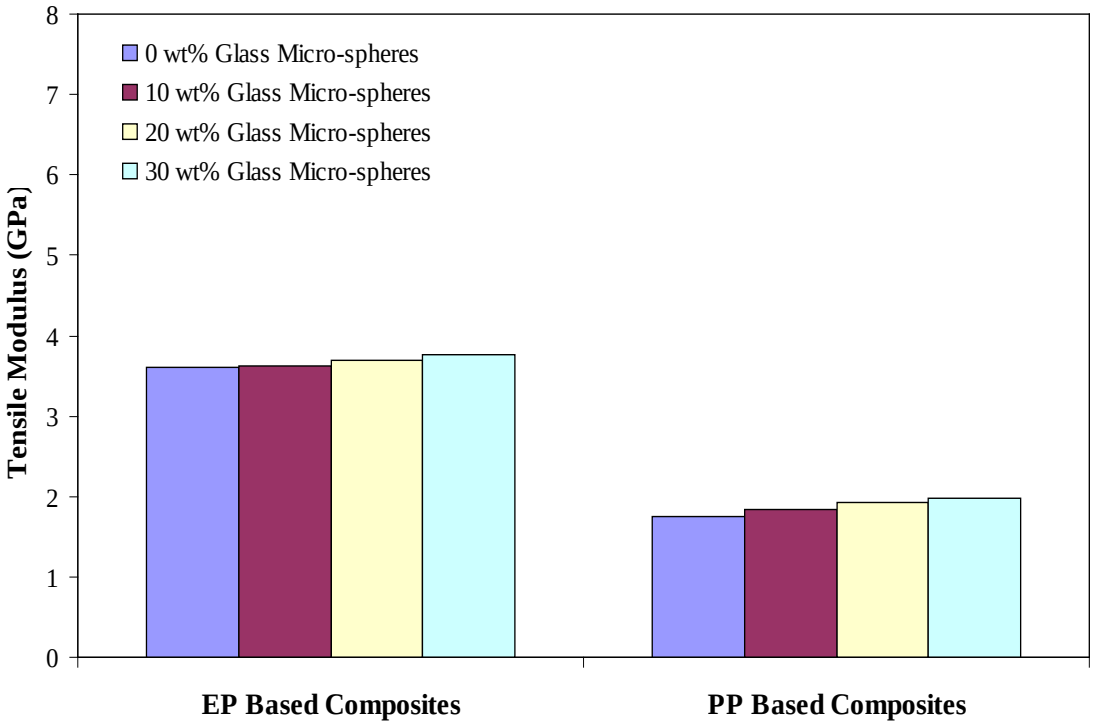


**Figure 6.3** Tensile modulus of glass micro-sphere filled composites

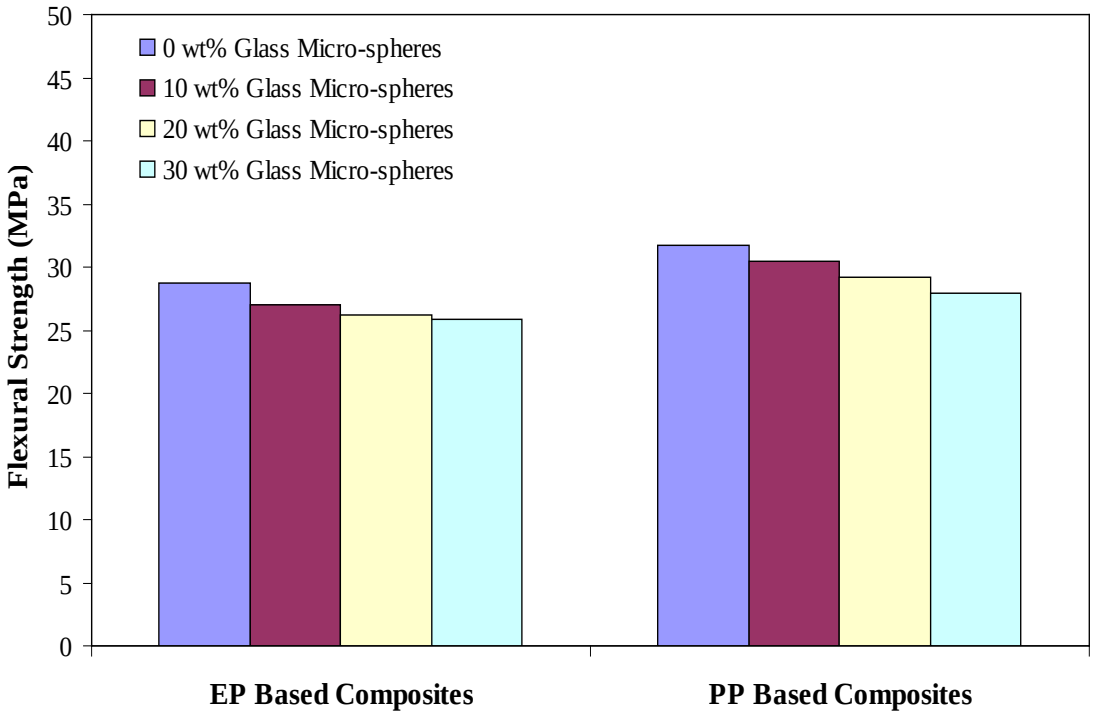


**Figure 6.4** Flexural strength of glass micro-sphere filled composites

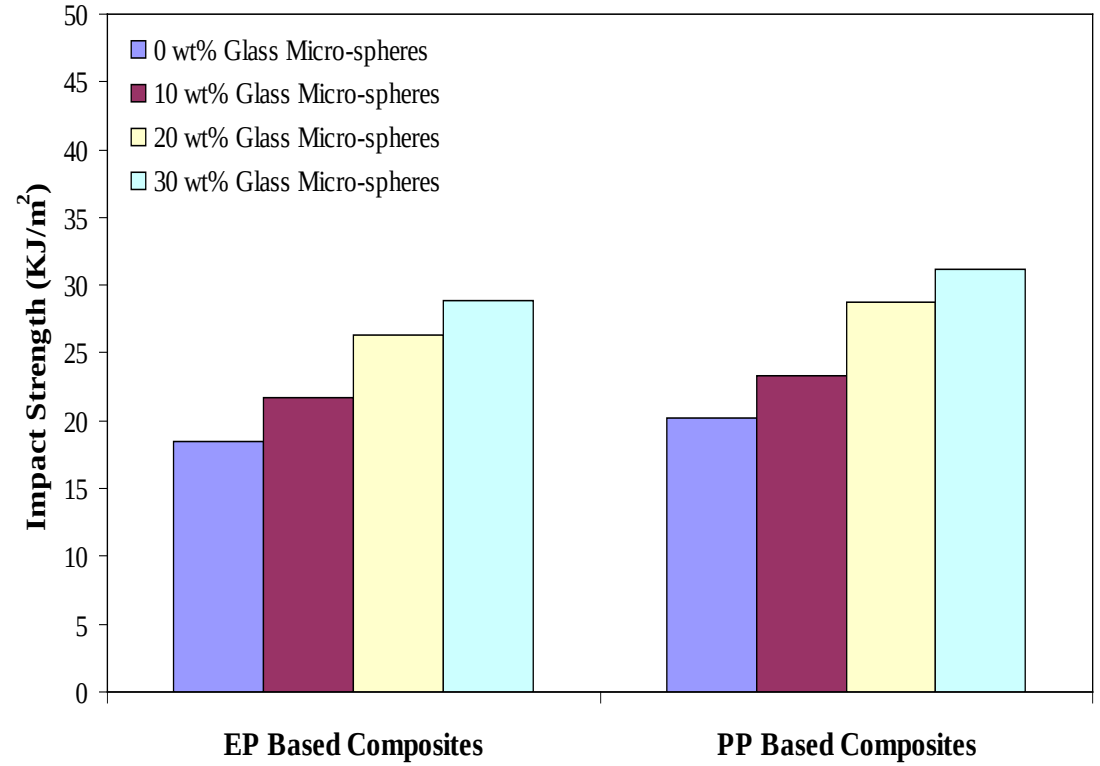


**Figure 6.5** Impact strength of glass micro-sphere filled composites

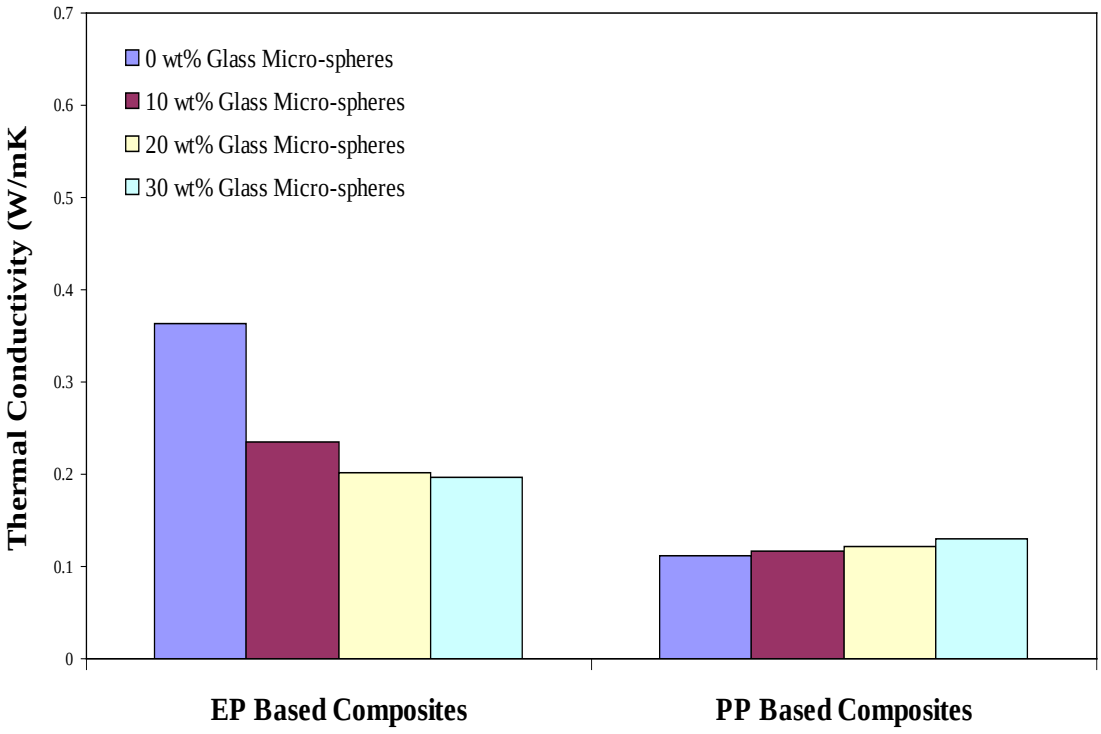


**Figure 6.6** Thermal conductivity of glass micro-sphere filled composites

Impact Strength

The impact strength of a material is its capacity to absorb and dissipate energies under impact or shock loading. The suitability of a composite for certain applications is determined not only by usual design parameters, but also by its impact or energy absorbing properties. Thus, it is important to have a good understanding of the impact behaviour of composites for both safe and efficient design of structures. Figure 6.5 shows measured impact energy values of glass micro-sphere filled composites under this investigation. It is seen from the figure that the impact energies of the composites increase gradually with filler content increasing from 0 to 30 wt% in case of both epoxy and PP composites. The reason for this is as follows: with the incorporation of glass micro-spheres, the mobility of polymer chain is constrained, which reduces their ability to deform freely and makes the material less ductile. Therefore the energy absorbing capability of the composites increases with the addition of glass micro-spheres.

Thermal Conductivity

Unitherm™ Model 2022 Thermal Conductivity Tester is used to measure the conductivity of the composites fabricated for this investigation in accordance with ASTM E-1530 test standards. Figure 6.6 presents the values of effective thermal conductivity as a function of the BGM content in the composites. It is encouraging to note that the incorporation of BGM results in significant drop in thermal conductivity of epoxy resin and thereby increases its thermal insulation capability. With addition of 30 wt% of BGM, the thermal conductivity decreases by about 84% as compared with neat epoxy resin. On the contrary, in case of polypropylene resin the thermal conductivity increases marginally with the addition of glass micro-spheres. This is obvious as the intrinsic thermal conductivity of PP is lower than that of glass.

**Chapter Summary**

This chapter has provided:

- The physical and mechanical characterization of epoxy and polypropylene composites filled with different weight fractions of glass micro-spheres.
- The effect of filler addition on the composite properties.

The next chapter presents the results and discussion for erosion wear performance of the epoxy and polypropylene based composites under different test conditions.

*****

Chapter 7

Results and Discussion - IV

# EROSION WEAR RESPONSE OF GLASS MICRO-SPHERE FILLED POLYMER COMPOSITES

In this chapter erosion wear characteristics of glass micro-sphere filled epoxy (EP) and polypropylene (PP) composites have been investigated following a plan of experiments based on the Taguchi technique which is used to acquire the erosion test data in a controlled way. This chapter reports the wear rates obtained from these erosion trials and presents a critical analysis of the test results. Further, erosion rate predictions following an ANN approach for different test conditions are presented. A correlation among various control factors influencing the erosion rate has also been proposed for predictive purpose. Possible wear mechanisms are identified from the scanning electron microscopy of the eroded surfaces.

## 7.1 Morphology of Composite Surfaces

It is well known that the properties of the composites are strongly dependent on the interaction of the filler and the matrix. In order to evaluate this interaction, the microstructure of the composites, including the dispersion of the glass micro-spheres in the polymer matrix were observed under scanning electron microscope.

Some typical scanning electron micrographs of the uneroded and eroded surfaces of glass micro-sphere filled epoxy composites are shown in Figure 7.1. The surface of the composite before being subjected to solid particle erosion, shown in Figure 7.1 (a), appears to be smooth with no wear grooves. It is also seen that glass microspheres are distributed in a reasonably uniform manner throughout the matrix body. Figure 7.1 (b) represents the magnified image of a single glass micro-sphere used in this work as the filler. Figures 7.1 (c) and (d) are the SEM images of the eroded composite surface in which formation of small craters and

initiation of cracks due to impact of hard sand particles are seen. Material removal from the relatively softer matrix regime as a result of erosion can also be noticed. Crack propagation in the filler particles is clearly visible in the micrograph Figure 7.1 (d). This is a case of the erodent particles striking aggressively the composite surface at high impact velocity. The material dislodged from the matrix body leads to a greater degree of surface damage.

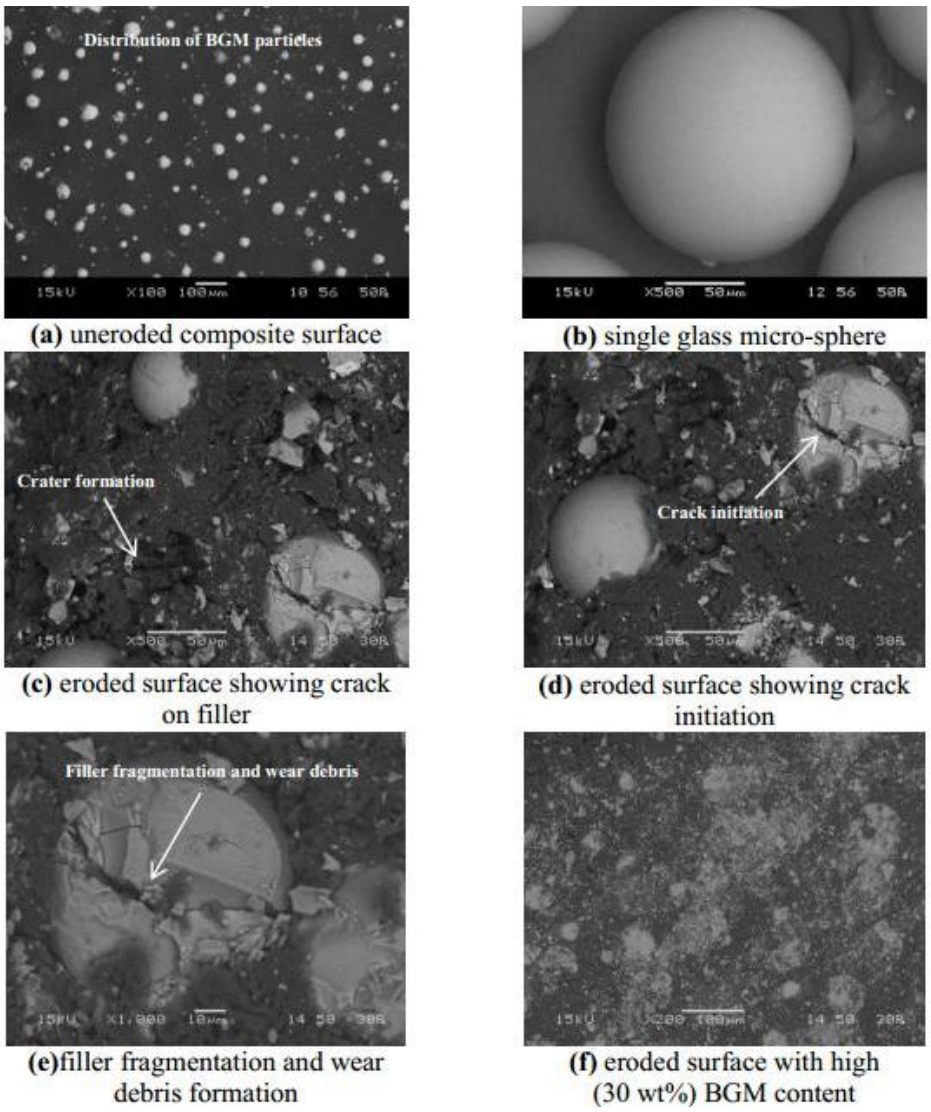


**(a)** uneroded composite surface
**(b)** single glass micro-sphere
**(c)** eroded surface showing crack on filler
**(d)** eroded surface showing crack initiation
**(e)**filler fragmentation and wear debris formation
**(f)** eroded surface with high (30 wt%) BGM content

**Figure 7.1** SEM micrographs of uneroded and eroded surfaces of the epoxy composites

Due to repeated impact of the erodent particles carrying higher kinetic energy, some of the glass micro-spheres in the matrix body break and subsequently get fragmented resulting in loose wear debris (Figure 7.1 (e)). But in the process, the hard filler particles also absorb a good fraction of the erodent kinetic energy and

thereby the energy available for the plastic deformation/fracture of soft epoxy body becomes less. This way material removal and surface degradation of particulate filled composites are mitigated to a large extent. Figure 7.1 (f) presents SEM micrograph of eroded epoxy composite with high filler content (30 wt%) clearly indicating this phenomenon of hard glass micro-spheres playing an important role in resisting the solid particle erosion of the composite as a whole.

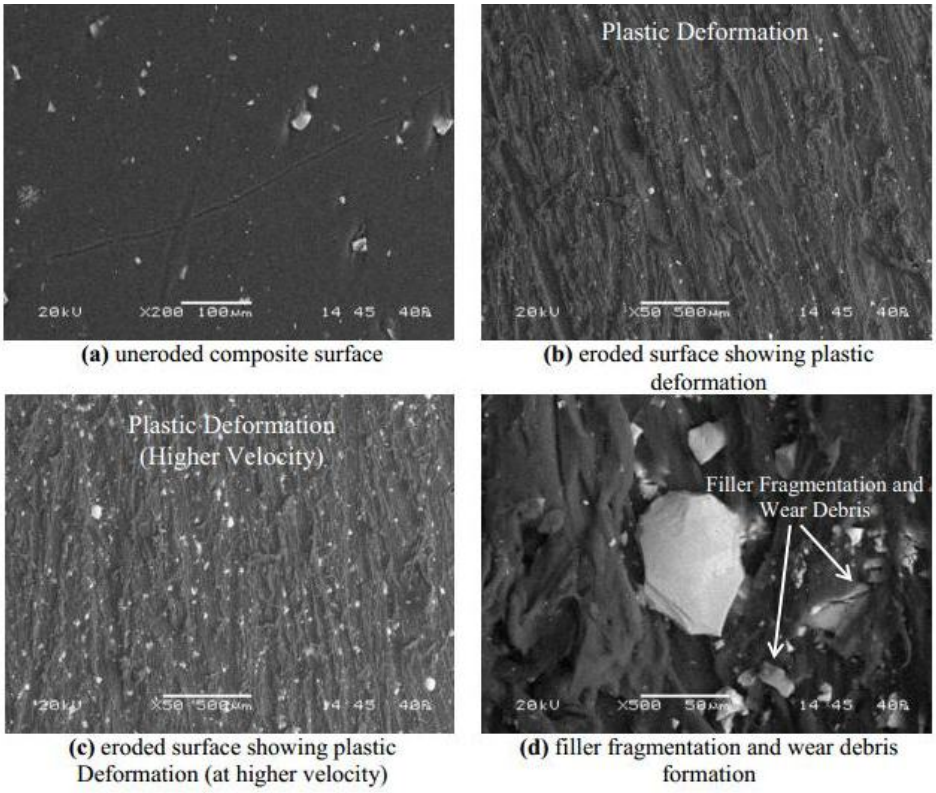


**(a)** uneroded composite surface

**(b)** eroded surface showing plastic deformation

**(c)** eroded surface showing plastic Deformation (at higher velocity)

**(d)** filler fragmentation and wear debris formation

**Figure 7.2** SEM micrographs of uneroded and eroded surfaces of the polypropylene composites

Figure 7.2 shows the scanning electron micrographs of the uneroded and eroded surfaces of glass micro-sphere filled polypropylene composites. Figure 7.2 (a) shows the surface of the composite prior to erosion. Figures 7.2 (b) and (c) are the SEM images of the eroded composite surface in which regions of plastic deformation are seen. The direction of material flow and the wear tracks are clearly visible. Softening of matrix as a result of repeated impact of the erodent particles is evident in these micrographs. Hard silica sand particles carrying higher kinetic energy cause the breaking and fragmentation in the matrix region resulting in loose wear debris (Figure 7.2 (d)). But in the process the hard BGM

particles also absorb a good fraction of the erodent kinetic energy and thereby the energy available for the plastic deformation/fracture of soft epoxy body becomes less. This way material removal and surface degradation of particulate filled composites are checked to a large extent.

### 7.2 Erosion Test Results and Taguchi Analysis

The erosion wear rates of glass micro-sphere filled epoxy and PP composites obtained for all the 16 test runs along with the corresponding signal-to-noise ratio are presented in Table 7.1.

**Table 7.1** Experimental design using $L_{16}$ orthogonal array and the wear test results for epoxy and polypropylene composites

| Test Run | A | B | C | D | E | EP-BGM | | PP-BGM | |
|---|---|---|---|---|---|---|---|---|---|
| | | | | | | ER | S/N Ratio | ER | S/N Ratio |
| 1 | 32 | 30 | 50 | 30 | 0 | 1.288 | -2.1983 | 1.246 | -1.9103 |
| 2 | 32 | 45 | 100 | 60 | 10 | 1.293 | -2.2319 | 1.208 | -1.6413 |
| 3 | 32 | 60 | 150 | 90 | 20 | 0.987 | 0.1136 | 1.195 | -1.5473 |
| 4 | 32 | 90 | 200 | 120 | 30 | 0.803 | 1.9056 | 1.111 | -0.9142 |
| 5 | 40 | 30 | 100 | 90 | 30 | 1.327 | -2.4574 | 1.122 | -0.9998 |
| 6 | 40 | 45 | 50 | 120 | 20 | 1.354 | -2.6323 | 1.205 | -1.6197 |
| 7 | 40 | 60 | 200 | 30 | 10 | 1.370 | -2.7344 | 1.252 | -1.9520 |
| 8 | 40 | 90 | 150 | 60 | 0 | 1.422 | -3.0579 | 1.268 | -2.0623 |
| 9 | 48 | 30 | 150 | 120 | 10 | 1.368 | -2.7217 | 1.221 | -1.7343 |
| 10 | 48 | 45 | 200 | 90 | 0 | 1.415 | -3.0151 | 1.294 | -2.2386 |
| 11 | 48 | 60 | 50 | 60 | 30 | 1.281 | -2.1509 | 1.196 | -1.5546 |
| 12 | 48 | 90 | 100 | 30 | 20 | 1.324 | -2.4377 | 1.274 | -2.1033 |
| 13 | 56 | 30 | 200 | 60 | 20 | 1.431 | -3.1127 | 1.302 | -2.2922 |
| 14 | 56 | 45 | 150 | 30 | 30 | 1.356 | -2.6451 | 1.130 | -1.0615 |
| 15 | 56 | 60 | 100 | 120 | 0 | 1.447 | -3.2093 | 1.356 | -2.6451 |
| 16 | 56 | 90 | 50 | 90 | 10 | 1.415 | -3.0151 | 1.209 | -1.6485 |

***Note :*** *Factor A denotes Impact Velocity (m/sec)*
*Factor B denotes Impingement Angle ($^0$)*
*Factor C denotes Erodent Size (µm)*
*Factor D denotes Erodent Temperature ($^0$C)*
*Factor E denotes BGM Content (wt%)*
*ER denotes Erosion Rate (mg/kg)*
*S/N Ratio denotes Signal to Noise Ratio (db)*
*EP: Epoxy, PP: Polypropylene, BGM: Borosilicate Glass Micro-sphere*

Each data point (value of erosion rate) is in fact the average of three replications. From this table, the overall mean for the S/N ratio of the wear rate for epoxy and PP composites are found to be -2.2250 db and -1.7453 db respectively. This is done using the software MINITAB-14 specifically used for design-of-experiment applications.

**Table 7.2** S/N ratio response table for erosion rate of EP-BGM composites

| **Level** | **A** | **B** | **C** | **D** | **E** |
|---|---|---|---|---|---|
| 1 | -0.6027 | -2.6226 | -2.4992 | -2.5039 | -2.8702 |
| 2 | -2.7205 | -2.6312 | -2.5841 | -2.6384 | -2.6758 |
| 3 | -2.5814 | -1.9953 | -2.0778 | -2.0935 | -2.0173 |
| 4 | -2.9956 | -1.6513 | -1.7392 | -1.6644 | -1.3370 |
| Delta | 2.3929 | 0.9799 | 0.8450 | 0.9740 | 1.5332 |
| **Rank** | **1** | **3** | **5** | **4** | **2** |

**Table 7.3** S/N ratio response table for erosion rate of PP-BGM composites

| **Level** | **A** | **B** | **C** | **D** | **E** |
|---|---|---|---|---|---|
| 1 | -1.503 | -1.734 | -1.683 | -1.757 | -2.214 |
| 2 | -1.659 | -1.640 | -1.847 | -1.888 | -1.744 |
| 3 | -1.908 | -1.925 | -1.601 | -1.609 | -1.891 |
| 4 | -1.912 | -1.682 | -1.849 | -1.728 | -1.133 |
| Delta | 0.409 | 0.284 | 0.248 | 0.279 | 1.082 |
| **Rank** | **2** | **3** | **5** | **4** | **1** |

The S/N ratio response analyses are presented in Tables 7.2 and 7.3 for EP-BGM and PP-BGM composites respectively. These tables show the hierarchical order of the control factors as per their significance on the composite erosion rate.

Figures 7.3 and 7.4 illustrate the effect of control factors on erosion rate for EP-BGM and PP-BGM composites respectively. Analysis of the results leads to the conclusion that factor combination of $A_1$ (Impact velocity), $B_4$ (Impingement angle), $C_4$(Erodent size), $D_4$ (Erodent temperature) and $E_4$ (BGM content) gives minimum erosion rate (Figure 7.3) for EP-BGM composites and factor combination $A_1$ (Impact velocity), $B_2$ (Impingement angle), $C_3$(Erodent size), $D_3$ (Erodent temperature) and $E_4$ (BGM content) gives minimum erosion rate (Figure 7.4) for PP-BGM composites.

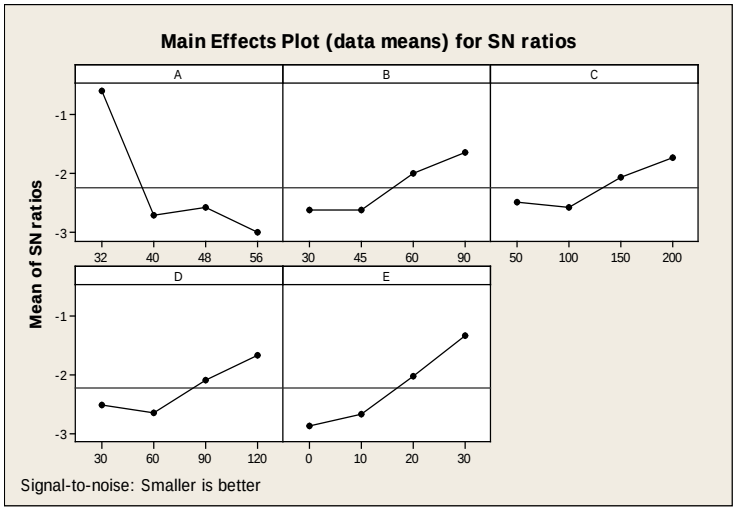


**Figure 7.3** Effect of control factors on erosion rate for EP-BGM composites

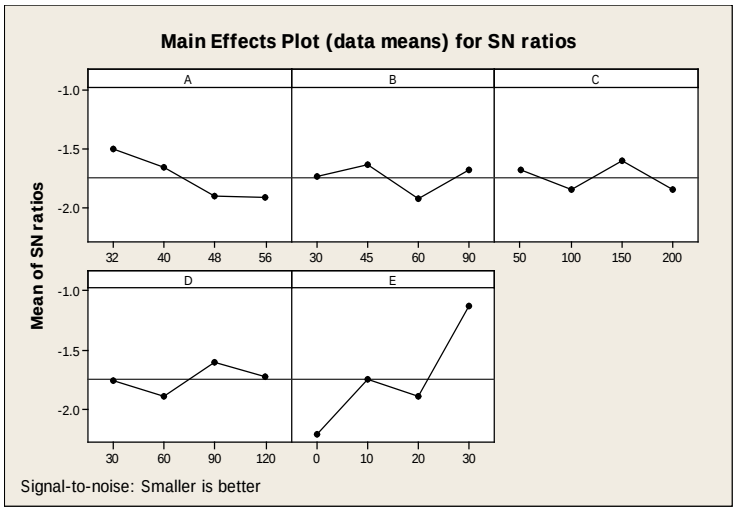


**Figure 7.4** Effect of control factors on erosion rate for PP-BGM composites

### 7.3 Confirmation Experiment

To validate the conclusions drawn during the analysis, confirmation experiment is performed by considering a new arbitrary set of factors other than the optimal factor setting to evaluate the erosion rate. For this investigation $A_4B_3D_2E_4$ and $A_3B_2D_2E_2$ for EP-BGM and PP-BGM composites respectively are chosen as the arbitrary set considering which a prediction equation can be formulated using Taguchi's approach to estimate S/N ratio for erosion rate as [301]:

$$\overline{\eta_1} = \overline{T} + \left(\overline{A_4} - \overline{T}\right) + \left(\overline{B_3} - \overline{T}\right) + \left(\overline{D_2} - \overline{T}\right) + \left(\overline{E_4} - \overline{T}\right) \quad \textbf{(7.1)}$$

$$\overline{\eta_2} = \overline{T} + \left(\overline{A_3} - \overline{T}\right) + \left(\overline{B_2} - \overline{T}\right) + \left(\overline{D_2} - \overline{T}\right) + \left(\overline{E_2} - \overline{T}\right) \quad \textbf{(7.2)}$$

| | |
|---|---|
| $\overline{\eta_1}$ , $\overline{\eta_2}$ | Predicted average for EP-BGM and PP-BGM composites respectively |
| $\overline{T}$ | Overall experimental average |
| $\overline{A}, \overline{B}, \overline{D}, \overline{E}$ | Mean response for factors |

By combining like terms, the equation reduces to

$$\overline{\eta_1} = \overline{A_4} + \overline{B_3} + \overline{D_2} + \overline{E_4} - 3\overline{T} \quad \textbf{(7.3)}$$

$$\overline{\eta_2} = \overline{A_3} + \overline{B_2} + \overline{D_2} + \overline{E_2} - 3\overline{T} \quad \textbf{(7.4)}$$

**Table 7.4** Results of the confirmation experiments for erosion rate

| | **Optimal Control Parameters** | | | |
|---|---|---|---|---|
| | **EP-BGM Composites** | | **PP-BGM Composites** | |
| | **Pred.** | **Exp.** | **Pred.** | **Exp.** |
| **Level** | $A_4B_3D_2E_4$ | $A_4B_3D_2E_4$ | $A_3B_2D_2E_2$ | $A_3B_2D_2E_2$ |
| **S/N ratio for erosion rate (db)** | -2.6501 | -2.7692 | -2.0476 | -2.1102 |
| **Percentage Error** | 4.30% | | 2.96% | |

For this chosen combination of factors, the S/N ratios for EP-BGM and PP-BGM composites are found to be -2.65014 and -2.04763 respectively. Further, an experiment is also conducted taking the same factor combination and the test results are compared with value obtained from the predictive Equations 7.3 and 7.4. The comparison of the experimental and the predicted results along with the

associated percentage errors are given in Table 7.4. Errors of 4.30 % and 2.96 % for the S/N ratios of erosion rate are recorded. The error can be further reduced if the number of measurements is increased. Thus, the proposed correlations seem to be capable of predicting erosion rate to a reasonable accuracy.

### 7.4 Wear Rate Estimation using Predictive Equation

The solid particle erosion wear rate of the composite samples can also be predicted using a nonlinear regressive predictive equation showing the relationship between the erosion rate and combination of control factors. This correlation is developed statistically using standard software SYSTAT 7.

**Table 7.5** Comparison between experimental and predicted values for erosion rate

| EP-BGM | | | PP-BGM | | |
|---|---|---|---|---|---|
| **ER Experimental** | **ER Predicted** | **% Error** | **ER Experimental** | **ER Predicted** | **% Error** |
| 1.288 | 1.417 | 10.015 | 1.246 | 1.269 | 1.845 |
| 1.293 | 1.237 | 4.331 | 1.208 | 1.229 | 1.738 |
| 0.987 | 1.057 | 7.092 | 1.195 | 1.189 | 0.502 |
| 0.803 | 0.847 | 6.256 | 1.111 | 1.149 | 6.256 |
| 1.327 | 1.193 | 10.097 | 1.122 | 1.173 | 4.545 |
| 1.354 | 1.253 | 7.459 | 1.205 | 1.213 | 0.663 |
| 1.370 | 1.233 | 10.000 | 1.252 | 1.253 | 0.079 |
| 1.422 | 1.263 | 11.181 | 1.268 | 1.293 | 1.971 |
| 1.368 | 1.349 | 1.388 | 1.221 | 1.277 | 4.586 |
| 1.415 | 1.369 | 3.250 | 1.294 | 1.317 | 1.777 |
| 1.281 | 1.309 | 2.185 | 1.196 | 1.197 | 0.083 |
| 1.324 | 1.299 | 1.888 | 1.274 | 1.237 | 2.904 |
| 1.431 | 1.385 | 3.214 | 1.302 | 1.261 | 3.149 |
| 1.356 | 1.365 | 0.663 | 1.130 | 1.221 | 8.053 |
| 1.447 | 1.505 | 4.008 | 1.356 | 1.341 | 1.106 |
| 1.415 | 1.455 | 2.826 | 1.209 | 1.301 | 7.609 |

***Note:*** *ER:Erosion Rate (mg/kg), EP: Epoxy, PP: Polypropylene, BGM: Borosilicate Glass Micro-sphere*

In order to express the erosion rate in terms of a nonlinear regressive mathematical equation, the following form is suggested:

$$ER = k_0 + k_1 \times A + k_2 \times B + k_3 \times C + k_4 \times D + k_5 \times E \quad \textbf{(7.5)}$$

Here, ER is the performance output term i.e. the erosion rate in mg/kg and $k_i$ (i = 0, 1, 2, 3, 4, 5) are the model constants. A is the impact velocity (m/sec), B is the impingement angle (degree), C is the erodent size (micron), D is the erodent temperature ($^0$C) and E is the BGM content in the composite (wt%).

By using the software, the values of all of the constants are calculated and the final nonlinear regression expressions for the EP-BGM and PP-BGM composites are obtained by the Equations 7.6 and 7.7 respectively.

$$ER = 1.173 + 0.012 \times A - 0.002 \times B - 0.001 \times C - 0.001 \times D - 0.007 \times E \quad \textbf{(7.6)}$$

$$ER = 1.173 + 0.003 \times A + 0.000 \times B + 0.000 \times C - 0.000 \times D - 0.004 \times E \quad \textbf{(7.7)}$$

The correctness of the calculated constants is confirmed because a very high correlation coefficients ($r^2$) of 0.997 and 0.999 for the EP-BGM and PP-BGM composites respectively are obtained for Equation (7.5); therefore, the models are quite suitable for further analysis. A comparison between the wear rate obtained from experimental results and the predictive equation for composite combination are shown in Table 7.5, which indicates that the percentage errors associated with the predicted values with respect to the experimental ones vary in the range of 0 to 11 %.

### 7.5 ANN Based Prediction

As mentioned earlier, artificial neural network (ANN) is a technique that involves database training to predict input-output evolutions. In this attempt to simulate the erosion wear process and to predict the erosion rates of EP-BGM and PP-BGM composites under different operating conditions, five input parameters (impact velocity, impingement angle, erodent size, erodent

temperature and BGM content) are taken, each of which is characterized by one neuron in the input layer of the ANN structure. Different ANN structures with varying number of neurons in the hidden layer are tested at constant cycles, learning rate, error tolerance, momentum parameter, noise factor and slope parameter. Based on least error criterion, one structure, shown in Tables 7.6 and 7.7, are selected for training of the input-output data for EP-BGM and PP-BGM composites respectively.

The optimized three-layer neural networks used in these simulations are shown in Figures 7.5 and 7.6. A software package NEURALNET for neural computing based on back propagation algorithm is used as the prediction tool for erosion wear rate of the composites under various test conditions.

**Table 7.6** Input parameters for training (EP-BGM)

| **Input Parameters for Training** | **Values** |
|---|---|
| Error tolerance | 0.001 |
| Learning rate (β) | 0.002 |
| Momentum parameter (α) | 0.002 |
| Noise factor (NF) | 0.001 |
| Number of epochs | 1,00,00,000 |
| Slope parameter (£) | 0.6 |
| Number of hidden layer neurons (H) | 11 |
| Number of input layer neurons (I) | 5 |
| Number of output layer neurons (O) | 1 |

**Table 7.7** Input parameters for training (PP-BGM)

| **Input Parameters for Training** | **Values** |
|---|---|
| Error tolerance | 0.001 |
| Learning rate (β) | 0.002 |
| Momentum parameter (α) | 0.002 |
| Noise factor (NF) | 0.001 |
| Number of epochs | 1,00,00,000 |
| Slope parameter (£) | 0.6 |
| Number of hidden layer neurons (H) | 9 |
| Number of input layer neurons (I) | 5 |
| Number of output layer neurons (O) | 1 |

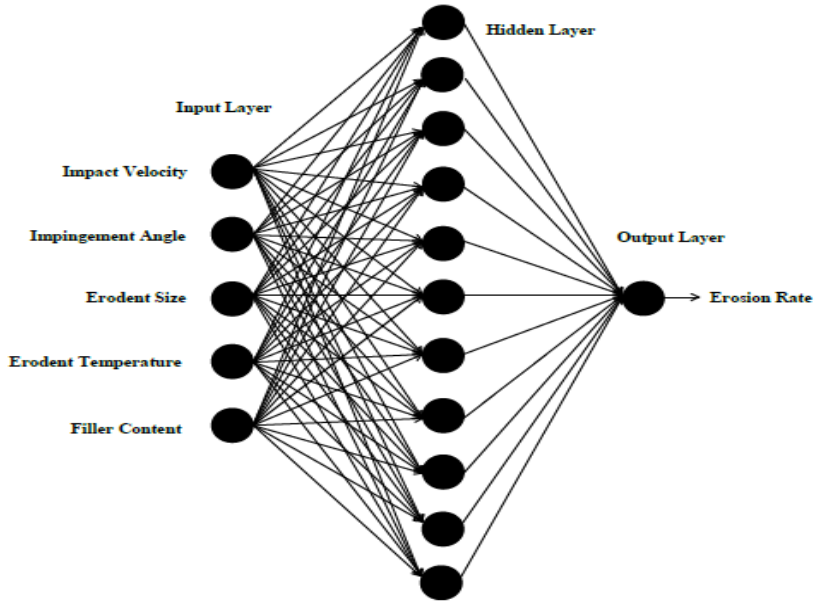


**Figure 7.5** Three layer neural network (EP-BGM)

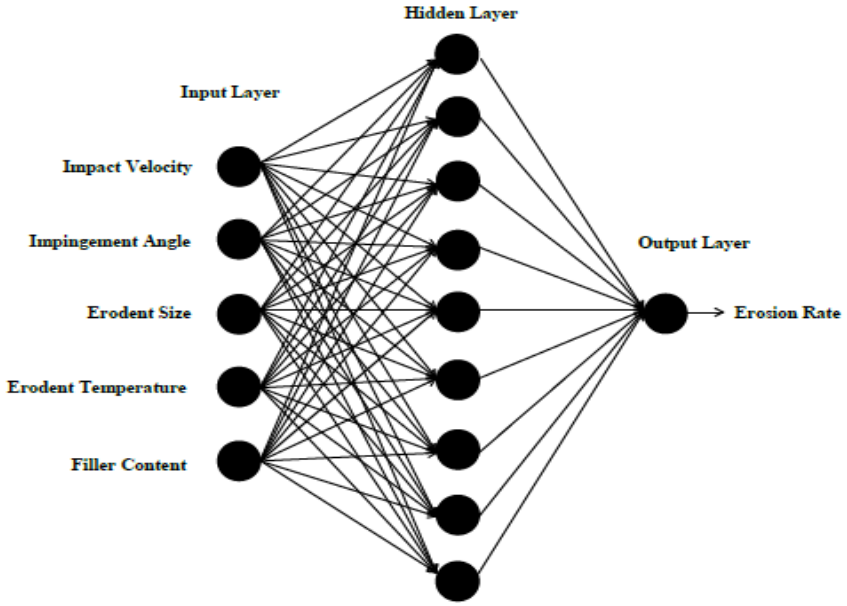


**Figure 7.6** Three layer neural network (PP-BGM)

The ANN predictive results of erosion wear rate for all the 16 test conditions and for all the composite combinations are shown and compared with the experimental values along with the associated percentage errors in Table 7.8. It is observed that the errors lie in the range of 0-10%, which establishes the validity of the neural computation. The errors, however, can still be reduced and the quality of predictions can be further improved by enlarging the data sets and optimizing the construction of the neural network.

**Table 7.8** Percentage error between experimental result and ANN prediction

| EP-BGM | | | PP-BGM | | |
|---|---|---|---|---|---|
| **ER Experimental** | **ER Predicted** | **% Error** | **ER Experimental** | **ER Predicted** | **% Error** |
| 1.288 | 1.351 | 4.891 | 1.246 | 1.243 | 0.240 |
| 1.293 | 1.365 | 5.581 | 1.208 | 1.2061 | 0.157 |
| 0.987 | 1.064 | 0.816 | 1.195 | 1.1667 | 2.368 |
| 0.803 | 0.810 | 0.873 | 1.111 | 1.1243 | 1.197 |
| 1.327 | 1.262 | 4.871 | 1.122 | 1.159 | 3.297 |
| 1.354 | 1.272 | 6.024 | 1.205 | 1.1751 | 2.481 |
| 1.37 | 1.290 | 5.804 | 1.252 | 1.251 | 0.079 |
| 1.422 | 1.321 | 7.091 | 1.268 | 1.2629 | 0.402 |
| 1.368 | 1.383 | 1.083 | 1.221 | 1.2609 | 3.267 |
| 1.415 | 1.397 | 1.267 | 1.294 | 1.3102 | 1.251 |
| 1.281 | 1.310 | 2.228 | 1.196 | 1.1756 | 1.705 |
| 1.324 | 1.310 | 1.029 | 1.274 | 1.2161 | 4.544 |
| 1.431 | 1.428 | 0.177 | 1.302 | 1.2748 | 2.089 |
| 1.356 | 1.385 | 2.153 | 1.13 | 1.232 | 9.026 |
| 1.447 | 1.494 | 3.261 | 1.356 | 1.3089 | 3.473 |
| 1.415 | 1.436 | 1.484 | 1.209 | 1.2582 | 4.069 |

***Note:*** *ER denotes Erosion Rate (mg/kg), EP: Epoxy, PP: Polypropylene BGM: Borosilicate Glass Micro-sphere*

A well-trained ANN is expected to be very helpful for the analysis of erosion wear characteristics of any given composites and permits to study quantitatively the effect of each of the considered input parameters on the wear rate. The range of any chosen parameter can be beyond the actual experimental limits, thus offering the possibility to use the generalization property of ANN in a large parameter space. In the present investigation, this possibility has been explored by selecting the most significant factor i.e. the impact velocity for EP-BGM composite in a range from 25 to 75 m/sec and the BGM content for PP-BGM composite in a range of 0 to 35 wt%. Sets of predictions for erosion wear rate of these composites of varied compositions at different impact velocities and

impingement angles are evolved and the predicted evolutions are presented in Figures 7.7 and 7.8. It is interesting to see that the erosion rate presents an almost linear type evolution with the impact velocity.

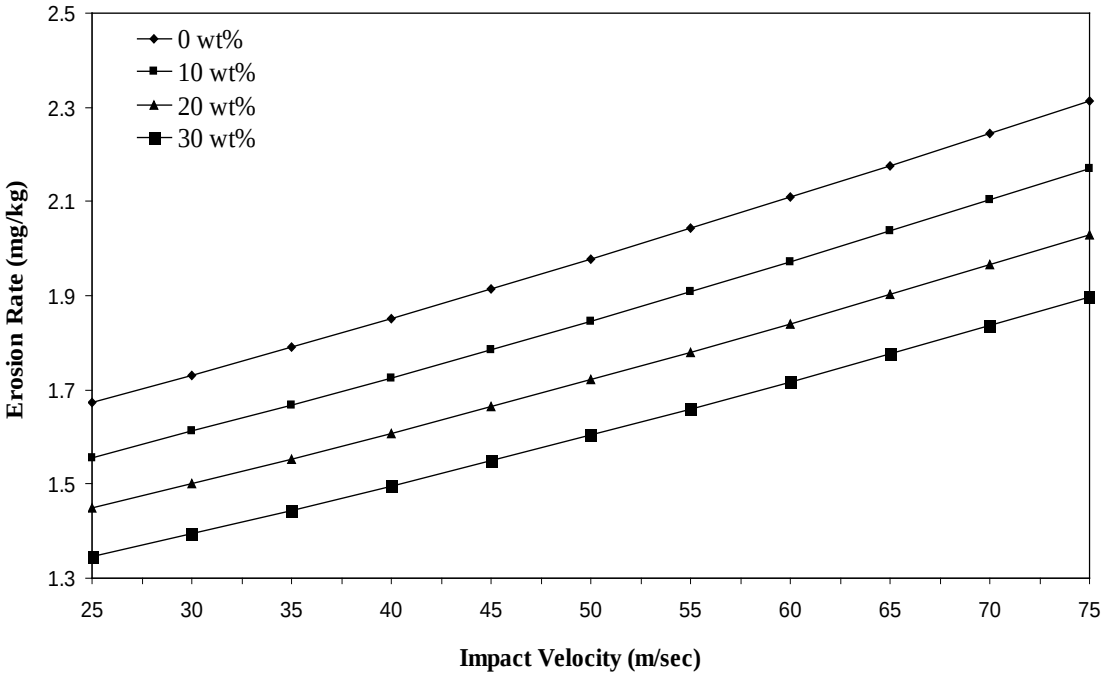


**(a)**

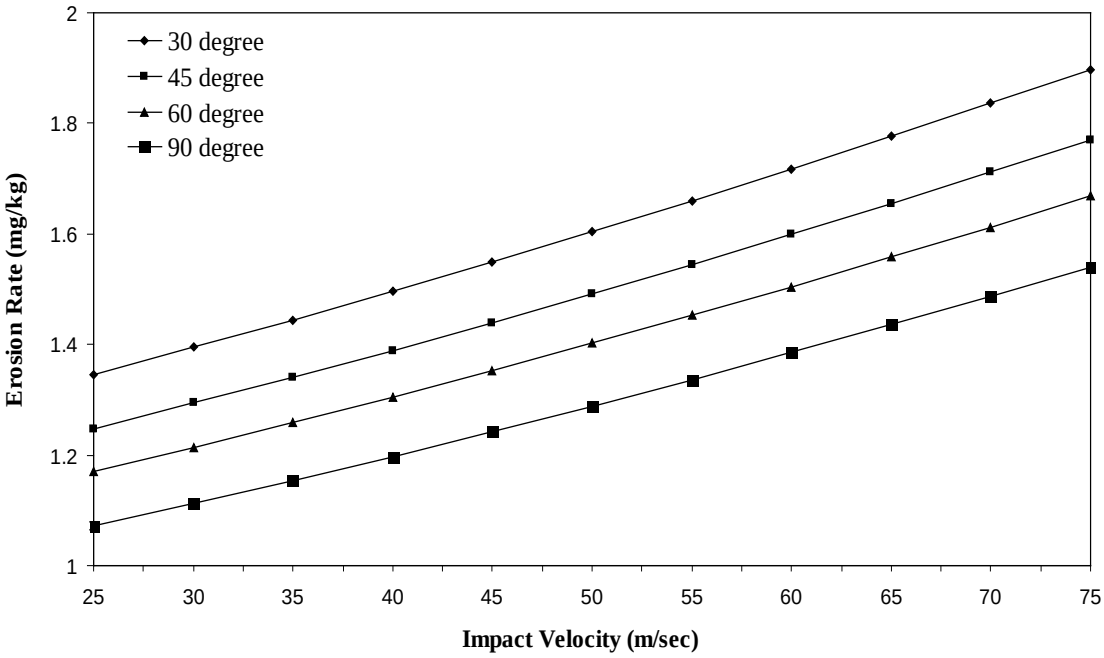


**(b)**

**Figure 7.7** Effect of impact velocity on erosion rate for different (a) BGM content (b) impingement angle for EP-BGM composite

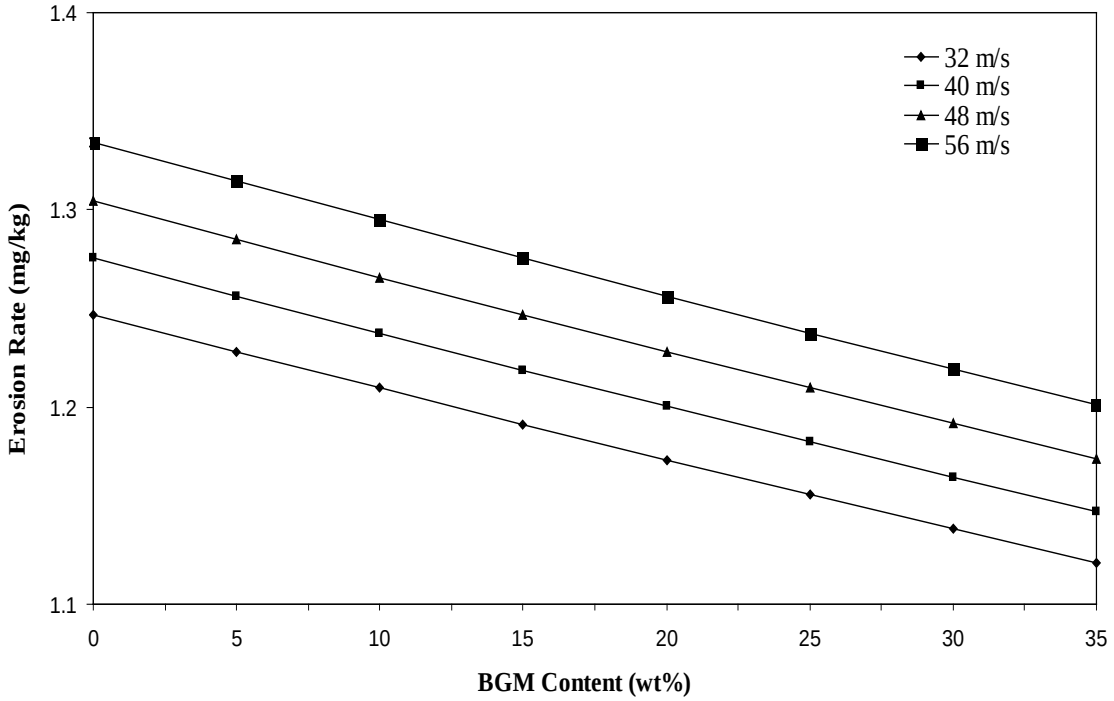


**(a)**

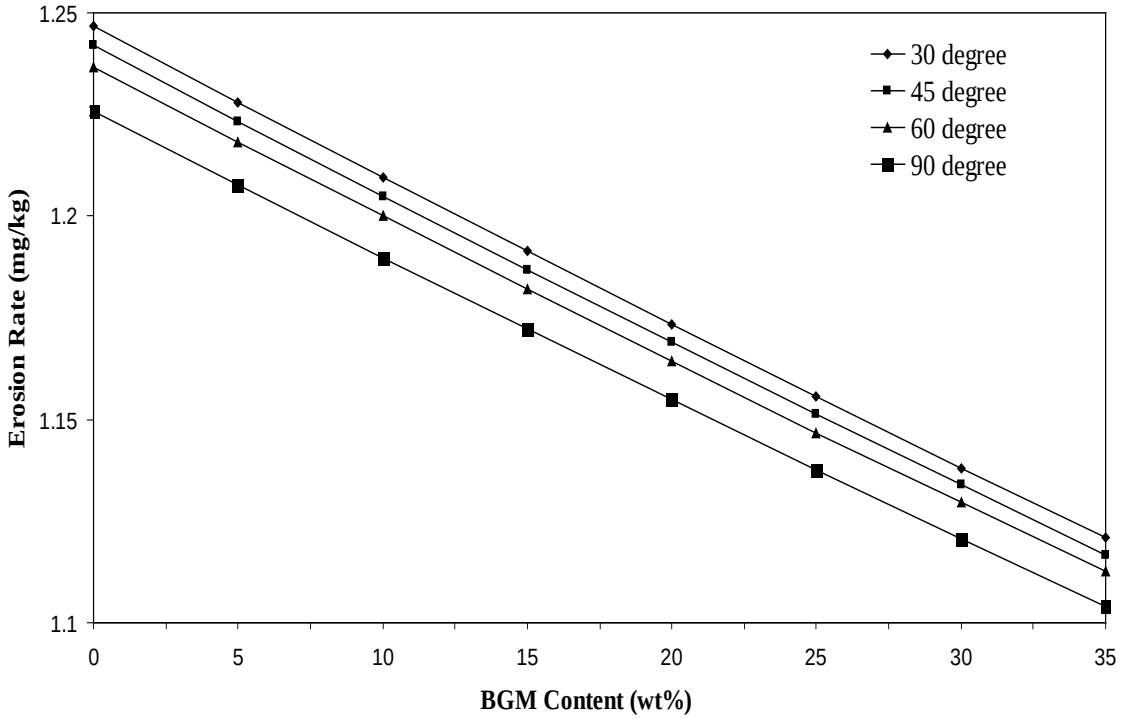


**(b)**

**Figure 7.8** Effect of BGM content on erosion rate for different (a) impact velocity (b) impingement angle for PP-BGM composite

Figures 7.9 and 7.10 present the comparison of the measured erosion rates with those obtained from the ANN prediction and from the proposed predictive

equation for EP-BGM and PP-BGM composites respectively. While the errors associated with the ANN predictions lie in the range of 0-10%, the same for results obtained from the proposed correlation lie in the range of 0-11%. Thus it can be concluded that both ANN and the proposed correlation can be used for predictive purpose as far as the estimation of erosion wear rate of the composites under this investigation is concerned.

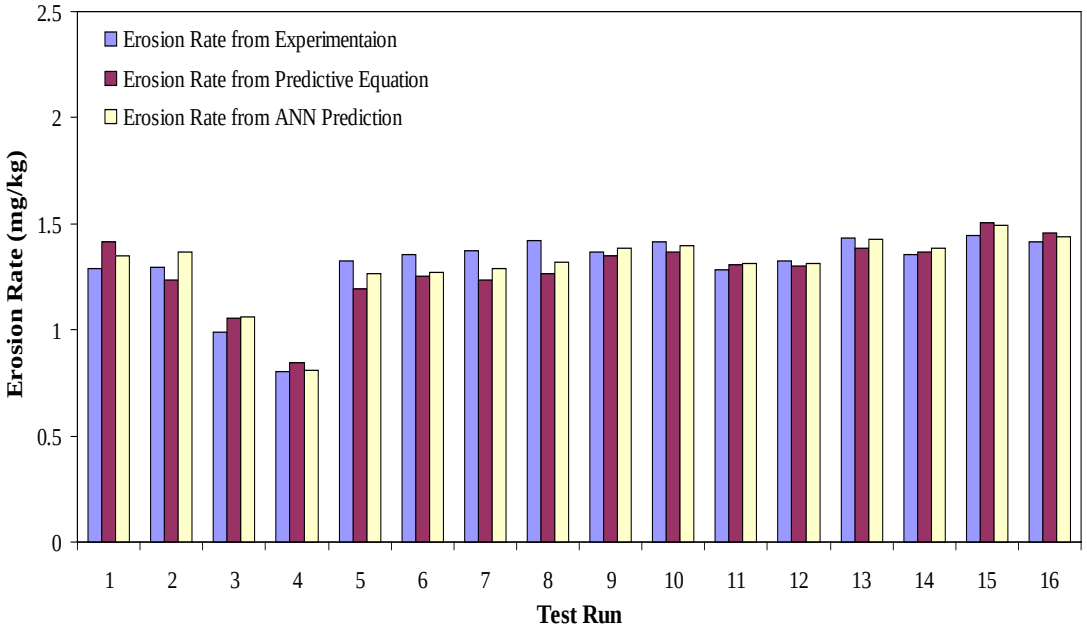


**Figure 7.9** Comparison of erosion rates of EP-BGM composites obtained from different methods

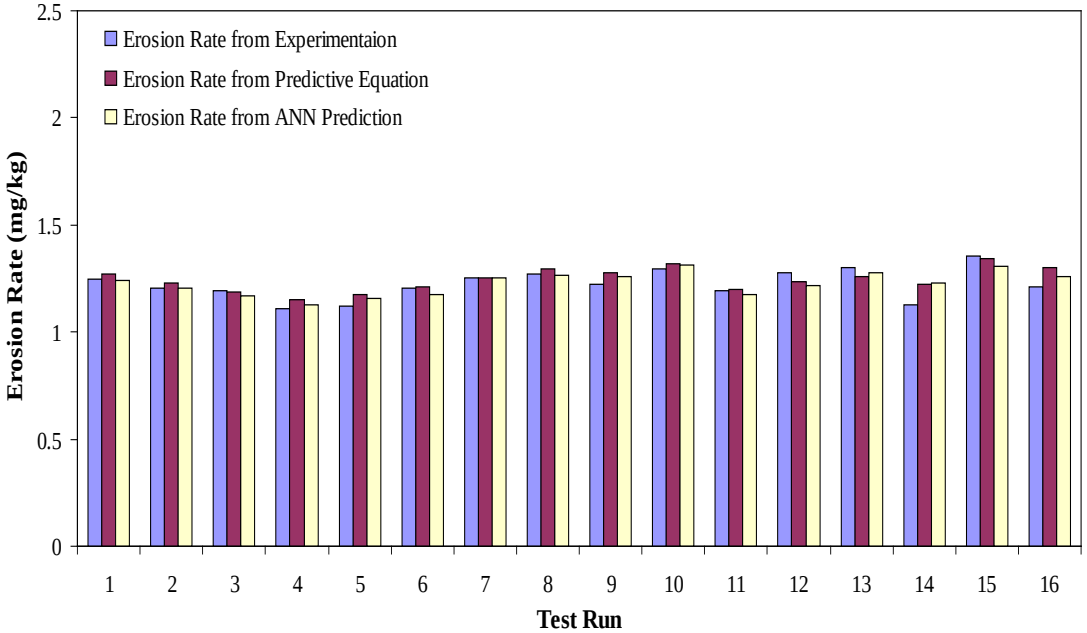


**Figure 7.10** Comparison of erosion rates of PP-BGM composites obtained from different methods

### 7.6 Effect of Impingement Angle on Erosion Rate

The erosion wear response of polymer composites can be grouped into ductile and brittle categories although this grouping is not definitive because the erosion characteristics depend on the experimental conditions as much as on the composition of the target material. It is well known that impingement angle is one of the important parameters in the erosion process and for ductile materials the peak erosion normally occurs at 15-30$^0$ angle while for brittle materials, the erosion damage is maximum usually at normal impact i.e. at 90$^0$ impingement angle.

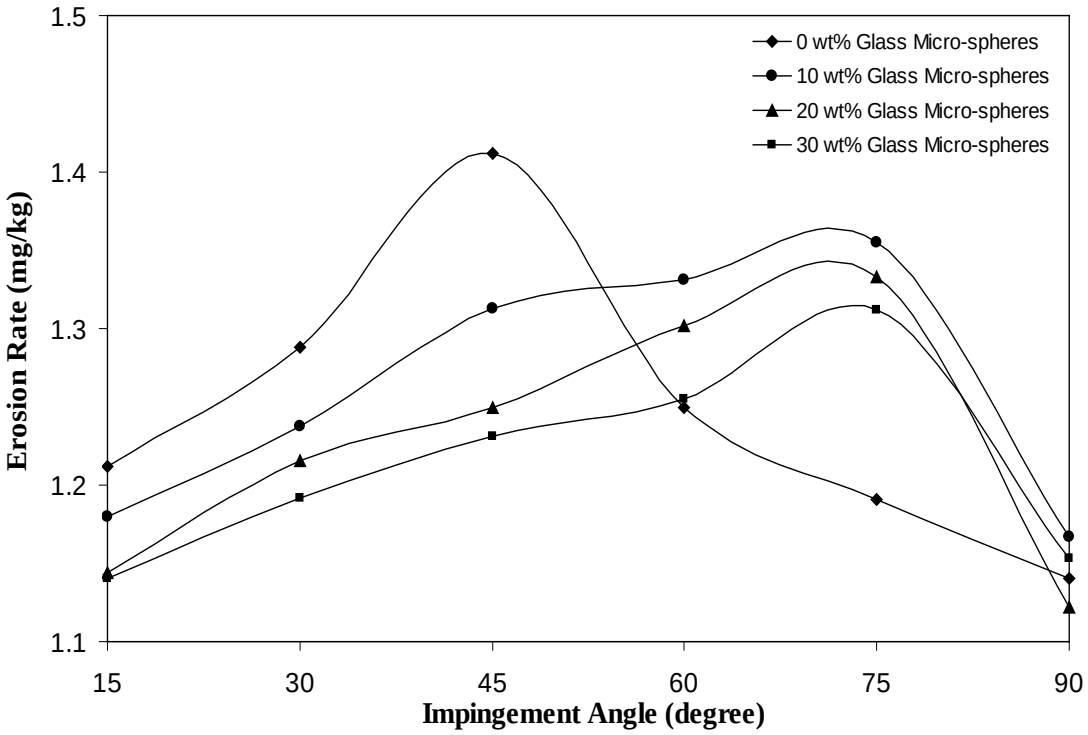


**Figure 7.11** Effect of impingement angle on erosion rate of epoxy-BGM composites (Impact vel. 32 m/sec, erodent size 50 micron, erodent temp. 30$^0$C)

In the present study, the variation of erosion wear rate of the composites with impingement angle is studied by conducting experiments under specified operating conditions. The results are presented in Figures 7.11 and 7.12 which shows that the peak erosion for hardened neat epoxy occurs at 45$^0$ impingement angle and for neat PP, peak erosion occurs at 30$^0$ impingement angle. It is obvious as thermoplastic polymers exhibit ductile erosion response. As shown in

Figures 7.11 and 7.12, the peak erosion takes place at an impingement angle of $75^0$ for EP-BGM composites and at $60^0$ for PP-BGM composites irrespective of the filler content, indicating a semi-brittle response. This behavior may be attributed to the incorporation of hard crystalline BGM particles within the matrix body.

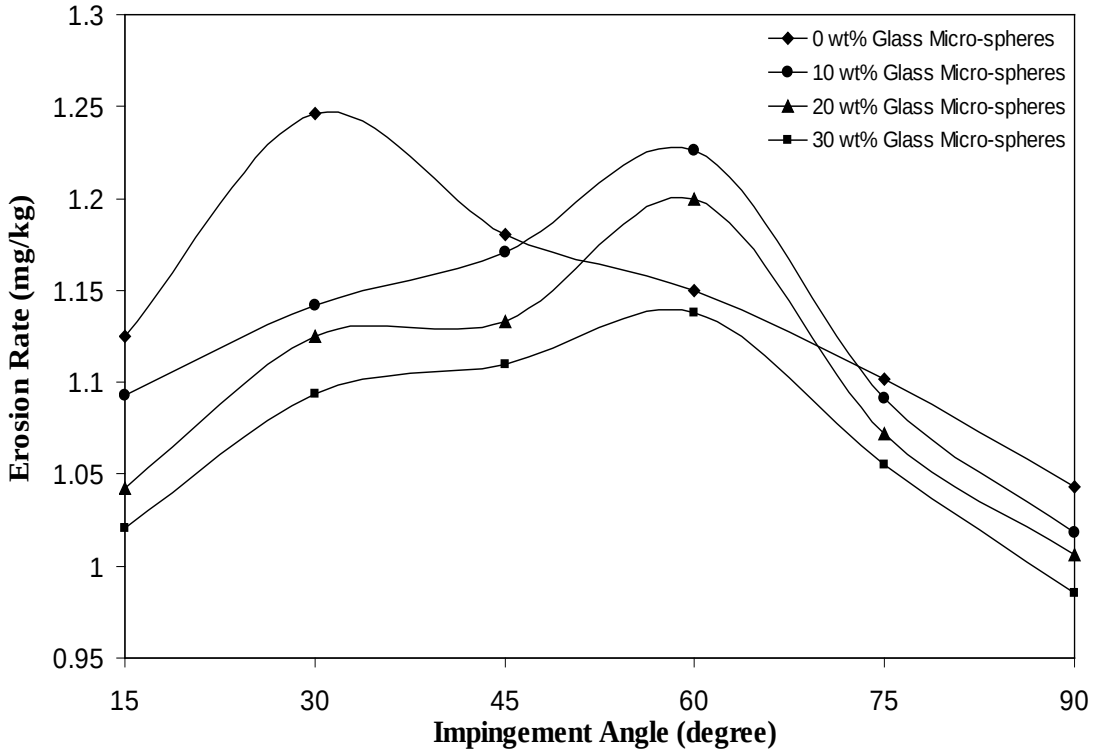


**Figure 7.12** Effect of impingement angle on erosion rate of PP-BGM composites (Impact vel. 32 m/sec, erodent size 50 micron, erodent temp. $30^0$C)

## 7.7 Discussion

The main experimental factor and the main material variable that are found to be influencing the erosion rate are the impact velocity and the filler (glass micro-sphere) content respectively. For all the composite types under this study, erosion rates are estimated at different impact velocities and BGM content. It is seen that invariably for all the composite samples, the erosion rates gradually and almost linearly increase with the increase in the impact velocity and decrease with the increase in BGM content. The increase in erosion rate can be attributed to the increased penetration of erodent particles on impact as a result

of dissipation of greater amount of particle kinetic energy to the target surface. This leads to more surface damage, enhanced sub-critical crack growth etc. and consequently to the reduction in erosion resistance. Similarly the drop in erosion rate with increasing BGM content can be attributed to the increase in the bulk hardness of the composite. Influence of BGM particles in reducing the erosion rates is very significant. In fact, the main advantage of adding hard phases to soft matrix is in increasing the stiffness of the matrix. While the friction is controlled by the self-lubricating property of the matrix, wear resistance is improved because of the improvement in composite micro-hardness due to the presence of hard and strong second phase. The hard BGM particles pose resistance to the erosive particles as first line of defense and thereby leading to a decrease in wear rates.

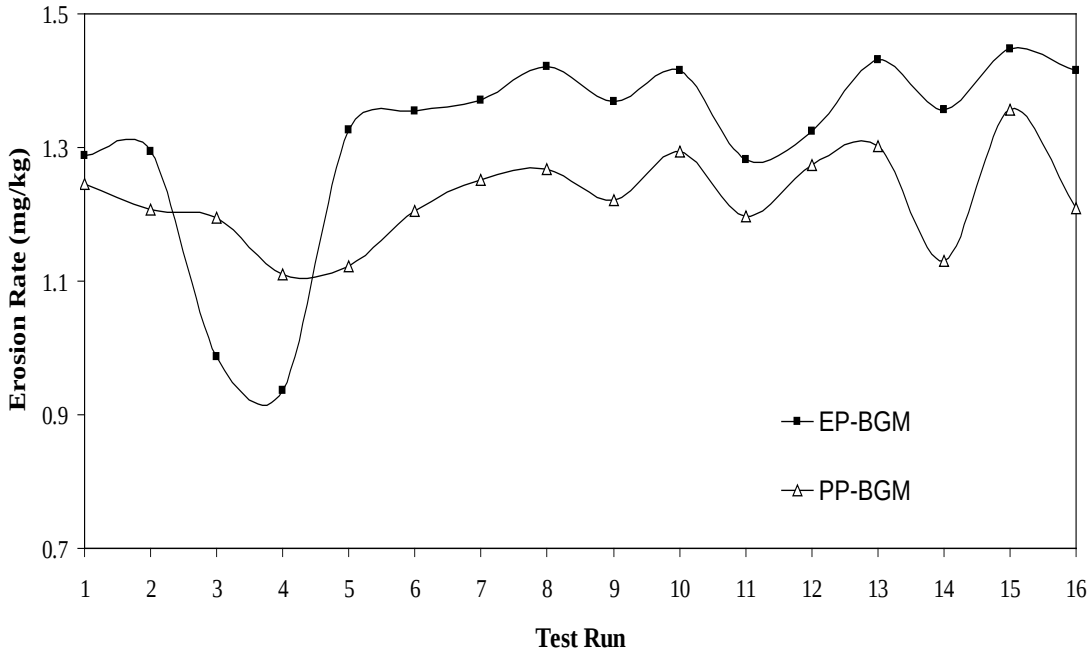


**Figure 7.13** Comparison of wear rates of composites under different test conditions

A comparison of the erosion responses of EP-BGM and PP-BGM composites is presented in Figure 7.13. The factors which govern the erosion rate of glass micro-sphere filled polymers are: the brittleness of the filler and the interfacial bond strength between the filler and the matrix. The sequence of damage due to

erosion is in this order (a) local removal of material in the polymer-rich zones, (b) erosion in the particulate filler zones associated with breakage of filler particles, and (c) erosion of the matrix-filler interface zones. Another factor which governs the erosion rate of EP-BGM and PP-BGM composites is the nature of the matrix being either thermosetting or thermoplastic. The difference in response of these two types of polymers to solid particle erosion have been reported and explained by a number of researchers in the past [1, 4, 5, 11, 159, 320, 321, 322]. Thermoplastic polymers become soft and formable when heated and the polymer melt can be formed or shaped when it is in this softened state. On the other hand, thermosetting polymers cannot be shaped or formed to any great extent and will definitely not flow. Hence in the present work, while plastic deformation is predominant in polypropylene (thermoplastic) based composites, features like micro-cutting and matrix-fracture characterize the epoxy (thermosetting) based composites.

**Chapter Summary**

This chapter has provided:

- The results of erosion tests for glass micro-sphere filled epoxy and polypropylene composites and their comparison
- The analysis of the experimental results using Taguchi method
- The surface morphologies of uneroded and eroded composites using SEM
- Simulated wear predictions under different test conditions within and beyond the experimental domain using ANN model
- The effect of the most influencing factor on erosion response of the composites

*****

Chapter 8

# SUMMARY AND CONCLUSIONS

The research reported in this thesis broadly consists of two parts:

- The first part has provided the description of the materials used, the experimental details and the methodologies adopted for analysis of experimental results. This part has also presented various physical and mechanical characteristics of the plasma sprayed coatings of glass micro-spheres (BGM, 'BGM + $Al_2O_3$' and 'BGM + $TiO_2$' coatings) and glass micro-sphere filled polymer composites (epoxy-BGM and polypropylene-BGM composites). An assessment of borosilicate glass micro-sphere (BGM) as a potential coating material and as a potential particulate filler in polymers has been made by evaluating the physical and mechanical properties of these coatings and composites under controlled laboratory conditions. A comparative evaluation of the effects of premixing of $Al_2O_3$ and $TiO_2$ powder on the physical and mechanical properties of glass micro-sphere coatings has also been made in this part.

- The second part reports on the solid particle erosion wear response of these coatings and composites. The erosion characteristics of both 'BGM + $Al_2O_3$' and 'BGM + $TiO_2$' coatings have been discussed separately and then a comparison has been presented. A comparison between glass micro-sphere filled epoxy and polypropylene composites has also been presented. Parametric appraisal of solid particle erosion wear process has been made for all coatings and composites using a statistical technique namely Taguchi experimental design. Correlations have been developed to predict the wear rate for these coatings and composites under different test conditions. Implementation of artificial neural networks for erosion

wear rate prediction of these coatings and composites has also been included in this part.

### 8.1 Summary of Research Findings

The performance of any engineering material is judged by its properties and behaviour under normal as well as adverse test environments. This information becomes essential for selecting the proper material for a given application as well as for designing purpose. To this end, the present work has reported the performance of a new class of glass micro-sphere based coatings and a new class of glass micro-sphere filled polymer based composites with emphasis on the general trends observed in their properties and behavior. A wealth of property data has been generated by conducting various characterization tests under controlled laboratory conditions. Some of the worth noting findings of these tests are summarized below.

Plasma spray coating is a complex process that combines particle injection, melting, quenching and consolidation in a single operation. The quality of coating in terms of mechanical, micro-structural and functional characteristics depends on a large number of variables that include both materials as well as operational parameters. While the composition of coating material and the substrate play an important role in determining the coating quality, the influence of plasma torch input power is also equally important; this is reflected in the research findings of the present investigation. The variations of different coating characteristics such as coating adhesion strength, deposition efficiency, coating thickness and micro-hardness with the plasma torch input power are evident in the illustrations presented in this thesis. The erosion resistance of 'BGM + $Al_2O_3$' and 'BGM + $TiO_2$' coatings are found to be lower than that of BGM coatings under similar test conditions. This has led to the conclusion that although the premixing of $Al_2O_3$/$TiO_2$ with BGM improves its coatabilty and some of the primary coating characteristics like coating adhesion strength,

coating thickness etc., the erosion wear resistance is compromised to some extent.

The present research shows that glass micro-sphere also has the potential to be successfully used as a functional filler material in both thermoset and thermoplastic polymers. It is noticed that the epoxy composites filled with glass microspheres have higher void fraction compared to that in the polypropylene composites. This difference is attributed to the difference in processing routes adopted while preparing the epoxy (hand layup) and polypropylene (injection/compression molding) composites. The presence of pores and voids in the composite structure significantly affects some of the mechanical properties and even the performance of the composites. Higher void contents usually mean lower fatigue resistance, greater susceptibility to water penetration and weathering. However, presence of void is unavoidable in composite making particularly through hand-lay-up route.

By incorporating glass microspheres in epoxy and polypropylene, synergistic effects, as expected are achieved in the form of modified mechanical properties and wear resistance. Inclusion of glass microspheres in these polymeric resins has not resulted in any improvement in the load bearing capacity (tensile strength) or in the ability to withstand bending (flexural strength) of the composites. On the other hand, hardness values have been found to have improved invariably for all the composites with addition of glass microspheres. This is obvious as the intrinsic hardness of glass is higher than those of the resin materials. The reduction in tensile strength and the improvement in hardness with the incorporation of glass microspheres can also be explained as follows: under the action of a tensile force, the filler-matrix interface is vulnerable to debonding depending on interfacial bond strength and this may lead to a break in the composite. But in case of hardness test, a compression or pressing stress is in action. So the polymeric matrix phase and the solid filler phase would be pressed

together and touch each other more tightly. Thus, the interface can transfer pressure more effectively although the interfacial bond may be poor.

This research shows that impact velocity and the composition of the target material are the factors that affect the wear rate significantly in case of solid particle erosion. The erosion wear rates of the coatings and composites are also found to be dependent on the impingement angle. In fact the angle of impingement determines the relative magnitude of the two components of the impact velocity, namely the components normal and parallel to the surface respectively. The normal component will determine how long the impact will last (that is the contact time and the load). The product of this contact time and the tangential (parallel) velocity component determines the amount of sliding that takes place. The tangential velocity component also provides a shear loading to the surface which is in addition to the normal load that the normal velocity component causes. Hence, as this angle changes, the amount of sliding that takes place also changes the nature and magnitude of the stress system. Both of these aspects influence the way a coating wears out. This study has indicated that composites with different constituents and compositions exhibit different angular dependency.

The objective of using Taguchi technique in this study of erosion response is to identify significant factors that affect the erosion rate of the coatings substantially. This method thus provides the researchers with a systematic and efficient approach for conducting experimentation to determine near optimum settings of design parameters for performance and cost. The Taguchi method utilizes orthogonal arrays to study a large number of variables with a small number of experiments. The greatest advantage of this method is that the use of these orthogonal arrays significantly reduces the number of experimental trials.

Functional coatings and composites have to fulfill various requirements when employed in tribological applications. The wear rate is one such requirement as it is directly related to the service life period of the coatings and composites. In

order to achieve certain degree of erosion wear resistance accurately and repeatedly, the influence parameters of the process have to be controlled accordingly. The present research has shown that neural computation can be successfully used as a predictive tool in such a case to process very large data related to a real time erosive situation and to simulate any desired parameter in a space larger than the domain of experimentation.

### 8.2 Conclusions

This analytical and experimental investigation on using borosilicate glass micro-spheres in wear resistant coatings and composites has led to the following specific conclusions:

1. This work suggests that glass micro-spheres are coatable and deposition of such coatings on metallic substrates using plasma spraying route is possible. During this experimental investigation, maximum deposition efficiencies of about 25% and 23% are recorded for glass micro-sphere coatings on mild steel and aluminium substrates respectively. These coatings possess desirable characteristics such as good adhesion strength, hardness etc.

2. Pre-mixing of micro-sized $Al_2O_3$ or $TiO_2$ particles improves the coatability of glass micro-spheres. The mixture of glass micro-spheres and $Al_2O_3$ particles is found to be eminently coatable with deposition efficiencies of 38.657% and 36.468% for mild steel and aluminium substrate respectively. Similarly, for the mixture of glass micro-spheres and $TiO_2$ particles, coating deposition efficiencies as high as 41.857% and 39.984% are achieved for mild steel and aluminium substrate respectively. It is found that coating deposition efficiency presents a sigmoid type evolution with the plasma torch input power.

3. Coatings of glass micro-spheres premixed with micro-sized $Al_2O_3$ or $TiO_2$ particles exhibit improved interfacial adhesion strength. The strength is greatly affected by the plasma torch input power. Maximum adhesion

strengths of about 32 MPa and 33 MPa are recorded for coatings of glass micro-spheres premixed with 30 wt% $Al_2O_3$ deposited at 20 kW on mild steel and aluminium substrates respectively. Similarly, maximum adhesion strengths of about 34 MPa and 35 MPa are recorded for coatings of glass micro-spheres premixed with 30 wt% $TiO_2$ deposited under similar conditions. The input power also affects the coating thickness, porosity and hardness appreciably.

4. Glass micro-sphere possesses ample reinforcing potential to be used as a functional filler in both thermoset and thermoplastic polymers. Successful fabrication of epoxy composites reinforced with glass micro-spheres is possible by simple hand-lay-up technique. Similarly, glass micro-sphere filled polypropylene composites can also be fabricated by injection molding and compression molding routes.

5. These glass micro-sphere filled composites possess very low amount of porosity (maximum $\approx$ 2%) and improved micro-hardness. They also exhibit improved impact strength as compared to that of the neat polymers. The tensile and flexural strength of the composites are affected, though marginally, by the weight fraction of glass micro-spheres in the composites. With improved hardness, these composites have the potential to be used in wear related applications.

6. Solid particle erosion wear characteristics of glass micro-sphere coatings and glass micro-sphere filled polymer composites have been successfully analyzed using Taguchi technique. Significant factors affecting the erosion rate of these coatings and composites are identified through successful implementation of signal-to-noise response approach. In the present work, it can be concluded that for all types of coatings and epoxy based composites, among all the factors, impact velocity is the most significant factor as far as the erosion wear rate is concerned. On the other hand, for the glass micro-sphere filled polypropylene composites, among

all the factors affecting the erosion rate, filler content emerged as the most significant factor followed by impact velocity. Factors like erodent size and erodent temperature have relatively much less significance on the erosion rate invariably in all the cases.

7. Impingement angle is identified as one of the major operating parameters significantly affecting the erosion rate of glass micro-sphere filled epoxy and polypropylene composites. A study on the variation of erosion rate with impingement angle reveals the semi-brittle erosion response of the composites under this investigation. The peak erosion rate is found to occur at $75^0$ impingement angle for all the epoxy based composites and at $60^0$ impingement angle for all the polypropylene based composites under similar experimental conditions.

8. Two predictive models; one based on artificial neural networks (ANN) approach and the other on Taguchi approach are proposed in this work. It is demonstrated that these models well reflect the effects of various factors on the wear loss and their predictive results are consistent with the experimental observations. Neural computation is successfully applied in this investigation to predict and simulate the wear response of these coatings and composites under various test conditions within and beyond the experimental domain.

### 8.3 Recommendations for Potential Applications

The plasma sprayed BGM, 'BGM + $Al_2O_3$' and 'BGM + $TiO_2$' coatings developed for this investigation are expected to have adequate potential for a wide variety of applications particularly in erosive environments. The use of such coatings is suggested in structural applications such as electric towers and engineering trusses in deserts and mining sites. These coatings can also be recommended for engineering applications such as pipelines and valves carrying particulate matters, transport tubes carrying abrasive materials in an air stream, coal bends carrying pulverized coal, rocket motors trail nozzle, gun barrel,

compressor, turbine and exhaust fan blades, burner nozzle, reheater, super heater and economizer tube banks etc.

Composite materials show excellent performance, these days, starting from their applications in manufacturing industries to house-hold appliances. It is due to their light weight, high stiffness-to-weight and strength-to-weight ratios and potentially high resistance to environmental degradation, resulting in lower lifecycle costs. The glass micro-sphere filled epoxy and polypropylene composites fabricated and experimented upon in this investigation are found to have adequate potential for a wide variety of applications particularly in wear prone environment. Their use may be suggested in applications like engineering structures in dusty environment and low cost building materials in deserts. Use of these composites, in general, may also be recommended for applications like partition boards, false ceilings, pipe lines carrying coal dust, pulley laggings, exhaust fan blades, nozzles and diffusers, light weight vehicles etc.

### 8.4 Scope for Future Work

The present research work leaves a wide scope for future investigators to explore many other aspects of glass micro-sphere coatings and glass micro-sphere filled polymer composites. Some recommendations for future research include:

- The possible use of ceramic/metallic powders other than $Al_2O_3$ and $TiO_2$ as additive in the development of glass micro-sphere based composite coatings.
- Possible use of polymeric resins other than epoxy and polypropylene in the development of new wear resistant glass micro-sphere filled composites.
- Study on the response of these coatings and composites to other wear modes such as sliding, corrosion and abrasion.
- Cost analysis of these coatings and composites to assess their economic viability in industrial applications.

*****

## REFERENCES


1. Sahu S. P., Satapathy A., Patnaik A., Sreekumar K. P. and Ananthapadmanabhan P. V. (2010), Development, characterization and erosion wear response of plasma sprayed fly ash–aluminum coatings, Materials and Design, 31, pp. 1165-1173.

2. Heimann R. B. (1996), Plasma spray coating-principles and applications, VCH Weinheim, Germany.

3. Satapathy A. (2006), Thermal spray coating of red mud on metals, Ph.D. Thesis, N.I.T., Rourkela, India.

4. Biswas S. (2010), Processing, characterization and wear response of particulate filled epoxy based hybrid composites, Ph.D. Thesis, N.I.T., Rourkela, India.

5. Nielsen L. E. and Landel R. F. (1994), Mechanical properties of polymers and composites, 2nd ed. NY: Marcel Dekker, pp. 557.

6. Peters S. T. (1998), Handbook of composites, 2nd ed. London: Chapman and Hall, pp. 242.

7. Stolarski T. A. (1990), Tribology in machine design, Heiman Newnes, UK.

8. Budinski K. G. (1998), Surface engineering for wear resistance, Prentice Hall, Englewood Cliffs, New Jerssy, USA, pp. 209.

9. Robinowicz E. (1965), Friction and wear of materials, John Wiley, NY, USA.

10. Barkoula N. M. and Karger-Kocsis J. (2002), Review-processes and influencing parameters of the solid particle erosion of polymers and their composites, Journal of Materials Science, 37, pp. 3807-3820.

11. Patnaik A., Satapathy A., Chand N., Barkoula N. M. and Biswas S. (2010), Solid particle erosion wear characteristics of fiber and particulate filled polymer composites: A review, Wear, 268, pp. 249-263.

12. Thomas H. Kosel (1992), Solid Particle Erosion, ASM Handbook, ASM International, 18, pp. 199-213.

13. Vuoristo P. M. J., Niemi K. J. and Mantyla T. A. (1992), Handbook of thermal spray technology, ASM International, Materials Park, OH, USA, pp. 171.

14. Ko P. L. and Robertson M. F. (2002), Wear characteristics of electrolytic hard chrome and thermal sprayed WC-10%Co-4%Cr coatings sliding against Al– Ni–Bronze in air at 21 $^0$C and at -40 $^0$C, Wear, 252 (11-12), pp. 880-893.

15. Saharoui T., Fenineche N. E., Montavon G. and Coddet C. (2004), Alternative to chromium: characteristics and wear behaviour of HVOF coatings for gas turbine shafts repair (heavy-duty), Journal of Materials Processing Technology, 152, pp. 43-55.

16. Rastegar F. and Richardson D. E. (1997), Alternative to chrome: HVOF cermet coatings for high horse power diesel engines, Surface and Coatings Technology, 90 (1-2), pp. 156-163.

17. Dorfman M. R. (2002), Thermal spray materials, Advanced Materials and Processes, 160 (8), pp. 49-51.

18. Herman H., Sampath S. and McCune R. (2000), Thermal spray: current status and future trends, in: Sampath S., McCune R. (Eds.), MRS Bulletin, pp. 17–25.

19. Wang Y., Jiang S., Wang M., Wang S., Xiao T. D. and Strutt P. R. (2000), Abrasive wear characteristics of plasma sprayed nanostructured alumina/titania coatings, Wear, 237 (2), pp. 176-185.

20. Xie Y. and Hawthorne H. M. (1999), Wear mechanism of plasma sprayed alumina coating in sliding contacts with harder asperities, Wear, 225-229 (1), pp. 90-103.

21. Fervel V., Normand B. and Coddet C. (1999), Tribological behaviour of plasma sprayed $Al_2O_3$-based cermet coatings, Wear, 230 (1), pp. 70–77.

22. Pantelis D. I., Psyllaki P. and Alexopoulos N. (2000), Tribological behaviour of plasma-sprayed $Al_2O_3$ coatings under severe conditions, Wear, 237 (2), pp. 197–204.

23. Normand B., Fervel V., Coddet C. and Nikitine V. (2000), Tribological properties of plasma sprayed alumina-titania coating: role and control of the microstructure, Surface and Coatings Technology, 123 (2-3), pp. 278–287.

24. Liu Z., Dong Y., Chu Z., Yang Y, Li Y. and Yan D. (2013), Corrosion behavior of plasma sprayed ceramic and metallic coatings on carbon steel in simulated seawater, Materials and Design, 52, pp. 630-637.

25. Netaji M., Rahimipour M. R. and Mobasherpour I. (2014), Evaluation of hot corrosion behavior of CSZ, CSZ/micro $Al_2O_3$ plasma sprayed thermal barrier coatings, Ceramics International, 40 (3), pp. 4579-4590.

26. Herrmann M., Toma F. L., Berger L. M., Kaiser G. and Stahr C. C. (2014), Comparative study of the corrosion resistance of thermally sprayed ceramic coatings and their bulk ceramic counterparts, Journal of the European Ceramic Society, 24 (2), pp. 493-504.

27. Perumal G., Geetha M., Asokamani R. and Alagumurthi N. (2014), Wear studies on plasma sprayed $Al_2O_3$-40 wt% 8YSZ composite ceramic coating on Ti-6Al-4V alloy used for biomedical applications, Wear, 311 (1-2), pp. 101-113.

28. Wang L. J., Qiu P. X., Liu Y., Zhou W., Gou Q. and Chen H. (2013), Corrosion behavior of thermal sprayed WC cermet coatings containing metallic binders in saline environment, Transactions of Nonferrous Metals Society of China, 23 (9), pp. 2611-2617.

29. Hawthorne H. M., Erickson L. C., Ross D., Tai H. and Troczynski T. (1997), The microstructure dependence of wear and indentation behaviour of some plasma sprayed alumina coatings, Wear, 203-204, pp. 709-714.

30. Ramachandran K., Selvarajan V., Ananthapadmanabhan P. V. and Sreekumar K. P. (1998), Microstructure, adhesion, micro-hardness, abrasive wear resistance and electrical resistivity of the plasma sprayed alumina and alumina-titania coatings, Thin Solid Films, 315 (1-2), pp. 144-152.

31. Wang D., Tian Z., Shen L., Liu Z. and Huang Y. (2014), Effects of laser remelting on microstructure and solid particle erosion characteristics of $ZrO_2$–7wt%$Y_2O_3$ thermal barrier coating prepared by plasma spraying, Ceramics International, 40 (6), pp. 8791- 8799.

32. Ramachandran C. S., Balasubramanian V. and Ananthapadmanabhan P. V. (2013), Erosion of atmospheric plasma sprayed rare earth oxide coatings under air suspended corundum particles, Ceramics International, 39 (1), pp. 649-672.

33. Pati P. R. and Satapathy A. (2014), Development of wear-resistant coatings using LD slag premixed with $Al_2O_3$, Journal of Materials Cycle and Waste Management, DOI: 10.1007/s10163-014-0234-1.

34. Bayrak G. and Yilmaz S. (2006), Crystallization kinetics of plasma sprayed basalt coatings, Ceramics International, 32 (4), pp. 441-446.

35. Yilmaz R., Kurt A. O., Demir A. and Tatli Z. (2007), Effects of $TiO_2$ on the mechanical properties of them $Al_2O_3$- $TiO_2$ plasma sprayed coating, Journal of the European Ceramic Society, 27 (2-3), pp. 1319-1323.

36. Auciello O. and Flamm D. L. (1989), Plasma diagnostics, Plasma-materials Interactions, Vol. 1, Academic Press, Boston, Mass.

37. Wang B. Q., Geng G. Q. and Levy A. V. (1992), Erosion and erosion-corrosion behavior of chromized-siliconized steel, Surface and Coatings Technology, 54-55 (2), pp. 529-535.

38. Modi M. D., Modi S. C. and Mayuram M. M. (1986), A case study on the use of plasma sprayed oxide ceramic coatings in hot extrusion dies for nonferrous metals, In: Proceedings of the 11th international thermal spraying conference, 8-12 September, Montreal, Canada, pp. 359-366.

39. Tucker (Jr.) R. C. (2002), Thermal spray coatings: broad and growing applications, International Journal of Powder Metallurgy, 38 (7), pp. 45-53.

40. Westergard R., Erickson L. C., Axen N., Hawthorne H. M. and Hogmark S. (1998), The erosion and abrasion characteristics of alumina coatings plasma sprayed under different spraying conditions, Tribology International, 31 (5), pp. 271-279.

41. Toma D., Brandl W. and Marginean G. (2001), Wear and corrosion behaviour of thermally sprayed cermet coatings, Surface and Coatings Technology, 138 (2-3), pp. 149-158.

42. Fu Y. Q., Batchelor A. W., Wang Y. and Khor K. A. (1998), Fretting wear behaviors of thermal sprayed hydroxyapatite (HA) coating under unlubricated conditions, Wear, 217 (1), pp. 132-139.

43. Liao H., Normand B. and Coddet C. (2000), Influence of coating microstructure on the abrasive wear resistance of WC/Co cermet coatings, Surface and Coatings Technology, 124 (2-3), pp. 235-242.

44. Sahu S. P., Satapathy A. and Mishra D. (2010), Development of protective coatings using fly ash premixed with metal powder on aluminium substrates, Journal of Solid Waste Technology and Management, 28 (7), pp. 660-666.

45. Little R. L. (1979), Welding and welding technology, TMH Publications, New Delhi, India.

46. Pawlowski L. (1995), The Science and Engineering of Thermal Spraying, Wiley, USA.

47. Metco Plasma Spraying Manual (1993), Metco, USA.

48. Novak R. C. (1988), Processing aspects of plasma sprayed ceramic coatings, Journal of Engineering for Gas Turbines and Power, 110 (4), pp. 617-620.

49. Nash D. R., Weare N. E. and Walker D. L. (1961), Process variables in plasma-jet spraying, Journal of Metals, 13 (7), pp. 483-486.

50. Gruner H. (1984), Vacuum plasma spray quality control, Thin Solid Films, 118 (4), pp. 409-420.

51. Eaton H. and Novak R. C. (1986), A study of the effects of variations in parameters on the strength and modulus of plasma sprayed zirconia, Surface and Coatings Technology, 27 (3), pp. 257-267.

52. Wielage B., Hofmann V., Steinhauser A. and Zimmerman G. (1998), Improving wear and corrosion resistance of thermal sprayed coatings, Surface Engineering, 14 (2), pp. 136-138.

53. Lee W. Y., Stinton D. P., Brandt C. C., Erdogan F., Lee Y. D. and Mutasim Z. Z. (1996), Thermal barrier coatings, Journal of Americal Ceramic Society, 79 (12), pp. 3003-3012.

54. Takei T., Hatta H. and Taya M. (1991), Thermal expansion behavior of particulate-filled composites with single reinforcing phase, Materials Science and Engineering, 131A, pp. 133-143.

55. Ranganath S. (1997), A review on particulate-reinforced titanium matrix composites, Journal of Materials Science, 32 (1), pp. 1-16.

56. Sawyer W. G., Freudenberg K. D., Praveen B. and Schadler L. S. (2003), A study on the friction and wear behavior of PTFE filled with alumina nanoparticles, Wear, 254 (5-6), pp. 573-580.

57. Kim J., Kang P. H. and Nho Y. C. (2004), Positive temperature coefficient behavior of polymer composites having a high melting temperature, Journal of Applied Polymer Science, 92 (1), pp. 394-401.

58. Nikkeshi S., Kudo M. and Masuko T. (1998), Dynamic visco-elastic properties and thermal properties of powder-epoxy resin composites, Journal of Applied Polymer Science, 69 (13), pp. 2593-2598.

59. Sumita M., Shizuma T., Miyasaka K. and Ishikawa K. (1983), Effect of reducible properties of temperature, rate of strain, and filler content on the tensile yield stress of nylon 6 composites filled with ultrafine particles, Journal of Macromolecular Science: Part B, 22 (4), pp. 601-618.

60. Bartczak Z., Argon A. S., Cohen R. E. and Weinberg M. (1999), Toughness mechanism in semi-crystalline polymer blends: II. High-density polyethylene toughened with calcium carbonate filler particles, Polymer, 40 (9), pp. 2347-2365.

61. Radford K. C. (1971), The mechanical properties of an epoxy resin with a second phase dispersion‖, Journal of Materials Science, 6 (10), pp. 1286-1291.

62. Young R. J. and Beaumont P. W. R. (1977), Failure of brittle polymers by slow crack growth Part 3 Effect of composition upon the fracture of silica particle-filled epoxy resin composites, Journal of Materials Science, 12 (4), pp. 684-692.

63. Kinloch A. J., Maxwell D. L. and Young R. J. (1985), The fracture of hybrid particulate composites, Journal of Materials Science, 20 (11), pp. 4169-4184.

64. Young R. J., Maxwell D. L. and Kinloch A. J. (1986), The deformation of hybrid particulate composites, Journal of Materials Science, 21 (2), pp. 380-388.

65. Koh S. W., Kim J. K. and Mai Y. W. (1993), Fracture toughness and failure mechanisms in silica-filled epoxy resin composites: effects of temperature and loading rate, Polymer, 34 (16), pp. 3446-3455.

66. Cantwell W. J. and Moloney A. C. (1994), Fractography and failure mechanisms of polymers and composites, Elesvier, Amsterdam, pp. 233.

67. Imanaka M., Takeuchi Y., Nakamura Y., Nishimura A. and Lida T. (2001), Fracture toughness of spherical silica-filled epoxy adhesives, International Journal of Adhesion Adhesives, 21 (5), pp. 389-396.

68. Wang H., Bai Y., Liu S., Wu J. and Wong C. P. (2002), Combined effects of silica filler and its interface in epoxy resin, Acta Materialia, 50 (17), pp. 4369-4377.

69. Yamamoto I., Higashihara T. and Kobayashi T. (2003), Effect of silica particle characteristics on impact/usual fatigue properties and evaluation of mechanical characteristics of silica-particle epoxy resins, JSME International Journal-Series A: Solid Mechanics and Material Engineering, 46 (2), pp. 145-153.

70. Nakamura Y., Yamaguchi M., Kitayama A., Okubo M. and Matsumoto T. (1991), Effect of particle size on fracture toughness of epoxy resin filled with angular-shaped silica, Polymer, 32 (12), pp. 2221-2229.

71. Nakamura Y., Yamaguchi M., Okubo M. and Matsumoto T. (1991), Effect of particle size on impact properties of epoxy resin filled with angular shaped silica particles, Polymer, 32 (16), pp. 2976-2979.

72. Nakamura Y., Yamaguchi M., Okubo M. and Matsumoto T. (1992), Effects of particle size on mechanical and impact properties of epoxy resin filled with spherical silica, Journal of Applied Polymer Science, 45 (7), pp. 1281-1289.

73. Pukanszky B. and Voros G. (1993), Mechanism of interfacial interactions in particulate filled composite, Composite Interfaces, 1 (5), pp. 411-427.

74. Nicolais L. and Nicodemo L. (1974), The Effect of particles shape on tensile properties of glassy thermoplastic composites, International Journal of Polymeric Materials, 3 (3), pp. 229-243.

75. Patnaik A., Satapathy A., Mahapatra S. S. and Dash R. R. (2009), A comparative study on different ceramic fillers affecting mechanical properties of glass-polyester composites, Journal of Reinforced Plastics and Composites, 28 (11), pp. 1305-1318.

76. Lauke B. and Fu S. Y. (2013), Aspects of fracture toughness modeling of particulate filled polymer composites, Composites Part B: Engineering, 45 (1), pp. 1569-1574.

77. Jerabek M., Major Z., Renner K., Moczo J., Pukanszky B. and Lang R. W. (2010), Filler/matrix-debonding and micro-mechanisms of deformation in particulate filled polypropylene composites under tension, Polymer, 51 (9), pp. 2040-2048.

78. Padhi P. K., Satapathy A. and Nakka A. M. (2013), Processing, characterization, and wear analysis of short glass fiber-reinforced polypropylene composites filled with blast furnace slag, Journal of Thermoplastic Composite Materials, DOI: 10.1177/0892705713486142.

79. Padhi P. K. and Satapathy A. (2012), Prediction and simulation of erosion wear behavior of glass-epoxy composites filled with blast furnace slag, Advanced Materials Research, 585, pp. 549-553.

80. Tagliavia G., Porfiri M. and Gupta N. (2010), Analysis of flexural properties of hollow-particle filled composites, Composites Part B: Engineering, 41 (1), pp. 86-93.

81. Weidenfeller B., Hofer M. and Schilling Frank R. (2005), Cooling behavior of particle filled polypropylene during injection molding process, Composites Part A: Applied Science and Manufacturing, 36 (3), pp.345-351.

82. Hassan S. B., Oghenevweta J. E. and Aigbodion V. S. (2012), Morphological and mechanical properties of carbonized waste maize stalk as reinforcement for eco-composites, Composites Part B: Engineering, 43 (5), pp. 2230-2236.

83. Omar M. F., Akil H. M. and Ahmad Z. A. (2013), Particle size-Dependent on the static and dynamic compression properties of polypropylene/silica composites, Materials and Design , 45, pp.539-547.

84. Nayak R., Dora P. T., Satapathy A. (2010), A computational and experimental investigation on thermal conductivity of particle reinforced epoxy composites, Computational Materials Science, 48 (3), pp. 576-581.

85. Bishay I. K., Abd-El-Messieh S.L., Mansour S.H. (2011), Electrical, mechanical and thermal properties of polyvinyl chloride composites filled with aluminum powder, Materials and Design, 32 (1), pp. 62-68.

86. Agrawal A. and Satapathy A. (2013), Development of a heat conduction model and investigation on thermal conductivity enhancement of AlN/epoxy composites, Procedia Engineering, 51, pp. 573-578.

87. Agrawal A. and Satapathy A. (2014), Effects of aluminium nitride inclusions on thermal and electrical properties of epoxy and polypropylene: An experimental investigation, Composites Part A: Applied Science and Manufacturing, 63, pp. 51-58.

88. Kenyon A. S. and Duffey H. J. (1967), Properties of a particulate-filled polymer, Polymer Engineering and Science, 7 (3), pp. 189-193.

89. Sahu S. and Broutman L. J. (1972), Mechanical properties of particulate composites, Polymer Engineering and Science, 12 (2), pp. 91-100.

90. Broutman L. J. and Sahu S. (1971), The effect of interfacial bonding on the toughness of glass filled polymers, Materials Science and Engineering, 8 (2), pp. 98-107.

91. Nielsen L. E. (1966), Simple theory of stress-strain properties of filled polymers, Journal of Applied Polymer Science, 10, pp. 97-103.

92. Hasselman D. P. H. and Fulrath R. M. (1966), Proposed fracture theory of a dispersion strengthened glass matrix, Journal of The American Ceramic Society, 49 (2), pp. 68-72.

93. Mallick P. K. and Broutman L. J. (1975), Mechanical and fracture behaviour of glass bead filled epoxy composites, Materials Science and Engineering, 18 (1), pp. 63-73.

94. Broutman L. J. and Kobayashi T. (1969), Facture studies in glassy polymers, Final report AMMRC CR 69-13, Contract DAAG 17-67-C-0133, Army Materials and Mechanics Research Center, Watertown, Massachusetts.

95. Kinloch A. J. and Young R. J. (1983), Fracture behaviour of polymers, Chapman & Hall, London.

96. Hertzberg R. W. (1989), Deformation and fracture mechanics of engineering materials 3rd ed., John Wiley & Sons, New York.

97. Williams J. G. and Cawood M. J. (1990), A linear elastic fracture mechanics (LEFM), european group of fracture standard for determining $K_c$ and $G_c$ methods for polymers, Polymer Testing, 9 (8) , pp. 15-26.

98. Moore D. R., Pavan A. and Williams J. G. (2001), Fracture mechanics testing methods for polymers adhesives and composites, ESIS Publication 28, Elsevier Science Ltd. Oxford, UK.

99. Sanchez-Soto M., Gordillo A., Maspoch M. L. L., Velasco J. I., Santana O. O. and Martinez A. B. (2002), Glass bead filled polystyrene composites: morphology and fracture, Polymer Bulletin, 47, pp. 587-594.

100. Lim T. T. S. (1971), Capillary extrusion of composite materials, Polymer Engineering and Science, 11 (3), pp. 240-246.

101. Faulkner D. L. and Schmidt L. R. (1977), Polymer Engineering & Science, 17 (9), pp. 657-665.

102. Lepez O., Choplin L. and Tanguy P. A. (1990), Thermorheological analysis of glass beads-filled polymer melts, Polymer Engineering & Science (1990), pp. 821-828.

103. Ou Y. C. and Yu Z. Z. (1995), Effects of interfacial adhesion on micro-damage and rheological behaviour of glass bead filled nylon 6, Polymer International, 37, pp. 113-117.

104. Li R. K. Y., Liang J. Z. and Tjong S. C. (1998), Morphology and dynamic mechanical properties of glass beads filled low density polyethylene composites, Journal of Material Processing Technology, 79, pp. 59-65.

105. Lee J. and Yee A. F. (2001), Inorganic particle toughening II: toughening mechanisms of glass bead filled epoxies, Polymer, 42, pp. 589-597.

106. Liang J. Z. (2005), Tensile and flexural properties of hollow glass bead-filled ABS composites, Journal of Elastomers and Plastics, 37 (4), pp. 361-370.

107. Liang J. Z. (2002), Tensile and impact properties of hollow glass bead-filled PVC composites, Macromolecular Materials and Engineering, 287 (9), pp. 588-591.

108. Gupta N., Ye R. and Porfiri M. (2010), Comparison of tensile and compressive characteristics of vinyl ester/glass microballoon syntactic foams, Composites Part B, 41 (3), pp. 236-245.

109. Gupta N., Woldesenbet E. and Kishore (2002), Compressive fracture features of syntactic foams-microscopic examination, Journal of Material Science, 37 (15), pp. 3199–3209.

110. Kim H. S. and Khamis M. A. (2001), Fracture and impact behaviours of hollow microsphere epoxy resin composites, Composites Part A, 32, pp. 1311-1317.

111. Ferreira J. A. M., Capela C. and Costa J. D. (2010), A study of the mechanical behaviour on fibre reinforced hollow microspheres hybrid composites, Composites Part A, 41 (3), pp. 345-352.

112. Kushvaha V. and Tippur H. (2014), Effect of filler shape, volume fraction and loading rate on dynamic fracture behavior of glass-filled epoxy, Composites Part B: Engineering, 64, pp. 126-137.

113. Yung K. C., Zhu B. L. and Yue T. M. (2009), Preparation and properties of hollow glass microsphere filled epoxy-matrix composites, Composites Science and Technology, 69 (2), pp. 260-264.

114. Zhu B. L., Ma J. and Wu J. (2010), Study on the properties of the epoxy-matrix composites filled with thermally conductive AlN and BN ceramic particles, Journal of Applied Polymer Science, 118 (5), pp. 2754-2764.

115. Liang J. Z. (2014), Estimation of thermal conductivity for polypropylene/ hollow glass bead composites, Composites Part B: Engineering, 56, pp. 431-434.

116. Mishra D. and Satapathy A. (2013), Development of theoretical model for effective thermal conductivity of glass microsphere filled polymer composites, Plastic and Polymer Technology, 2 (2), pp. 39-47.

117. Mishra D. and Satapathy A. (2012), Processing and thermal conductivity characterization of solid glass micro-sphere filled polymer composites, Advanced Materials Research, 445, pp. 526-529.

118. Organization for Economic Co-operation and Development (1969), Research Group on Wear of Engg. Materials, Glossary of terms in the field of friction, wear and lubrication, Tribology, Paris, pp. 169.

119. Burwell J. T. and Strang C. D. (1952), On the empirical law of adhesive wear, Journal of Applied Physics, 23 (1), pp. 18-28.

120. Burwell (Jr.) J. T. (1957/1958), Survey of possible wear mechanisms, American-Standard Corp., New York, U.S.A., Wear, 1, pp. 119-141.

121. Guessasma S., Bounazef M., Nardin P. and Sahraoui T. (2006), Wear behavior of alumina Titania coatings: analysis of process and parameters, Ceramics International, 32, pp. 13-19.

122. Ouyang J. H. and Sasaki S. (2005), Tribological characteristics of low pressure plasma-sprayed $Al_2O_3$ coating from room temperature to $800^0$C, Tribology International, 38 (1), pp. 49-57.

123. Kovarik O., Siegl J., Nohava J. and Chraska P. (2005), Young's modulus and fatigue behavior of plasma-sprayed alumina coatings, Journal of Thermal Spray Technology, 14, pp. 231-238.

124. Xie Y. and Hawthorne H. M. (1999), The damage mechanisms of several plasma sprayed ceramic coatings in controlled scratching, Wear, 233-235, pp. 293-305.

125. Erickson L. C., Hawthorne H. M. and Troczynski T. (2001), Correlations between microstructural parameters, micromechanical properties and wear resistance of plasma-sprayed ceramic coatings, Wear, 250 (1), pp. 569-575.

126. Fernandez J. E., Rodriguez R., Wang Y., Vijande R. and Rincon A. (1995), Sliding wear of a plasma-sprayed $Al_2O_3$ coating, Wear, 181-183 (1), pp. 417-425.

127. Budinsky K. G. (1995), Abrasion resistance of transport roll surfaces, Wear, 181-183 (2), pp. 938-943.

128. Bolelli G., Cannillo V., Lusvarghi L. and Ricco S. (2006), Mechanical and tribological properties of electrolytic hard chrome and HVOF-sprayed coatings, Surface and Coatings Technology, 200, pp. 2995-3009.

129. Hsu S. M. and Shen M. (2004), Wear prediction of ceramics, Wear, 256, pp. 867-878.

130. Kato K. and Adachi K. (2002), Wear of advanced ceramics, Wear, 253, pp. 1097-1104.

131. Adachi K., Kato K. and Chen N. (1997), Wear map of ceramics, Wear, 203-204, pp. 291-301.

132. Pragatheeswaran A., Ananthapadmanabhan P.V., Chakravarthy Y., Bhandari S., Thiyagarajan T. K., Tiwari N., Saha T. K. and Ramachandran K. (2014), Plasma spray deposition and characterization of strontium zirconate coatings, Ceramics International, 40 (7B), pp. 10441-10446.

133. Garcia A., Cadenas M., Fernandez M. R. and Noriega A. (2013), Tribological effects of the geometrical properties of plasma spray coatings partially melted by laser, Wear, 305 (1-2), pp. 1-7.

134. Aruna S. T., Balaji N., Shedthi J. and William Grips V.K. (2012), Effect of critical plasma spray parameters on the microstructure, micro-hardness and wear and corrosion resistance of plasma sprayed alumina coatings, Surface and Coatings Technology, 208, pp. 92-100.

135. Sivakumar G., Dusane R. O. and Joshi S. V. (2013), A novel approach to process phase pure α- $Al_2O_3$ coatings by solution precursor plasma spraying, Journal of the European Ceramic Society, 33 (13-14), pp. 2823-2829.

136. Monica V., Bannier E., Moreno R., Salvador M. D. and Sanchez E. (2013), Atmospheric plasma spraying coatings from alumina-titania feedstock comprising bimodal particle size distributions, Journal of the European Ceramic Society, 33 (15-16), pp. 3313-3324.

137. Sadri E. and Ashrafizadeh F. (2013), Structural characterization and mechanical properties of plasma sprayed nanostructured $Cr_2O_3$-Ag composite coatings, Surface and Coatings Technology, 236, pp. 91-101.

138. Tucker (Jr.) R. C. (1995), On the relationship between the microstructure and the wear characteristics of selected thermal spray coatings, In: Proceeding of ITSC, Kobe, Japan.

139. Erickson L. C., Troczynski T., Ross D., Tai H. and Hawthorne H. M. (1997), Processing dependent microstructure and wear related surface properties of plasma sprayed alumina coatings, Presented on World Tribology Congress, Londan, UK.

140. Erickson L. C., Troczynski T., Hawthorne H. M., Tai H. and Ross D. (1998), Alumina coatings by plasma spraying of mono size sapphire powders, In: Proceeding of ITSC, Nice, France.

141. Ohmori A., Li C. J. and Arata Y. (1990), Influence of Plasma spray conditions on the structure of $Al_2O_3$ coatings, Transaction of Joining and Welding Research Institute, 19 (2), pp. 99-110.

142. Alonso F., Fagoaga I. and Oregui P. (1991), Erosion Protection of carbon epoxy composites by plasma sprayed coatings, Surface and Coatings Technology, 49 (1-3), pp. 482-488.

143. Tabakoff W. and Shanov V. (1995), Erosion rate testing at high temperature for turbo machinery use, Surface and Coatings Technology, 76-77 (1), pp.75-80.

144. Kulu P., Hussainova I. and Veinthal R. (2005), Solid particle erosion of thermal sprayed coatings, Wear, 258 (1-4), pp. 488-496.

145. Kulu P. (1989), The abrasive erosion resistance of powder coatings, Journal of Tribologia: Finnish J. Tribology, 8 (4), pp. 12-25.

146. Kulu P., Tumanok A. and Zimakov S. (1999), Treatment of recycled hard metals, In: Proceedings of 4th ASM International Conference and Exhibition on the Recycling of Metals, ASM International, Vienna, Austria, pp. 319-327.

147. Kulu P., Phil T. and Halling J. (1998), Wear-resistant WC–Co–NiCrSiB composite coatings, In (NORDTRIB'98): Proceedings of the 8th International Conference of Tribology, S.S. Eskilden, D.S. Larsen, H. Reitz, E.J. Bienk, and A. Straede, ed., DTI Tribology Centre, Aarhus, Denmark, pp. 809-817.

148. Wert J. J. and Oppliger S. J. (1992), Influence of composition and processing parameters on mechanical properties and erosion response of Ni0-$TiB_2$ coatings, Materials Science and Technology, 8, pp. 825-835.

149. Finnie I. (1995), Some reflections on the past and future of erosion, Wear, 186-187 (1), pp. 1-10.

150. Hamed A., Tabakoff W. and Wenglarz R. (2006), Erosion and deposition in turbo-machinery, Journal of Propulsion and Power, 22 (2), pp. 350–360.

151. Finnie I. and McFadden D. H. (1978), On the velocity dependence of the erosion of ductile metals by solid particles at low angles of incidence, Wear, 48, pp. 181-190.

152. He C., Wang Y. S., Wallace J. S. and Hsu S. M. (1993), Effect of microstructure on the wear transition of zirconia-toughened alumina, Wear, 162-164 (1), pp. 314-321.

153. Ajayi O. O. and Ludema K. C. (1988), Surface damage of structural ceramics: Implications for wear modeling, Wear, 124 (2), pp. 237-257.

154. McPherson R. (1989), A review of microstructure and properties of plasma sprayed ceramic coatings, Surface and Coatings Technology, 39-40, pp. 173-181.

155. Wang B. (1996), Erosion-corrosion of thermal sprayed coatings in FBC boilers, Wear, 199 (1), pp. 24-32.

156. Eyre T. S. (1975), Effect of Boronising on Friction and Wear of Ferrous Metals, Wear, 34, pp. 383-397.

157. Zhang X. S., Clyne T. W. and Hutchings I. M. (1997), Relationship between microstructure and erosive wear resistance of plasma sprayed alumina coatings, Surface Engineering, 13 (5), pp. 393-401.

158. Branco J. R. T., Gansert R., Sampath S., Berndt C. C. and Herman H. (2004), Solid particle erosion of plasma sprayed ceramic coatings, Materials Research, 7 (1), pp. 147-153.

159. Mishra S. C., Sahu A., Das R., Satapathy A., Sen S., Ananthapadmanabhan P. V. and Sreekumar K. P. (2008), Microstructure, adhesion and erosion wear of plasma sprayed alumina-titania composite coatings, Journal of Reinforced Plastics And Composites, Doi: 10.1177/0731684407087758.

160. Ercenk E., Sen U. and Yilmaz S. (2012) The erosive wear behavior of basalt based glass and glass-ceramic coatings, Tribology International, 52, pp. 94-100.

161. Krishnamurthy N., Murali M. S., Venkataraman B. and Mukunda P. G. (2012), Characterization and solid particle erosion behavior of plasma sprayed alumina and calcia-stabilized zirconia coatings on Al-6061 substrate, Wear, 274-275, pp. 15-27.

162. Sahu S. P., Satapathy A., Mishra D., Patnaik A. and Sreekumar K. P. (2010), Tribo-performance analysis of fly ash-aluminum coatings using experimental design and ANN, Tribology Transactions, 53 (4), pp. 533-542.

163. Engel P. A. (1976), Impact wear of materials, Elsevier, Amsterdam, New York, pp. 277-290.

164. Tilly G. P. (1979), Erosion caused by impact of solid particles, in Herman H. (ed.), Treatise on Materials Science and Technology, v13:D. Scott(ed), Wear, Academic Press: New York, pp. 287-320.

165. Rochester M. C. and Brunton J. H. (1979), In: J. E. Field (Ed.), 5th International Conference on Erosion by Liquid and Solid Impact, Cavendish Laboratory, Cambridge, U.K., Paper 6.

166. Lesser M. B. and Ezekoye O. A. (1987), Proceedings of 7th International Conference on Erosion by Liquid and Solid Impact (eds. Field J. E. and Dear J. P.), Cavendish Laboratory, Cambridge, U.K.

167. Evans A. G. (1979), Impact Damage Mechanism-Solid Projectile, in Herman H. (ed.), Treatise on Materials Science and Technology, Vol. 16: Preece C. M. (ed.), Materials Erosion, (Academic Press: New York, pp. 1-67.

168. Engel P. A. (1978), Percussive impact wear: A study of repetitively impacting solid components in engineering, Tribology International, 11 (3), pp. 169-176.

169. Preece C. M. and Macmillan N. H. (1977), Erosion, Annual Review of Materials Science, 7, pp. 95-121.

170. Hutchings I. M. (1981), A model for the erosion of metals by spherical particles at normal incidence, Wear, 70 (3), pp. 269-281.

171. Finnie I., Levy A. and McFadden D. H. (1979), The fundamental mechanisms of the erosion wear of ductile metals by solid particles, ASTM STP 664, Erosion: Prevention and Useful Applications, pp. 36-58.

172. Ruff A. W. and Wiederhorn S. M. (1979), Erosion by solid particle impact (Preece C. M., (Ed.) Treatise on Materials Science and Technology), Academic Press, New York, 16, pp. 65-70.

173. Shewmon P. and Sundararajan G. (1983), The erosion of metals, Annual Review of Materials Science, 13, pp. 301-318.

174. Sundararajan G. (1983), Solid particle erosion of metals and alloys, Transactions of the Indian Institute of Metals, 36 (6), pp. 474-495.

175. Levy A. V. (1995), Solid particle erosion and erosion-corrosion of materials, In: 2nd Ed., ASM International, Materials Park, Ohio, USA.

176. Guo D. Z., Li F. L., Wang Y. and Sun J. S. (1995), Effects of post-coating processing on structure and erosive wear characteristics off tame and plasma spray coatings, Surface and Coatings Technology, 73, pp. 73-78.

177. Hidalgo V. H., Varela F. J. B. and Fernandez R. E. (1997), Erosion wear and mechanical properties of plasma-sprayed nickel and iron-based coatings subjected to service conditions in boilers, Tribology International, 30 (9), pp. 641-649.

178. Mishra S. B., Chandra K. and Prakash S. (2013), Erosion-corrosion performance of NiCrAlY coating produced by plasma spray process in a coal-fired thermal power plant, Surface & Coatings Technology, 216, pp. 23-34.

179. Mishra S. B., Prakash S. and Chandra K. (2006), Studies on erosion behaviour of plasma sprayed coatings on a Ni-based superalloy, Wear, 260, pp. 422-432.

180. Proudhon H., Savkova J., Basseville S., Guipont V., Jeandin M. and Cailletaud G. (2014), Experimental and numerical wear studies of porous rweactive plasma sprayed Ti-6Al-4V/TiN composite coating, Wear, 311, pp. 159-166.

181. Yugeswaran S., Kobayashi A., Suresh K., Rao K. P. and Subramanian B. (2012), Wear behavior of gas tunnel type plasma sprayed Zr-based metallic glass composite coatings, Applied Surface Science, 258, pp. 8460-8468.

182. Singh V. P., Sil A. and Jayaganthan R. (2011), Study on sliding and erosive wear behaviour of atmospheric plasma sprayed conventional and nanostructured alumina coatings, Materials and Design, 32, pp. 584-591.

183. Hsiao W. T., Su C. Y., Huang S. and Liao W. H. (2013), Wear resistance and microstructural properties of Ni–Al/h-BN/WC–Co coatings deposited using plasma spraying, Materials Characterization, 79, pp. 84-92.

184. Sahab A. R. M., Saad N. H., Kasolang S. and Saedon J. (2012), Impact of Plasma Spray Variables Parameters on Mechanical and Wear Behaviour of Plasma Sprayed Al2O3 3%wt TiO2 Coating in Abrasion and Erosion Application, Procedia Engineering, 41, pp. 1689-1695.

185. Pool K. V., Dharan C. K. H. and Finnie I. (1986), Erosion wear of composite materials, Wear, 107, pp. 1-12.

186. Pepi M., Squillacioti R., Pfledderer L. and Phelps A. (2012), Solid particle erosion testing of helicopter rotor blade materials, Journal of Failure Analysis and Prevention, 12, pp. 96-108.

187. Aglan H. A. and Chenock Jr. T. A. (1993), Erosion damage features of polyimide thermoset composites, SAMPEQ, 24,pp. 41-47.

188. Rao P. V. (1995), Characterization of optical and surface parameters during particle impact damage, ASME/Fluids Engineering Publication, 23, pp. 87-96.

189. Tennyson R. C. (1991), LDEF mission up year: composites in space, Advanced Materials and Processes, 5, pp. 33-36.

190. Kaundal R. (2014), Role of process variables on the solid particle erosion of polymer composites: a critical review, Silicon, 6, pp. 5-20.

191. Meng H. C and Ludema K. C. (1995), Wear models and predictive equations: their form and content, Wear, 181-183, pp. 443-457.

192. Friedrich K., Reinicke R. and Zhang Z. (2002), Wear of polymer composites, Journal of Engineering Tribology, 216, pp. 415-426.

193. Stachowiak G. W. and Batchelor A. W. (2001), Engineering Tribology, 2nd edition, Butterworth-Heinemann, Jordan Hill, Oxford, UK.

194. Friedrich K. (1986), Erosive wear of polymer surfaces by steel ball blasting, Journal of Materials Science, 21 (9), pp. 3317-3332.

195. Gross K. J. (1988), Dissertation, University of Stuttgart, Germany.

196. Miyazaki N. and Takeda N. (1993), Solid Particle erosion of fiber reinforced plastics, Journal of Composite Materials, 27 (1), pp. 21-31.

197. Miyazaki N. and Hamao T. (1994), Solid particle erosion of thermoplastic resins reinforced by short fibers, Journal of Composite Materials, 28 (9), pp. 871-883.

198. Tilly G. P and Sage W. (1970), The interaction of particle and material behaviour in erosion process‖, Wear, 16 (6), PP. 447-465.

199. Hovis S. K., Pallout Y. A. and Talia J. E. (1990), Erosion in glass fiber reinforced epoxy composites, 24, pp. 195-200.

200. Thai C. M., Tsuda K. and Hojo H. (1981), Erosion behaviour of polystyrene, Journal of Testing and Evaluation, 9, pp. 359-365.

201. Walley S. M., Field J. E. and Yennadhiou P. (1984), Single solid particle impact erosion damage on polypropylene, Wear, 100 (1-3), pp. 263-280.

202. Barkoula N. M and Karger-Kocsis J. (2002), Effects of fiber content and relative fiber-orientation on the solid particle erosion of GF/PP composites, Wear, 252 (1-2), pp. 80-87.

203. Rajesh J. J., Bijwe J., Tewari U. S. and Venkataraman B. (2001), Erosive wear of various polyamides, Wear, 249 (8), pp. 702-714.

204. Walley S. M and Field J. E. (1987), The erosion and deformation of polyethylene by solid particle impact, Philosophical Transactions of The Royal Society A, London, 321 (1558), pp. 277-303.

205. Wang Y. Q., Huang L. P., Liu W. L. and Li J. (1998), The blast erosion behavior of ultrahigh molecular weight polyethylene, Wear, 218 (1), pp. 128-133

206. Walley S. M., Field J. E. and Greengrass M. (1987), An impact and erosion study of polyetheretherketone, Wear, 114 (1), pp. 59-72.

207. Pei X. and Friedrich K. (2012), Erosive wear properties of unidirectional carbon fiber reinforced PEEK composites, Tribology International, 55, pp. 135-140.

208. Rao P. V. and Buckley D. H. (1986), Angular particle impingement studies of thermoplastic materials at normal incidence, Tribology Transactions, 29 (3), pp. 283-298.

209. Srivastava V. K. and Pawar A. G. (2006), Solid particle erosion of glass fiber reinforced fly ash filled epoxy resin composites, Composites Science and Technology, 66, pp. 3021-3028.

210. Kulkarni S. M. and Kishore (2001), Influence of matrix modification on the solid particle erosion of glass/epoxy composites, Polymers and Polymer Composites., 9, pp. 25-30.

211. Yang N. H., Nayeb-Hashemi H. and Vaziri A. (2008), Non-destructive evaluation of erosion damage on E-glass/epoxy composites, Composites: Part A, 39 (1), pp. 56-66.

212. Harsha A. P. and Jha S. K. (2008), Erosive wear studies of epoxy-based composites at normal incidence, Wear, 265, pp. 1129-1135.

213. Satapathy A., Patnaik A. and Pradhan M. K. (2009), A study on processing, characterization and erosion behavior of fish (Labeo-rohita) scale filled epoxy matrix composites, Materials and Design, 30 (7), pp. 2359-2371.

214. Fouada Y., El-Meniawib M. and Afific A. (2011), Erosion Behaviour of epoxy based unidirectional (GFRP) composite materials‖, Alexandria Engineering Journal, 50, pp. 29-34.

215. Bagci M. and Imrek H. (2011), Solid particle erosion behavior of glass fiber reinforced boric acid filled epoxy resin composites, Tribology International, 44 (12), pp. 1704-1710.

216. Rout A. K. and Satapathy A. (2012), Study on mechanical and tribo performance of rice-husk filled glass-epoxy hybrid composites, Materials and Design, 41, pp. 131-141.

217. Mohan N., Natarajan S., Kumaresh Babu S. P., Siddaramaiah and Lee H. J. (2010), Solid particle erosion of UHMWPE filled aramid fabric epoxy hybrid composites, Advanced Materials Research, 123-125, pp. 1051-1054.

218. Tewari U. S., Harsha A. P., Hager A. M. and Friedrich K, (2003), Solid particle erosion of carbon fiber and glass fiber-epoxy composites, Composites Science and Technology, 63 (3), pp. 549-557.

219. Bagci M. and Imrek H. (2013), Application of Taguchi method on optimization of testing parameters for erosion of glass fiber reinforced epoxy composite materials, Materials and Design, 46, pp. 706-712.

220. Qian D., Bao L., Takatera M., Kemmochi K. and Yamanaka A. (2010), Fiber reinforced polymer composite materials with high specific strength and excellent solid particle erosion resistance, Wear, 268, pp. 637-642.

221. Brandstadter A., Goretta K. C, Routbort J. L, Groppi D. P and Karasek K. R. (1991), Solid particle erosion of bismaleimide polymers, Wear, 147 (1), pp. 155-164.

222. Hutchings I. M., Deuchar D. W. T and Muhr A. H. (1987), Erosion of unfilled elastomers by solid particle impact, Journal of Materials Science, 22(11), pp. 407-4076.

223. Li J. and Hutchings I. M. (1990), Resistance of cast polyurethane elastomers to solid particle erosion, Wear, 135 (2), pp. 293-303.

224. Arnold J. C. and Hutchings I. M. (1990), The mechanisms of erosion of unfilled elastomers by solid particle impact, Wear, 138, pp. 33-46.

225. Besztercey G, Karger-Kocsis J and Szaplonczay P. (1999), Solid particle erosion of electrically insulating silicone and EPDM rubber compounds, Polymer Bulletin, 42 (6), pp. 717-724.

226. Zhou R., Lu D. H., Jiang Y. H. and Li Q. N. (2005), Mechanical properties and erosion wear resistance of polyurethane matrix composites, Wear, 259 (1-6), pp. 676-683.

227. Harsha A. P., Tewari U. S. and Venkataraman B. (2003), Solid particle erosion behaviour of various polyaryletherketone composites, Wear, 254 (7-8), pp. 693-712.

228. Patnaik A., Satapathy A., Mahapatra S. S. and Dash R. R., (2008), A Taguchi approach for investigation of erosion of glass fiber-polyester composites, Journal of Reinforced Plastics and Composites, 27 (8), pp. 871-888.

229. Patnaik A., Satapathy A., Mahapatra S. S. and Dash R. R. (2008), Parametric optimization of erosion wear of polyester-GF-alumina hybrid composites using Taguchi method, Journal of Reinforced Plastics and Composites, 27 (10), pp. 1039-1058.

230. Patnaik A., Satapathy A., Mahapatra S. S. and Dash R. R., (2008), Implementation of Taguchi design for erosion of fiber reinforced polyester composite systems with SiC filler, Journal of Reinforced Plastics and Composites, 27 (10), pp. 1093-1111.

231. Patnaik A., Satapathy A., Mahapatra S. S. and Dash R. R. (2008), A modeling approach for prediction of erosion behaviour of glass fiber-polyester composites, Journal of Polymer Research, 15 (2), pp. 147-160.

232. Patnaik A., Satapathy A., Mahapatra S. S. and Dash R. R., (2009), Tribo- performance of polyester hybrid composites: damage assessment and parameter optimization using Taguchi design, Materials and Design, 30 (1), pp. 57-67.

233. Patnaik A., Kaundal R., Satapathy A., Biswas S. and Kumar P. (2010), Solid particle erosion of particulate filled short glass fiber reinforced polyester resin composites, Advanced Materials Research, 123-125, pp. 213-216.

234. Sinmazcelik T. and Taskiran I. (2007), Erosive wear behavior of polyphenylenesulphide (PPS) composites, Materials and Design, 28, pp. 2471-2477.

235. Sinmazcelik T., Fidan S. and Gunay V. (2008), Residual mechanical properties of carbon/polyphenylenesulphide composites after solid particle erosion, Materials and Design, 29, pp. 1419-1426.

236. Rattan R. and Bijwe J. (2007), Influence of impingement angle on solid particle erosion of carbon fabric reinforced polyetherimide composite, Wear, 262, pp. 568-574.

237. Sari N. and Sinmazcelik T. (2007), Erosive wear behavior of carbon fiber/polyetherimide composites under low particle speed, Materials and Design, 28, pp. 351-355.

238. Harsha A. P. and Thakre A. A. (2007), Investigation on solid particle erosion behaviour of polyetherimide and its composites, Wear, 262, pp. 807-818.

239. Arjula S., Harsha A. P. and Ghosh M. K. (2008), Erosive wear of unidirectional carbon fiber reinforced polyetherimide composite, Materials letters, 62, pp. 3246-3249.

240. Kumar S., Satapathy B. K. and Patnaik A. (2012), Thermo-mechanical correlations to erosion performance of short glass/carbon fiber reinforced vinyl ester resin hybrid composites, Computational Materials Science, 60, pp. 250-260.

241. Karsli N. G., Yilmaz T., Aytac A. and Ozkoc G. (2013), Investigation of erosive wear behavior and physical properties of SGF and/or calcite reinforced ABS/PA6 composites, Composites: Part B, 44 (1), pp. 385-393.

242. Arjula S. and Harsha A. P. (2006), Study of erosion efficiency of polymers and polymer composites, Polymer Testing, 25 (2), pp. 188-196.

243. Panda P., Mantry S., Mohapatra S., Singh S. K. and Satapathy A. (2013), A study on erosive wear analysis of glass fiber-epoxy-AlN hybrid composites, Journal of Composite Materials, 48 (1),pp. 107-118.

244. Mohan N., Mahesha C. R. and Rajaprakash B. M. (2013), Erosion wear behaviour of WC filled glass epoxy composites, Procedia Engineering, 68, pp. 694-702.

245. Zhao G., Hussainova I., Antonov M., Wang Q., Wang T. and Yung D. L. (2014), Effect of temperature on sliding and erosive wear of fiber reinforced polyimide hybrids, Tribology International, In Press, DOI: 10.1016/j.triboint.2014.01.019

246. Zhang N., Yang F., Shen C., Castro J. and Lee L. J. (2013), Particle erosion on carbon nano fiber paper coated carbon fiber/epoxy composites, Composites Part B: Engineering, 54, pp. 209-214.

247. Padhi P. K. and Satapathy A. (2014), Solid particle erosion behaviour of BFS-filled epoxy-SGF composites using Taguchi's experimental design and ANN, Tribology Transactions, 57 (3), pp. 396-407.

248. Bagci M., Imrek H. and Khalfan O. M. (2015), Optimization of test parameters that Influence erosive wear behaviors of glass fiber-reinforced epoxy composites by using the Taguchi method, Journal of Tribology, 197, DOI: 10.1115/1.4028226.

249. Roy M., Vishwanathan B. and Sundararajan G. (1994), The solid particle erosion of polymer matrix composites, Wear, 171, pp. 149-161.

250. Bakar M., Kostrzewa M., Okulska-Bożek M. and Jacewicz E. (2011), Mechanical and morphological properties of polycarbonate and montmorillonite filled epoxy hybrid composites, Journal of Applied Polymer Science, 119, pp. 752-759.

251. Deo C. and Acharya S. K. (2009), Solid particle erosion of lantana camara fiber-reinforced polymer matrix composite, Polymer-Plastics

Technology and Engineering, 48, pp. 1084-1087.

252. Taguchi G. and Konishi S. (1987), Taguchi methods: orthogonal arrays and linear graphs: tools for quality engineering, American Supplier Institute Inc., Dearborn, MI.

253. Taguchi G. (1986), Introduction to quality engineering, Asian Productivity Organization, UNIPUB, White Plains, NY.

254. Phadke M. S. (1989), Quality engineering using robust design, Prentice Hall, Englewood Cliffs, NJ.

255. Wu Y. and Moore W. H. (1986), Quality engineering: product & process design optimization, American Supplier Institute Inc., Dearborn, MI.

256. Logothetis N. and Haigh A. (1987), The statistical flexibility of Taguchi method in the optimization of multi-response processes, Professional Statistician, 6 (7), pp. 10-16.

257. Logothetis N. and Haigh A. (1988), Characterizing and optimizing multi response processes by the Taguchi method, Quality and Reliability Engineering International, 4 (2), pp. 159-169.

258. Shoemaker A. C. and Kackar R. N. (1988), A methodology for planning experiments in robust product and process design, Quality and Reliability Engineering International, 4 (2), pp. 95-103.

259. Phadke M. S. and Dehnad K. (1988), Optimization of product and process design for quality and cost, Quality and Reliability Engineering International, 4 (2), pp. 105-112.

260. Mahapatra S. S. and Patnaik A. (2006), Optimization of parameter combinations in wire electrical discharge machining using Taguchi method, Indian Journal of Engineering and Materials Sciences, 13, pp. 493-502.

261. Mahapatra S. S. and Patnaik A. (2006), Optimization of wire electrical discharge machining (WEDM) process parameters using Taguchi method, The International Journal of Advanced Manufacturing Technology, 34 (9-10), pp. 911-925.

262. Mahapatra S. S. and Patnaik A. (2007), Parametric optimization of wire electrical discharge machining (WEDM) process using Taguchi method, Journal of the Brazilian Society of Mechanical Sciences and

Engineering, 28 (4), pp. 423-430.

263. Mahapatra S. S. and Patnaik A. (2006), Determination of optimal parameters settings in wire electrical discharge machining (WEDM) process using Taguchi method, Journal of The Institution of Engineers (India), 87, pp. 16-24.

264. Patnaik A., Satapathy A., Mahapatra S. S. and Dash R. R. (2010), Modified erosion wear characteristics of glass-polyester composites by silicon carbide filling: a parametric study using Taguchi technique, International Journal of Materials and Product Technology, 38 (2-3), pp. 131-152.

265. Patnaik A., Satapathy A., Mahapatra S. S. and Dash R. R. (2008), Erosive wear assesment of glass reinforced polyester-fly ash composites using Taguchi method, International Polymer Processing, 13, pp. 192-199.

266. Pang J. S., Ansari M. N. M., Zaroog O. S., Ali M. H. and Sapuan S. M. (2013), Taguchi design optimization of machining parameters on the CNC end milling process of halloysite nanotube with aluminium reinforced epoxy matrix (HNT/Al/Ep) hybrid composite, HBRC Journal, DOI: 10.1016/j.hbrcj.2013.09.007.

267. Rubio J. C. C., Silva L. J. D., Leite W. D. O., Panzera T. H., Filho S. L. M. R. and Davim J. P. (2013), Investigations on the drilling process of unreinforced and reinforced polyamides using Taguchi method, Composites Part B: Engineering, 55, pp. 338-344.

268. Ramesh B. N. and Suresha B. (2014), Optimization of tribological parameters in abrasive wear mode of carbon-epoxy hybrid composites, Materials and Design, 59, pp. 38-49.

269. Vankanti V. K. and Ganta V. (2014), Optimization of process parameters in drilling of GFRP composite using Taguchi method, Journal of Materials Research and Technology, 3 (1), pp. 35-41.

270. Kartalopoulos S. V. (1996), Understanding neural networks and fuzzy logic: basic concepts and applications, IEEE Press, Piscataway, NJ.

271. Zhang Z. and Friedrich K. (2003), Artificial neural networks applied to polymer composites: a review, Composites Science and Technology, 63 (14), pp. 2029-2044.

272. Kadi H. E. (2006), Modeling the mechanical behavior of fiber-reinforced polymeric composite materials using artificial neural

networks-A review, Composite Structures, 73 (1), pp. 1-23.

273. Jiang Z., Zhang Z. and Friedrich K. (2007), Prediction on wear properties of polymer composites with artificial neural network, Composites Science and Technology, 67, pp. 168-176.

274. Gyurova L. A., Minino-justel P. And Sclarb A. K. (2010), Modelling the sliding wear and friction properties of polyphenylene sulfide composites using artificial neural networks, Wear, 268 (5-6), pp. 708-714.

275. Abdelbary A., Abouelwafa M. N., El Fahham I. M. and Hamdy A. H. (2012), Modeling the wear of Polyamide 66 using artificial neural network, Materials and Design, 41, pp. 460-469.

276. Satapathy A., Tarkes D. P. and Nayak N. B. (2010), Wear response prediction of $TiO_2$-polyester composites using neural networks, International Journal of Plastics Technology, 14 (1), pp. 24-29.

277. Kranthi G. and Satapathy A. (2010), Evaluation and prediction of wear response of pine wood dust filled epoxy composites using neural computation, Computational material science, 49, pp. 609-614.

278. Gyurova L. A. (2010), Sliding friction and wear of polyphenylene sulfide matrix composites: experimental and artificial neural network approach, Ph.D. Thesis, Institut fur Verbundwerkstoffe GmbH: Kaiserslautern, Germany.

279. Suresh A., Harsh A. P. and Ghosh M. K. (2009), Solid particle erosion studies on polyphenylene sulfide composites and prediction on erosion data using artificial neural networks, Wear, 266 (1-2), pp. 184-193.

280. Genel K., Kurnaz S. C. and Durman M. (2003), Modeling of tribological properties of alumina fiber reinforced zinc-aluminum composites using artificial neural network, Materials Science and Engineering, A363, pp. 203-210.

281. Zhang Z., Friedrich K. and Velten K. (2002), Prediction on tribological properties of short fibre composites using artificial neural networks, Wear, 252, pp. 668-675.

282. Padhi P. K. and Satapathy A. (2014), Processing and wear analysis of blast furnace slag filled polypropylene composites using Taguchi model and ANN, International Polymer Processing, 29 (2), pp. 233-

244.

283. Mishra D. (2014), A study on thermal and dielectric characteristics of solid glass microsphere filled epoxy composites, Ph.D. Thesis, N.I.T. Rourkela, India.

284. Sahu M. (2014), A study on thermal characteristics of polymer composites filled with micro sized $TiO_2$ particles, M.Tech (R) Thesis, N.I.T., Rourkela, India.

285. Mishra S. (2012), Processing, characterization and erosion wear response of particulate filled ZA-27 metal matrix composites, M.Tech (R) Thesis, N.I.T., Rourkela, India.

286. Barbero Ever J. (1999), Introduction to composite materials design, Taylor & Francis, Philadelphia, PA.

287. Chen H., Lee S. W., Du H., Ding C. X. and Cho C. H. (2004), Influence of feed stock and spraying parameters on the deposition efficiency and micro-hardness of plasma sprayed zirconia coatings, Materials Letters, 58 (7-8), pp. 1241-1245.

288. Agarwal B. D. and Broutman L. J. (1990), Analysis and performance of fiber composites, Second edition, John Wiley & Sons, pp. 2-16.

289. Padhi P. K. and Satapathy A. (2013), Analysis of sliding wear characteristics of BFS filled composites using an experimental design approach integrated with ANN, Tribology Transactions, 56, pp. 786-796.

290. Zeng P. (1998), Neural computing in mechanics, Applied Mechanics, 51 (2), pp. 173-197.

291. Haykin S. (1999), Neural networks: A comprehensive foundation, Prentice Hall, Upper Saddle River, NJ.

292. Rajasekaran S. and Vijayalakshmi Pai G. A. (2003), Neural networks, fuzzy logic and genetic algorithms-synthesis and applications, Prentice Hall of India, New Delhi.

293. Sobolev V. V., Guilemany J. M., Nutting J. and Miquel J.R. (1997), Development of substrate-coating adhesion in thermal spraying, International Materials Reviews, 42 (3), pp. 117-136.

294. Sahu S. P. (2010), A study on solid particle erosion wear response of plasma sprayed fly ash coatings, Ph.D. Thesis, Sambalpur University, Burla, India.

295. Yilmaz S., Okumus S. C., Demirkiran A. S. and Bindal C. (2004), Fly ash based plasma spray coating, Key Engineering Materials, 264-268, pp. 533-536.

296. Lima C. R. C. and Trevisan R. E. (1997), Graded Plasma Spraying of Premixed Metal Ceramic Powders on Metallic Substrates, Journal of Thermal Spray Technology, 62, pp. 199-204.

297. Lalleman G. and Tallaron (1996), Study of Microstructure and adhesion of spinelles coatings formed by plasma spraying, Ph. D. Thesis No. 96-58, E. C. Lyon, France.

298. Hansson C. M. (1992), Cavitation Erosion, In: ASM Handbook, Friction, Lubrication and Wear Technology, ASM International, USA, 18, pp. 214-220.

299. Satapathy A., Mishra S. C., Ananthapadmanabhan P. V. and Sreekumar K. P. (2007), Development of ceramic coatings using red mud: a solid waste of alumina plants, Journal of Solid Waste Technology and Management, 33, pp. 48-53.

300. Sarikaya O. (2005), Effect of some parameters on microstructure and hardness of alumina coatings prepared by air plasma spraying process, Surface and Coatings Technology, 190, pp. 388-393.

301. Glen S. P. (1993), Taguchi Methods: A Hand on Approach, Addison-Wesley.

302. Roberto J., Branco T., Gansert R., Sampath S., Berndt C. C. and Herman H. (2004), Solid particle erosion of plasma sprayed ceramic coatings, Materials Research, 7 (1), pp. 147-153.

303. Mishra S. C., Das S., Satapathy A., Ananthapadmanabhan P. V. and Sreekumar K. P. (2009), Erosion wear analysis of plasma sprayed ceramic coating using the Taguchi technique, Tribology Transactions, 52, pp. 401-404.

304. Lindsley B. A. and Marder A. R. (1999), The effect of velocity on the solid particle erosion rate of alloys, Wear, 225-229, pp. 510-516.

305. Chen Q. and Li D. Y. (2003), Computer simulation of solid particle erosion, Wear 254 (3-4), pp. 203-210.

306. Rajesh J., John J., Bijwe B., Venkataraman B. and Tewari U. S. (2004), Effect of impingement velocity on the erosion wear behavior of polyamides, Tribolology International, 37 (3), pp. 219-226.

307. Lopez D., Congote J. P., Cano J. R., Toro A. and Tschiptschin A. P. (2005), Effect of particle velocity and impact angle on the corrosion-erosion of AISI 304 and AISI 420 stainless steel, Wear, 25 (1-6), pp. 118-124.

308. Biswas S. and Satapathy A. (2009), Tribo-performance analysis of red mud filled glass-epoxy composites using Taguchi experimental design, Materials and Design, 30, pp. 2841-2853.

309. Biswas S. and Satapathy A. (2010), A study on tribological behavior of alumina-filled glass-epoxy composites using Taguchi experimental design, Tribology Transactions, 53, pp. 520-532.

310. Kretsis G. (1987), A review of the tensile, compressive, flexural and shear properties of hybrid fibre-reinforced plastics, Composites, 18 (1), pp. 13-23.

311. Singh B., Gupta M. and Verma A. (1995), Mechanical behavior of particulate hybrid composite laminates as potential building materials, Construction and Building Materials, 9, pp. 39-44.

312. Selzer R. and Friedrich K. (1997), Mechanical properties and failure behavior of carbon fibre-reinforced polymer composites under the influence of moisture, Composites: Part A, 28A, pp. 595-604.

313. Jawaid M., Khalil A. and Abu Baker A. (2011), Woven hybrid composites: tensile and flexural properties of oil-palm woven jute fiber based epoxy composites, Materials Science and Engineering A, 528, pp. 5190-5195.

314. Singh S., Mohanty A.K. and Misra M. (2010), Hybrid bio-composite from talc, wood fiber and bioplastic: fabrication and characterization, Composites: Part A, 41, pp. 304-312.

315. Liu S. P., Hwang S. S., Yeh J. M. and Hung C. C. (2011), Mechanical properties of polyamide-6/montmorillonite nanocomposites - prepared by the twin screw extruder mixed technique, International

Communications in Heat And Mass Transfer, 38 (1), pp. 37-43.

316. Jacob M., Thomas S. and Varughese K. T. (2004), Mechanical properties of sisal/oil palm hybrid fiber reinforced natural rubber composites, Composites Science and Technology, 64, pp. 955-965.

317. Arib R. M. N., Sapuan S. M. and Ahmad M. M. H. M (2004), Mechanical properties of pineapple leaf fibre reinforced polypropylene composites, Materials and Design, 27, pp. 391-396.

318. Vu-Khaanh T., Denault J., Habib P. and Low A. (1991), The effect of injection moulding on the mechanical behavior of long-fibre reinforced PBT/PET blends, Composites Science and Technology, 40, pp. 423-435.

319. Pati P. R. and Satapathy A. (2014), Processing, characterization and erosion wear response of Linz-Donawitz (LD) slag filled polypropylene composites, Journal of Thermoplastic Composite Materials, DOI: 10.1177/0892705714563122.

320. Ahmed T. J., Nino G. F., Bersee H. E. N. and Beukers A. (2009), Improving erosion resistance of polymer reinforced composites, Journal of Thermoplastic Composite, 22, pp. 703-725.

321. Pati P. R. and Satapathy A. (2015), Prediction and simulation of wear response of Linz-Donawitz (LD) slag filled glass-epoxy composites using neural computation, Polymers Advanced Technologies, 26, pp. 121-127.

322. Pati P. R. and Satapathy A. (2015), Tribo-performance analysis of coatings of LD slag premixed with $TiO_2$ using experimental design and ANN, Tribology Transactions, 58, pp. 349-356.

*****

# Appendix A1

## LIST OF PUBLICATIONS OUT OF THIS WORK

### International Journals

1. **Gaurav Gupta** and Alok Satapathy (2012), "Preparation and Characterization of Thermal Spray Coating of Glass Microspheres on Metal Substrate*"*, ***Advanced Materials Research*** *585****,*** pp. 502-506.

2. **Gaurav Gupta** and Alok Satapathy (2013), **"**Plasma Sprayed Coatings of Glass Micro-Spheres Premixed with $Al_2O_3$", ***Surface Engineering*** *29(10),* pp. 755-760.

3. **Gaurav Gupta** and Alok Satapathy (2014), "Erosion Wear Response of Glass Micro-sphere Coatings: Parametric Appraisal and Prediction using Taguchi Method and Neural Computation", ***Tribology Transactions*** *57(5),* pp. 899-907.

4. **Gaurav Gupta** and Alok Satapathy (2014), "Studies on Erosion Behavior of Plasma Sprayed Coatings of Glass Micro-spheres Premixed with $Al_2O_3$ Particles", ***Advances in Tribology*** *2014,* pp. 1-11.

5. **Gaurav Gupta** and Alok Satapathy, "Processing, Characterization and Erosion Wear Characteristics of Boro-silicate Glass Microspheres Filled Epoxy Composites", ***Polymer Composites***, DOI: 10.1002/pc.23079.

6. **Gaurav Gupta** and Alok Satapathy, "Characterisation and Wear Performance of Plasma Sprayed Borosilicate Glass Micro-sphere Coatings on Metallic Substrates", ***Surface Science and Engineering*** *(9)1,* pp. 81-95.

7. **Gaurav Gupta** and Alok Satapathy**,** "Erosive Wear Characteristics of Plasma Sprayed Coatings of Glass Micro-spheres Premixed with $TiO_2$ Particles", ***Tribology Transactions***. (Under review)

*Contd….*

## Conferences

1. **Gaurav Gupta** and Alok Satapathy, "Modified Mechanical and Wear Characteristics of Epoxy Filled with Borosilicate Glass Micro-spheres", ***Proceedings of APM-2013, March 1-3, 2013, CIPET, Luckhnow.***

2. **Gaurav Gupta** and Alok Satapathy, "A Study on Tribological Performance of Borosilicate Glass Micro-spheres Filled Epoxy Composites Modified Mechanical and Wear Characteristics of Epoxy Filled with Borosilicate Glass Micro-spheres", ***Proceedings of APM-2013, Feb 14-16, 2014, CIPET, Bhubaneswar.***

3. **Gaurav Gupta** and Alok Satapathy**,** "Tribo-performance prediction of glass micro-spheres coatings using artificial neural network", ***PLASMA-2012, Dec 10-13, 2012, Pondicherry University, Puducherry.***

4. **Gaurav Gupta** and Alok Satapathy, "Solid particle erosion of plasma sprayed coatings of glass micro-spheres premixed with $TiO_2$ particles", ***ICAT-2014, Feb 21-24, 2014, NIT, Calicut.***

5. **Gaurav Gupta** and Alok Satapathy**,** "Physical, Mechanical and Thermal Characterization of Glass Micro-sphere filled Epoxy", ***ASEAI-2014, April 11-13, 2014, Assumption University, Bangkok, Thailand.***

*****

# Appendix A2

## Brief bio-data of the author

The author, **Gaurav Gupta**, born on 29-06-1986 graduated in Mechanical Engineering from Shri Shankaracharya College of Engineering and Technology, Bhilai, India in the year 2007. He completed his Post-graduate study (M.Tech.) in Mechanical Engineering with specialization in Thermal Engineering from the National Institute of Technology, Rourkela, India in the year 2009. Immediately after completion of M.Tech. programme, he joined as an Assistant Professor in the Department of Mechanical Engineering at Shri Shankaracharya College of Engineering and Technology, Bhilai, India and served for about 2 years. He joined National Institute of Technology, Rourkela in the year 2011 as a Research Scholar in the Department of Mechanical Engineering.

The author is engaged in active research in the area of plasma spray coatings and composite materials since 2011. He has 7 research papers to his credit which have been published in various international journals of repute. He has also presented 5 research papers in the area of coatings and composites at various national and international conferences held in India and abroad.

*****